The role of claudin-2 in the proximal tubule and kidney stone disease

By
Joshua Curry

Submitted to the graduate degree program in Molecular and Integrative Physiology and the Graduate Faculty of the University of Kansas in partial fulfillment of the requirements for the degree of Doctor of Philosophy.

Co-Chair: Alan Yu, M.B., B.Chir.

Co-Chair: Gustavo Blanco, M.D., Ph.D.

Bruno Hagenbuch, Ph.D.

Timothy Fields, M.D., Ph.D.

Peter Rowe, Ph.D.

Darren Wallace, Ph.D.

Jason Stubbs, M.D.

Date Defended: 7 May 2018

The dissertation committee Joshua Curry certifies that this is the approved version of the following dissertation:

The role of claudin-2 in the proximal tubule and kidney stone disease

_____
Co-Chair: Alan Yu, M.B., B.Chir.

_____
Co-Chair: Gustavo Blanco, M.D., Ph.D.

Date Approved: 7 May 2018

Abstract

The concentration of circulating blood calcium is vital to the function of many cellular processes. As such, it is maintained within a narrow range through the actions of gastrointestinal, bone, kidney, and endocrine tissues. In the kidney, the first portion of the nephron, called the proximal tubule (PT), performs the majority of solute reabsorption including about two-thirds of calcium. *In vivo* and *ex vivo* studies of PTs have shown that the major component of calcium reabsorption is passive and tightly linked to sodium reabsorption. This passive transport has long been suspected to be paracellular. The precise mechanisms and molecular facilitators of calcium reabsorption in the PT, however, remain unknown. Claudins are a group of transmembrane tight junction (TJ) proteins that are vital to the regulation of paracellular transport. In the PT, claudin-2 is a highly expressed isoform. Claudin-2 increases the calcium permeability of renal epithelial cells upon overexpression. In addition, it was previously shown that mice with deletion of claudin-2 have increased urinary calcium excretion. I hypothesized that PT calcium reabsorption is facilitated by claudin-2. My overall hypothesis was tested in several ways.

First, I examined the patterns of claudin expression in the proximal nephron and found that claudins-2 and -10a are expressed throughout the PT, in both convoluted and straight segments. In contrast, claudin-3 is expressed only within the proximal straight tubule (PST). Furthermore, claudin-2 and claudin-3 expression are found in separate and distinct subpopulations of thin descending limbs. Next, I used co-immunoprecipitation experiments to show that claudin-2 physically interacts with claudin-3. Then I generated renal epithelial cell lines with inducible expression of PT claudins, claudin-2 and either claudin-3 or claudin-10a. I found no effect of claudin-3 overexpression on conductance or sodium permeability (P_{Na}), with or without claudin-2 expression. However, overexpression of both claudins-2 and -10a led to a highly conductive cell monolayer with loss of charge selectivity. The results of calcium permeability assays show that calcium transport was reduced with co-expression of claudins-2 and -10a but unchanged with co-expression of claudins-2 and -3. In order to test the potential contribution of

claudin hetero-oligomerization on these permeability properties, I measured permeability of claudin-2/claudin-10a cells with titrated expression of each protein and with blockage of the claudin-2 pore. My results suggest that, rather than forming a hybrid channel with novel characteristics, claudin-2 and claudin-10a form pores in parallel.

Next, I tested the hypothesis that deletion of the claudin-2 gene *Cldn2* in mice causes nephrocalcinosis similar to human kidney stone disease using micro-computed tomography (micro-CT) and histological analyses. My findings indicate that this papillary pattern of nephrocalcinosis shares striking similarities to human kidney stone disease. I also examined the mechanism of hypercalciuria in these animals and found both a reduction in renal calcium reabsorption and a large increase in intestinal calcium absorption. Our colleagues subsequently identified multiple SNPs in the *CLDN2* locus that associate with human kidney stone disease. Importantly, *cis*-acting expression quantitative trait loci (eQTL) analysis reveals that these same risk variants correlate with reduced claudin-2 mRNA expression in human tissues.

My work suggests that proximal delivery of calcium to the loops of Henle is important in the pathogenesis of nephrocalcinosis and kidney stone formation. In addition, claudin-2 expression is an important mediator of calcium transport that is associated with kidney stone disease in humans. These findings have led to a better understanding of renal physiology and paracellular transport and provide a novel treatment target for disorders of calcium balance and homeostasis.

Acknowledgements

There are many people who have supported me and assisted me thus far along the path towards my ultimate goal to become a physician scientist. There is so much inspiration to be drawn from the people who surround me and have helped shape the person I am today. I would of course like to thank my mentor, Dr. Alan Yu, for being a guiding force; thank you for giving me the independence I needed to grow as a scientist while navigating me through this work. The impeccably logical and organized way you have in approaching problems is a skill I hope to master as I progress through my training. You have given me the template with which to build a successful academic career, and I could not have possibly chosen a better lab to develop as a scientist.

I would also like to show appreciation to the colleagues at the Oregon Health and Science University that led me to this career path. First, thank you to Jean McCormick, Charlie Borzy, and Dr. Ali Olyaei, my mentors in clinical research, for allowing me to slip into the translational research realm as I was drawn towards bench research. Thank you to Dr. David Ellison for being a supportive leader in the lab and the field, and another shining example of what it means to be a successful physician scientist. For Dr. Jim McCormick, who was my basic science mentor and a fierce supporter - thank you. I doubt I would be here without your advocacy, including authorships, letters of support, and career advice. It means more than you know, and I hope to be such an indefatigable champion for my own trainees one day. I would also especially like to thank Dr. Andy Terker, who is currently a resident on the physician-scientist track. Thank you, Andy, for the many words of wisdom and paving the road ahead.

This work would not have been possible without the aid of many outside collaborations. I would like to thank Dr. Andrew Evan (Indiana University) for assistance in the interpretation of histological data, as well as Dr. Andre J. Sommer (Miami University of Ohio) for analysis of papillary mineral deposition. I would also like to thank Drs. Koichi Matsuda (University of Tokyo), Chizu Tanikawa (University of Tokyo), and Yoichiro Kamatani (RIKEN Center for Integrative Medical Sciences) for the analysis of human genetic data in association with kidney stone

disease. Finally, I am grateful for the technical skill and expertise of Barbara Fegley. Thank you so much Barbara with your help throughout my PhD training.

I want to thank the members of my committee; Drs. Gustavo Blanco, Timothy Fields, Bruno Hagenbuch, Peter Rowe, Jason Stubbs, and Darren Wallace. Your support, guidance, and collaboration along the way has helped me reach this moment, and I will forever be grateful to you for challenging me and steering me throughout this journey.

I want to show appreciation for the Department of Molecular and Integrative Physiology, especially Dr. Gustavo Blanco, Shari Standiferd, and Jennifer Wallace. The department's commitment to students and your desire to keep us involved and impassioned, including your support for the Physiology Society, in so many ways has made this a fun place to complete this dissertation work. I also would like to thank the scientists and physicians at the Jared Grantham Kidney Institute for showing me what a collaborative, disease-focused translational research group looks like.

I would like to acknowledge the financial support I received from the National Institute of Diabetes and Digestive and Kidney Diseases at the National Institutes of Health (NIH) through the Ruth L. Kirschstein National Research Service Award (NRSA) Individual Predoctoral MD/PhD or Other Dual-Doctoral Degree Fellowship (F30 DK109605). Support from NIH and the process of grant application and reporting has been a key part of my training thus far.

I would of course like to thank the MD/PhD program. To Janice Fletcher- thank you for all of your hard work and advocacy throughout the years. To Dr. Timothy Fields- I am lucky to have a renal pathologist as a mentor and scientific guide through this program. Thank you, Dr. Fields, for your open door and being the steady force throughout times of anxiety-ridden transitions. Dr. Brenda Rongish- thank you for being one of the most kind and supportive scientists I know, and thank you for your dedication to prepare me for success in writing with scientific clarity. To all of the students, thank you for always being there for guidance, support, commiseration, and quite a

few backyard barbecues. I am proud to be associated with the University of Kansas MD/PhD program.

I could not have accomplished much in the lab without encouragement from members of the Yu lab. First, thank you to Dr. “Pearl” Pei; you were a second mentor in the lab and I wish you tremendous success in the future. To Patrick McAnulty, thanks for paving the way for some of this work and providing me with the supplies and good conversation. To Dr. Madhu Rajagopal, thank you for making us feel like a team. To Dr. Shinsaku Tokuda, it has been a pleasure working for you this short time and I look forward to seeing the amazing things you do in the lab. There are so many to thank, but the people in the lab have made it a nice place to hang my hat these years, including the Drs. Jiahua and Min Li, Dr. Morten Engelund, Kayleigh Peterson, Mike Filla, and Lynn Magenheimer.

I am so thankful for the love and support of my parents, my sisters and their families, who have always encouraged me to follow my dreams. I love you.

Last, but not least, I would like to thank my wife, Alyssa. You and Elowyn are my everything. I know this has not always been an easy road, so thank you for taking it with me and being my “rock-k-k” (Elowyn’s pronunciation). I love you both to the moon and back.

Table of Contents

List of Abbreviations

AQP1/2	aquaporin-1/2
ATR	attenuated total internal reflection
BMD	bone mineral density
CaOx	calcium oxalate
CB28K/D9k	calbindin-D28k/D9k
CCD	cortical collecting duct
CLC-K	chloride channel K
CLDNX	claudin-(number X)
CRISPR	Clustered Regularly Interspaced Short Palindromic Repeats
DCT	distal convoluted tubule
DEXA	dual energy X-ray absorptiometry
ECL1/2	extracellular loop 1/2
eQTL	expression quantitative trait loci
$FECa^{2+}$	fractional excretion of calcium
FHHNC	familial hypomagnesemia with hypercalciuria and nephrocalcinosis
FTIR	Fourier transform infrared
GTEx	Genotype-Tissue Expression project
GWAS	genome-wide association study
Hek293	human embryonic kidney 293
J-MICC	Japan Multi-Institutional Collaborative Cohort
JPHC	Japan Public Health Center
LLC-PK1	Lilly Laboratory Cell – Porcine Kidney 1
MDCKI/II/C7	Madin Darby Canine Kidney cells I/II/C7
MECA32	mouse panendothelial cell antigen 32
Micro-CT	micro-computed tomography
MTSEA	methanethiosulfonate ethylammonium
NCX1	sodium calcium exchanger
NHERF1	sodium hydrogen exchange regulator factor-1
NIPS	novel interstitial plaque structures
NKCC2	Na^+-K^+-$2Cl^-$ cotransporter 2
Npt2a	type II sodium phosphate cotransporter
OPN	osteopontin
PCT	proximal convoluted tubule
PDZ	postsynaptic density 95/discs large/ZO-1
PMCA1	plasma membrane calcium ATPase
PST	proximal straight tubule
PT	proximal tubule
PTH	parathyroid hormone
P_X	permeability to ion X
SNP	single nucleotide polymorphism
TAL	thick ascending limb of the loop of Henle
TALEN	transcription activator-like effector nuclease
tdL	thin descending limb of the loop of Henle
TER	transepithelial resistance
THP	Tamm-Horsfall protein (THP)
TJ	tight junction
tLOH	thin limbs of the loop of Henle
ToMMo	Tohoku Medical Megabank Organization
TRPV5/ TRPV6	transient vanilloid type 5 / 6 channel

List of Figures and Tables

Chapter 1: Claudins and Kidney Stones

I am investigating the role of claudin-2 in calcium transport in the PT and gastrointestinal tract, as well as its role in the development of nephrocalcinosis and kidney stone disease. Claudin-2 increases calcium flux of cell monolayers *in vitro* (Yu, Cheng et al. 2009) while mice with deletion of claudin-2 develop hypercalciuria (Muto, Hata et al. 2010). This work describes novel findings in the pathogenesis of nephrocalcinosis and suggests a role for claudin-2 in the formation of kidney stones in humans.

This introductory chapter will first cover our current knowledge regarding the role of TJs in calcium transport and calcium homeostasis. I will provide an introduction to TJ biology and underscore the fundamental role of TJs in normal mammalian physiology and disease. In particular, I will discuss the role of claudins in physiology by exploring human diseases caused by loss-of-function mutations in claudin genes. Next, I will describe our current knowledge of paracellular transport within the PT of the kidney, with a particular focus on mechanisms of calcium transport. Following this, the clinical features of the two most common forms of kidney stone disease in humans will be summarized. This includes a discussion of the pathogenetic mechanisms for stone formation and the gaps that remain in our present understanding. Finally, I will discuss the evidence that reduced PT calcium transport is a common feature of kidney stone formers, and explore the potential role that claudin-2 plays in calcium transport in the PT.

In chapter 2, I explore the role of PT claudins in the paracellular permeability of renal epithelial cells *in vitro*. We have generated a novel dual-claudin inducible model with which to investigate the effects of dual claudin expression on permeability of cell monolayers. My findings show that the most prominent claudins within the PT, claudins-2 and -10a, form cation and anion pores, respectively. I hypothesized that the permeabilities imparted by claudins-2 and -10a would be additive. However, co-expression of claudin-2 and claudin-10a reduced the permselectivity imparted by either claudin alone and led to a low resistance monolayer with approximately equal

permeabilities to both sodium (P_{Na}) and chloride (P_{Cl}). Thus, I investigated a potential model of claudin interaction in which co-expression of PT claudins leads to a hybrid channel with novel permeability properties. Subsequent experiments support the conclusion that PT claudins influence the permselectivity as parallel ion channels, with claudin-2 and claudin-10a forming separate pores rather than a hybrid pore in the TJ.

In chapter 3, I investigate the mechanisms of hypercalciuria and explore the nephrocalcinosis phenotype of animals with deletion of claudin-2 (*Cldn2*$^{-/y}$ mice). My findings show that claudin-2 loss results in both a decrease in renal calcium reabsorption and an increase in intestinal calcium absorption. These data suggest that *Cldn2*$^{-/y}$ mice exhibit many similarities to human kidney stone formers. First, I describe a form of calcium deposition within the medullary region of the kidney which resembles deposits in human kidney stone formers. My characterization suggests that these deposits form in the lumina of loops of Henle. These intraluminal deposits resemble deposits found in humans that are hypothesized to precede human kidney stone formation. Genomic analysis of a large database of stone formers and non-stone formers reveals that multiple common SNPs at the *CLDN2* locus associate with kidney stone disease in a Japanese population. These SNPs are common worldwide and associate with the reduced tissue mRNA expression of claudin-2. Thus, I suggest that reduced claudin-2 expression in the kidney is a common risk factor for kidney stone disease in humans.

1.1 Junctional complexes and TJs

Junctional complexes are massive multi-protein structures found at the interface between adjacent cells that help to maintain the integrity of the epithelial cell barrier. In vertebrates, the junctional complex is organized into three major components: the *zonula adherens* (intermediary junction), the *macula adherens* (desmosome), and the *zonula occludens* (TJ, Figure 1-1A) (Farquhar and Palade 1963). Another category of structures often found within the junctional complex of epithelia is the communicating junction, an example being the gap junctions (Figure 1-1A) that allow passage of small molecules from cell to cell through hexameric channels called

connexons (Alberts 2002). Junctional complex components are large enough to be recognized by transmission electron microscopy (TEM) and freeze-fracture microscopy (Alberts 2002). Intermediary junctions and desmosomes both function to anchor cells firmly to each other, and their composition is largely made up of proteins from the *cadherin* family (Alberts 2002). The TJ is the most apical structure of the junctional complex. Whereas intermediary junctions and desmosomes are found associated with an intercellular space, no such space is observed at TJs (Farquhar and Palade 1963). In addition, TJs are found continuously along the apical membrane of adjacent cells, as opposed to the often discontinuous pattern of the other junctional complex components (Farquhar and Palade 1963). Given this, it is not surprising that the TJs form a seal separating the apical and basolateral environment of epithelia. This can even be appreciated using TEM, where electron-dense proteins such as hemoglobin or zymogens within epithelial lumina are barred passage at the TJ (Farquhar and Palade 1963).

Farquhar and Palade described the structure of TJs across a wide range of epithelial tissues, and found that within the kidney, in particular, the morphology of TJs changes from one portion of the nephron to another (Farquhar and Palade 1963). For instance, the most leaky portion of the nephron, the PT, has a relatively shallow TJ (~0.03μm in depth) and wide intercellular spaces, whereas the TJs of the high transepithelial resistance (TER) distal tubule segments are deep (~0.3μm in depth) and intercellular spaces are narrow (Farquhar and Palade 1963).

A few decades ago, several key proteins were discovered in association with TJs. Zonula occludens-1 (ZO-1) was first identified as a large (220 kDa) peripheral membrane protein localized to the TJ of epithelial cells (Stevenson, Siliciano et al. 1986). The discovery of ZO-1 led to the isolation of membrane fractions of liver specific to the TJ, allowing the identification and cloning of another TJ protein: the transmembrane protein, occludin (65 kDa) (Furuse, Hirase et al. 1993). Subsequent work identified a functional role for ZO-1 as a scaffolding protein joining occludin with the actin cytoskeleton (Fanning, Jameson et al. 1998).

1.2 The claudin family of proteins

In 1998, Furuse et al. sequenced peptides from a 22 kDa transmembrane protein found in TJ membrane fractions and identified and cloned two full-length cDNAs with predicted peptide sequence similarity (Furuse, Fujita et al. 1998). These cDNAs encoded for two distinct four-pass transmembrane proteins that localize to the TJ of epithelial cells *in vitro* but do not share sequence homology with occludin (Furuse, Fujita et al. 1998). Furuse named the two proteins claudin-1 and claudin-2 after the Latin word *claudere*, or "to close" (Furuse, Fujita et al. 1998). Genetic ablation of claudin-1 in mice caused severe dehydration and neonatal death but did not result in morphologic alterations to the TJ or mislocalization of occludin (Furuse, Hata et al. 2002). Interestingly, despite normal TJ ultrastructure, loss of claudin-1 in mice allowed diffusion of a 600 Da tracer towards the skin surface, indicating that it plays a vital role in creating an impermeable barrier between cells (Furuse, Hata et al. 2002). While claudin-1 appears to be a barrier claudin and is expressed in most tissues (Furuse, Fujita et al. 1998), claudin-2 is expressed exclusively in tissues with leaky epithelia such as the intestinal crypts (Rahner, Mitic et al. 2001) and the PT (Enck, Berger et al. 2001). *In vitro* expression of claudin-2 decreases the TER (Furuse, Furuse et al. 2001) by increasing the paracellular cation permeability of an epithelial cell monolayer (Amasheh, Meiri et al. 2002, Yu, Cheng et al. 2009). The extracellular cation pore formed by claudin-2 is estimated to be approximately 6.5 Å (Yu, Cheng et al. 2009, Li, Zhuo et al. 2014). These two initially characterized claudins demonstrate the range of functions of claudins at the TJ; claudins may function either to bar the passage of small molecules such as ions and water or facilitate the diffusion of such molecules across an epithelial layer, akin to extracellular ion channels.

Since the initial discovery of claudins-1 and -2, at least 24 additional members of the claudin family have been identified (Hou, Rajagopal et al. 2013). All of these proteins consist of four-transmembrane domains, 2 extracellular loops, and cytoplasmic C- and N-terminal tails (Hou, Rajagopal et al. 2013) (Figure 1-1B). The first extracellular loop (ECL1) of each claudin contains

a GLWCC motif and amino residues that confer the paracellular ion selectivity of a given isoform (Hou, Rajagopal et al. 2013). In addition, all claudins contain a postsynaptic density 95/discs large/ZO-1 (PDZ) binding domain at the C-terminal tail (Figure 1-1B). This domain is crucial for interaction with peripheral membrane scaffolding proteins such as ZO-1 (Itoh, Furuse et al. 1999). The first crystal structure of a claudin was resolved for mouse claudin-15 in 2014 (Suzuki, Nishizawa et al. 2014). Homologous proteins with analogous ECL1 motifs and PDZ binding domains are found throughout the animal kingdom, including in sponges, which are believed to be the closest living relatives of the earliest branch of Metazoa (Leys and Riesgo 2012). Given this, it is easy to speculate that claudins were a vital ingredient in the fundamental evolutionary recipe for formation of a multicellular epithelial layer.

1.3 Claudins in Mendelian disease

The role of claudins in normal physiology can perhaps best be explored by the spectrum of human diseases caused by claudin mutations.

1.3.1 Familial hypomagnesemia with hypercalciuria and nephrocalcinosis

In 1999, the first disease-causing mutations within the claudin family were described for the claudin-16 gene (*CLDN16*, originally identified as Paracellin-1, or *PCLN-1*) (Simon, Lu et al. 1999). These are loss of function *CLDN16* mutations that cause the autosomal recessive disorder familial hypomagnesemia with hypercalciuria and nephrocalcinosis (FHHNC) (Weber, Schneider et al. 2001, Konrad, Hou et al. 2008). FHHNC is characterized by impaired renal reabsorption of magnesium and calcium, bilateral calcification within the kidneys (nephrocalcinosis), and rapidly progressing tubulointerstitial kidney disease leading to kidney failure in adolescence or young adulthood (Weber, Schneider et al. 2001). Claudin-16 is located within the thick ascending limb of the loops of Henle (TAL) in the human kidney (Kirk, Campbell et al. 2010), the site of defective calcium and magnesium reabsorption in FHHNC (Blanchard, Jeunemaitre et al. 2001). The role of claudin-16 in TAL calcium and magnesium transport is likely to be complex. First, overexpression of claudin-16 in MDCK C7 cells increases paracellular magnesium permeability

(but not calcium) (Gunzel, Amasheh et al. 2009) and isolated TAL from claudin-16 knockout mice have reduced permeability to magnesium and calcium (Will, Breiderhoff et al. 2010). This suggests that claudin-16 may act as a divalent cation pore and directly mediate paracellular reabsorption in the TAL. On the other hand, claudin-16 also seems to modulate basolateral chloride secretion through calcium activated chloride channels (Gunzel, Amasheh et al. 2009) and increase paracellular P_{Na} (Hou, Paul et al. 2005), thereby increasing the positive lumen potential which drives magnesium and calcium reabsorption in the TAL (Hou, Shan et al. 2007).

In 2006, mutations in the gene for claudin-19, *CLDN19*, were discovered in patients with ocular abnormalities and visual impairment in addition to all of the characteristic symptoms of FHHNC (Konrad, Schaller et al. 2006). Claudin-19 seems to act as a chloride barrier and physically interact with claudin-16 *in vitro*, thereby increasing the cation to anion selectivity ratio of the paracellular pathway (Hou, Renigunta et al. 2008). Interestingly, in transgenic mice with knockdown of either claudin-16 or -19, it has been observed that the localization of both claudins-16 and -19 are lost from the TAL TJ (Hou, Renigunta et al. 2009). Indeed, several FHHNC mutations have been shown to interfere with the physical interaction of claudins-16 and -19 (Hou, Renigunta et al. 2008), highlighting the complexity of heterogeneous claudin expression *in vivo*.

1.3.2 Autosomal Recessive Deafness DFNB29

In 2001, mutations in *CLDN14*, the gene for claudin-14, were first described as the cause of a form of nonsyndromic recessive deafness (Wilcox, Burton et al. 2001). Overexpression of claudin-14 in MDCK II cells (a low resistance renal epithelial cell line) leads to an increase in TER and reduction in cation permeability, suggesting that it functions primarily as a cation barrier (Ben-Yosef, Belyantseva et al. 2003). The Organ of Corti of the inner ear contains sensory hair cells that depend on a high concentration of potassium within the endolymph of the scala media for adequate depolarization (Wilcox, Burton et al. 2001). Claudin-14 is expressed at the apical portion of hair cells in the organ of Corti (Wilcox, Burton et al. 2001). Mirroring the human disorder, claudin-14 knockout mice are also deaf, and this has been determined to be primarily due to the

degeneration of the sensory hair cells (Ben-Yosef, Belyantseva et al. 2003). This disease serves as an example of the physiological importance of claudins in the formation of a paracellular barrier. Claudin-14 is also expressed in liver and kidney tissues (Ben-Yosef, Belyantseva et al. 2003), and genetic associations between *CLDN14* and nephrolithiasis will be discussed in more detail in the sections below.

1.3.3 Neonatal Sclerosing Cholangitis Associated With Ichthyosis

Mutations resulting in a premature stop codon in claudin-1 (*CLDN1*) were identified in 2004 as the cause of an autosomal recessive disorder, neonatal sclerosing cholangitis associated with ichthyosis (Hadj-Rabia, Baala et al. 2004). In humans, claudin-1 is expressed in both hepatocytes and chloangiocytes (Hadj-Rabia, Baala et al. 2004). The disease presents in infants with jaundice and pale stools, similar to symptoms caused by obstruction of the bile duct, and ultimately leads to biliary cirrhosis and liver failure (Hadj-Rabia, Baala et al. 2004). The disorder is suspected to arise as a result of increased permeability of bile across these cells and subsequent bile duct injury (Hadj-Rabia, Baala et al. 2004). Loss of claudin-1 in mice leads to severe dehydration and a loss of barrier function in skin (Furuse, Hata et al. 2002), perhaps mirroring the symptom of ichthyosis in humans but with heightened severity (Furuse, Hata et al. 2002). Likewise, early neonatal death in these mice may explain why liver disease and biliary obstruction were not identified (Furuse, Hata et al. 2002). These findings illuminate a central role for claudin-1 in the formation of epithelial barriers in various tissues.

1.3.4 HELIX Syndrome

Recently, a number of mutations have been described in the gene for claudin-10 (*CLDN10*) which cause a complex multisystem syndrome that includes hypokalemic metabolic alkalosis, salt wasting, and increased renal magnesium and calcium reabsorption (Bongers, Shelton et al. 2017, Klar, Piontek et al. 2017, Hadj-Rabia, Brideau et al. 2018). *CLDN10* transcripts are alternatively spliced into separate isoforms that differ in their localization and permeability properties (Gunzel, Stuiver et al. 2009). Claudin-10a is a variant expressed only in

kidney and uterus. Claudin-10a localizes to the TJ and imparts chloride selectivity when overexpressed in MDCK II cells (Van Itallie, Rogan et al. 2006, Gunzel, Stuiver et al. 2009). In contrast, claudin-10b is a cation-selective isoform that is found throughout the body, including in the distal nephron (Gunzel, Stuiver et al. 2009) and the glandular tissue such as sweat glands (Klar, Piontek et al. 2017) and salivary glands (Hadj-Rabia, Brideau et al. 2018). Interestingly, one of the reports of *CLDN10* mutations described two missense mutations specific only to isoform claudin-10b, leading to a syndrome of hypohidrosis, electrolyte imbalance, lacrimal gland dysfunction, ichthyosis, and xerostomia and thus termed HELIX syndrome (Hadj-Rabia, Brideau et al. 2018). There are subtle differences in the reported cases of *CLDN10* mutations and disease but taken together these studies suggest that the major manifestations of the described tubulopathy are the result of defective claudin-10b function.

1.4 Claudins within the PT of the kidney

Similar to the patterns in TJ morphology, the expression pattern of claudins in the kidney is highly heterogeneous from one segment to another (Kirk, Campbell et al. 2010, Lee, Chou et al. 2015). Among many important functions, the kidneys remove waste products from blood and maintain ion homeostasis via regulation of blood pressure and the electrolyte composition of extracellular fluid (Hall and Guyton 2011). Each human kidney is composed of roughly one million individual units called nephrons. Each nephron is composed of a modified capillary bed that serves as a filtration unit (glomerulus) followed by a series of tubule segments with distinct functional properties. These properties allow the kidneys to filter waste products out of blood at an incredible rate (around 180L of plasma is filtered per day in a healthy human adult) while reabsorbing >99% of solutes and water (Hall and Guyton 2011).

The PT is responsible for the reabsorption of approximately two thirds of sodium, chloride, water, and calcium by the kidney (Hall and Guyton 2011). A significant proportion of PT reabsorption of these ions is passive, following the electrochemical gradients set up by sodium-coupled cotransport of nutrient osmolytes such as glucose and amino acids (Figure 1-2A) (Green

and Giebisch 1989). Active sodium-coupled cotransport is coupled with bicarbonate reabsorption, which leads to generation of a chloride gradient in the mid-PT (Figure 1-2C) (Liu and Cogan 1984). Since the paracellular pathway is highly permeable to chloride, chloride is passively reabsorbed (Green and Giebisch 1989) and a positive lumen potential is generated. This small lumen potential, paired with an incredibly low TER, is believed to drive the paracellular reabsorption of sodium and calcium (Figure 1-2B-C) (Barratt, Rector et al. 1974). Figure 1-2 depicts transport along the PT in early and mid-late portions of the segment. Claudin-2, as mentioned above, is a cation-selective isoform with high expression within the PT and the first portion of the thin descending limb (Enck, Berger et al. 2001). Using a knockout mouse model, Muto et al. (2010) showed that loss of claudin-2 *in vivo* leads to a reduction in the P_{Na} of isolated PTs (Muto, Hata et al. 2010). In addition, claudin-2 knockout mice excrete more sodium than wild type following administration of hypertonic sodium chloride, suggesting that claudin-2 mediates paracellular sodium reabsorption in the PT (Muto, Hata et al. 2010). Claudin-2 also has been demonstrated to function as a water pore (Rosenthal, Milatz et al. 2010) and likely accounts for a fraction of water reabsorption in the PT (Schnermann, Huang et al. 2013).

Considering that the kidneys reabsorb well over 100L of fluid and solutes per day, the chemical energy needed to drive transcellular transport of this quantity would seem to make glomerular filtration an evolutionarily precarious strategy for waste excretion. Previous work in our lab showed that loss of claudin-2 greatly increases renal energy consumption and predisposes kidneys to acute ischemic injury (Pei, Solis et al. 2016). This, we argue, is due to the ability of claudin-2 to allow passive transport of sodium in the PT, which otherwise must be reabsorbed through active, energy-consuming transcellular processes. As a result, claudin-2 allows PT reabsorption to be much more energy efficient (Pei, Solis et al. 2016). In a teleological sense, such a heavy reliance on passive wholesale ion transport is acceptable in the PT because much of the fine-tuning of electrolyte and acid-base homeostasis is regulated within the more distal nephron.

In addition to claudin-2, claudin-10 is also expressed within the PT (Kirk, Campbell et al. 2010, Lee, Chou et al. 2015). As mentioned in Section 1-3-4, the *CLDN10* gene is transcribed as multiple splice variants. The two major variants differ in their ECL1 loops and charge selectivity (Van Itallie, Rogan et al. 2006). In the PT of mice, the anion-selective variant claudin-10a is expressed (Gunzel, Stuiver et al. 2009). Thus, it is possible that claudin-10a provides the paracellular route for chloride reabsorption in the PT, although this has not been directly tested in animal models. In the distal portion of the PT, claudin-3 is highly expressed in the rat (Lee, Chou et al. 2015). Claudin-3 is believed to act primarily as a barrier claudin, and overexpression of claudin-3 in the highly cation-selective MDCK II cells reduces the cation permeability and increases TER (Milatz, Krug et al. 2010). Characterization of claudin expression in the human kidney has thus far focused on cortical sections only (Kirk, Campbell et al. 2010), and so the expression pattern of claudin-3 within the PSTs of *homo sapiens* is unknown.

1.5 Nephrolithiasis in man

Kidney stone disease, or nephrolithiasis, was common enough to be written about in ancient Mesopotamian medical texts, and a stone was even discovered in the bladder of a 5000 year-old mummy (Tefekli and Cezayirli 2013)! Hippocrates' *Oath of Medical Ethics*, a document written in the B.C. epoch and still taken by physicians today, states "*I will not cut for stone, but will leave this to be done by practitioners of this work*." Indeed, kidney stones were operated on thousands of years ago with decidedly less evidence-based approaches than today such as urethral lavage of "medicated" milk, or, failing that, perineal lithotomy (in the age before antibiotics or anesthesia, an operation with considerable mortality) (Tefekli and Cezayirli 2013). Today, great strides have been made but many obstacles remain in the prevention and treatment of kidney stones.

1.5.1 Prevalence and Clinical Manifestations of Stone Disease

Nephrolithiasis continues to present a massive public health concern, afflicting an estimated 1 in 11 people in the United States (Scales, Smith et al. 2012). This number has

skyrocketed from about 1 in 26 people in 1974 (Stamatelou, Francis et al. 2003), and there is a strong association between nephrolithiasis and obesity and diabetes in the U.S. (Scales, Smith et al. 2012). With this in mind, environmental factors such as diet and lifestyle seem to be playing an increasing role in the pathogenesis of the disorder. Unfortunately, most patients who experience a kidney stone will experience another, as it has a relapse rate of 75% within a 20 year period (Moe 2006).

Nephrolithiasis is considerably more common in males, affecting approximately 10.6% of males, compared with 7.1% of women (Scales, Smith et al. 2012). It is of note that at least some component of the disparity between sexes is related to polygenic inheritance (Resnick, Pridgen et al. 1968). Stone disease is more common in white, non-Hispanic people than black or Hispanic populations in the U.S. (Scales, Smith et al. 2012).

Rather than being a diagnosis in and of itself, nephrolithiasis is often a manifestation of an underlying cause, and evidence is lacking to show that kidney stones can cause symptoms in the absence of an obstruction (Moe 2006). Thus, the clinical symptoms of kidney stones are related to the disorder causing the stone to form and ureteral obstruction by the stone itself. Obstruction classically causes symptoms of renal colic, a highly characteristic onset of pain as the stone passes from the renal pelvis through the ureter, occasionally accompanied by hematuria and, as the stone enters the lower urinary tract, dysuria (Moe 2006). The underlying cause of stone disease ultimately depends on the type of stones formed. For instance, the major risk factors for uric acid stones are a high concentration of urate and/or low pH of the urine, cystine stones are caused by a hereditary disorder causing the renal leak of basic amino acids, and magnesium ammonium phosphate stones are caused by an infection of the urinary tract by urea-splitting bacteria (Moe 2006). The most common stones are composed of calcium, accounting for over 80% of stones. A host of risk factors are involved in calcium stone pathogenesis (Moe 2006). In 1939, Flocks first described the association between calcium stones and high urinary calcium excretion, or hypercalciuria, which he was able to identify in 23 out of 35 patients with kidney

stones (Flocks 1939). While hypercalciuria may be caused by a monogenic disorder or systemic disease such as hypercalcemia, it is most often discovered in the absence of an identifiable cause and thus termed idiopathic hypercalciuria (Pak 1979). The risk factors for calcium stone formation will be discussed in more detail in the sections below.

1.5.2 Basic Pathogenetic Mechanisms of Hypercalciuria

In order for many vital processes in the body to function appropriately, serum calcium must be kept within a tight range. The body achieves this in large part via the action of the calcium-sensing receptor (CASR) in various tissues along with the calciotropic hormones, parathyroid hormone (PTH) and the active form of vitamin D, 1,25$(OH)_2$-vitamin D_3. These in turn regulate intestinal absorption, bone resorption, and renal reabsorption of calcium (Hoenderop, Nilius et al. 2005). Thus, it should come as no surprise that hypercalciuria can be due to increased intestinal absorption, increased bone resorption, or decreased renal reabsorption of calcium (Figure 1-3). Indeed, patients with idiopathic hypercalciuria are a heterogeneous group with characteristics of one or multiple of these abnormalities underlying the elevation in urine calcium (Pak 1979).

Bone is the major site of calcium storage in the body, and, as such, a central tissue in the regulation of extracellular calcium (Hoenderop, Nilius et al. 2005). When serum calcium is low, reduced activity by CASR in the parathyroid glands leads to secretion of PTH (Hoenderop, Nilius et al. 2005). PTH acts on bone to stimulate bone resorption and thus increase serum calcium and phosphate concentrations (Taal, Brenner et al. 2012). Concurrently, PTH acts on the renal PT to reduce phosphate reabsorption and increase the activity of 25(OH)-vitamin D 1-α-hydroxylase, which converts the hormone vitamin D to its active form (Taal, Brenner et al. 2012). Additionally, PTH acts on the renal TAL and distal tubule to increase calcium reabsorption (Taal, Brenner et al. 2012). Hypercalciuria with bone resorption as a primary cause is termed ”resorptive hypercalciuria” and is usually due to hyperparathyroidism, prolonged immobilization, or osteolytic metastases; unlike idiopathic hypercalciuria, this type of hypercalciuria is typically accompanied by an increase in serum calcium (Pak, Kaplan et al. 1975, Stewart, Adler et al. 1982, Moe 2006).

Abnormally high bone resorption in the absence of hyperparathyroidism would be expected to be accompanied by fasting hypercalciuria and suppression of PTH and 1,25$(OH)_2$-vitamin D_3 (Worcester and Coe 2008).

In the case of increased intestinal calcium absorption, rising serum calcium leads to 1) increased filtered load of calcium in the kidney and 2) the suppression of PTH secretion and consequent reduction in renal calcium reabsorption (Pak 1979). In addition, urinary calcium excretion will decrease during fasting periods, although some patients experience a reduction but remain hypercalciuric (Heller, Zerwekh et al. 2007). Intestinal calcium absorption is mediated by both paracellular and transcellular processes (Bronner 1998). The majority of active calcium transport occurs in the duodenum, where it is regulated in part through the action of 1,25$(OH)_2$-vitamin D_3 (Bronner 1998). Patients with intestinal hyperabsorption may have elevated or reduced 1,25$(OH)_2$-vitamin D_3 levels, depending on whether hyperabsorption is a primary defect in the intestine or secondary (Pak 1979). Active calcium transport in the duodenum is transcellular, mediated by transporters that will be discussed in more detail in Chapter 3. Passive paracellular calcium reabsorption in the intestine is determined by the passive permeability of the tissue to calcium, the degree to which calcium is solubilized, and the transit time of calcium through the alimentary canal (Bronner 1998).

In the kidney, a large number of potential mechanisms exist to affect renal calcium reabsorption, many of which will be discussed below in the context of known genetic factors influencing nephrolithiasis. It is estimated that approximately 70% of calcium is reabsorbed in the PT, 20% in the TAL, and 8% in the distal convoluted tubule (DCT), with the remainder being excreted in the urine (Taal, Brenner et al. 2012). Figures 1-2, 1-5A, and 1-5B depict PT, TAL, and DCT mechanisms of calcium transport, respectively. As mentioned above, renal reabsorption is regulated by PTH and 1,25$(OH)_2$ vitamin D_3. Additionally, CASR is expressed in the TAL where it regulates the reabsorption of calcium and magnesium (Gong, Renigunta et al. 2012, Gong and Hou 2014). Regulation of renal calcium reabsorption will be discussed further in Chapter 3.

It is important to reiterate that bone, the gastrointestinal tract, and the kidney interplay heavily in the context of idiopathic hypercalciuria; for example, intestinal hyperabsorption reduces both renal calcium reabsorption and bone resorption, and vice versa in patients with a renal leak of calcium (Moe 2006). In addition, the existence of absorptive hypercalciuria with fasting hypercalciuria suggests that idiopathic hypercalciuria occurs along a spectrum, and, while the mechanisms are not well known, some patients appear to have defects in both intestinal calcium absorption and renal calcium reabsorption.

1.5.3 Other Risk Factors in Calcium Nephrolithiasis

In addition to hypercalciuria, a high concentration of urinary oxalate is a major risk factor in calcium nephrolithiasis by increasing the supersaturation of calcium oxalate (CaOx), the most common type of calcium stone (Moe 2006). Similarly, urine phosphate levels affect the saturation of calcium phosphate in the urine and contribute to stone risk. Urine pH is a major factor affecting calcium phosphate stone formation, specifically, as these types of calcium salts are much less soluble at a high urinary pH (Moe 2006). Citrate is an inhibitor of calcium phosphate stone formation largely due to its role in allowing excretion of base without raising urine pH, and so low urine citrate can contribute to calcium phosphate nephrolithiasis (Moe 2006). In addition, a high sodium diet increases urine calcium excretion and reduces citrate, thereby posing another risk factor in stone formation (Moe 2006).

The common link between virtually all risk factors for kidney stone formation is the supersaturation of crystallizing solutes (Moe 2006). Given this, decreased urine volume is a risk factor underlying all forms of nephrolithiasis, including calcium nephrolithiasis (Moe 2006). Low urine volume increases the risk of stone due to 1) increased concentration of solutes during urine formation and 2) relative urinary stasis (Moe 2006).

Besides these urinary abnormalities, which by and large affect the supersaturation of calcium crystals, a major factor in the pathogenesis of kidney stones is thought to be the deposition of calcium crystals within the kidney itself, a phenomenon known as nephrocalcinosis.

1.5.4 Stone composition and the role of nephrocalcinosis in stone formation

Several types of nephrocalcinosis have been implicated to have a major role in nephrolithiasis. In 1937, Randall first observed and described hydroxyapatite (a calcium phosphate mineral) plaque formation as the initiating step in the pathogenesis of calcium stones, so called Randall's plaques (Randall 1937). Randall's theory has been validated and extended, including by key work showing that these plaques form on the basement membrane of thin limbs of the loops of Henle and provide the base for concomitant precipitation of calcium crystals (Evan, Lingeman et al. 2003). These plaques are located within the deepest part of the renal medulla, termed the papilla (Figure 1-4A and 1-4B). While humans have multiple papillae within each kidney, mice only have one solitary papilla (Figure 1-4C). Subsequent work by Evan, et al. (2006) revealed that Randall's plaques are relatively specific to CaOx stone formers; plaques that are close to the papillary surface allow growth of CaOx stones on the wall within the renal calyces. Indeed, removal of attached papillary CaOx stones can reveal underlying plaques (Evan, Lingeman et al. 2006). A separate form of nephrocalcinosis is found in patients with stones composed of primarily hydroxyapatite. These patients commonly have large intratubular plugs of calcium phosphate within the terminal portions of the collecting ducts (termed Bellini's ducts) (Evan, Lingeman et al. 2014). In addition to these intratubular plugs, these patients also have calcium phosphate aggregations within the papillary interstitium termed novel interstitial plaque structures (NIPS) (Evan, Lingeman et al. 2014). NIPS may form due to the local interstitial calcium concentrations, as they do not appear to originate from within tubules (Evan, Lingeman et al. 2014). Similarities between NIPS and nephrocalcinosis described in several animal models may suggest a common pathogenetic mechanism (Evan, Lingeman et al. 2014). Figures 1-4C and 1-4D show the expected locations of Randall's plaques and intratubular deposits associated with calcium phosphate stones, respectively, on deep papillary cross-sections of mouse kidney (location denoted by magenta "X").

Several mouse models have been generated that exhibit papillary nephrocalcinosis, although no animal models currently exist which exactly mimic human stone disease (Wu 2015). Chapter 3 will go into more detail regarding the characteristics of these various mouse models of nephrocalcinosis.

1.5.5 Genetics of Hypercalciuria and Calcium Nephrolithiasis

The significant contribution of genetics to nephrolithiasis is well established. In a large study comparing the families of kidney stone formers with relatives of unaffected spouses, it was found that polygenic inheritance is a major factor in risk for kidney stones (Resnick, Pridgen et al. 1968). Likewise, a male-male twin study showed a stronger concordance rate among monozygotic twins (Goldfarb, Fischer et al. 2005). While polygenic inheritance is a major factor, almost one sixth of patients with kidney stone disease may have an underlying monogenic cause (Halbritter, Baum et al. 2015). A number of common variants and rare genetic mutations contribute to stone risk without causing hypercalciuria. For instance, causes of renal tubular acidosis can lead to failure to acidify urine and thereby increase the risk of stone formation. In addition, genetic causes of hyperoxaluria or hyperphosphaturia will increase the risk for calcium stone formation (Sayer 2017). Finally, several kidney-stone associated SNPs have been identified in the genes for calcium stone inhibitors *OPN* (coding for osteopontin) (Gao, Yasui et al. 2007) and *UMOD* (coding for uromodulin or Tamm-Horsfall protein) (Gudbjartsson, Holm et al. 2010).

Regarding intestinal absorption, one study found that nearly half of the patients with absorptive hypercalciuria have a family history of kidney stones (Pak 1979). Despite this, relatively few genetic factors have been identified as direct causes of intestinal calcium hyperabsorption. One such putative absorptive hypercalciuria gene is *ADCY10*, which codes for the soluble adenylate cyclase 10; *ADCY10* is thought to be mutated in autosomal dominant forms of nephrolithiasis (Reed, Heller et al. 1999, Halbritter, Baum et al. 2015). In addition, gain-of-function mutations in the intestinal calcium transporter, transient receptor potential vanilloid type 6 channel (TRPV6), have been identified in absorptive hypercalciuric kidney stone formers (Suzuki, Pasch

et al. 2008). SNPs in *VDR*, the gene for the vitamin D receptor, are also associated with kidney stone disease, and VDR is expressed in both intestine and kidney (Zhang, Nie et al. 2013). Hypercalciuria and nephrocalcinosis also occur in Mendelian intestinal diseases such as congenital sucrose/isomaltase deficiency (Belmont, Reid et al. 2002) and glucose/galactose malabsorption (Pahari, Milla et al. 2003), but these disorders occur in infancy and include hypercalcemia.

Considerably more is known about the contribution of genetics to renal calcium reabsorption and nephrolithiasis. In the PT, a number of genetic factors have been identified. However, none of these seem to directly involve PT calcium transport mechanisms. For instance, a risk variant in close proximity to *AQP1*, the gene for aquaporin-1, implicates PT water transport in the development of nephrolithiasis (Urabe, Tanikawa et al. 2012). *AQP1* knockout mice exhibit severe dehydration upon water restriction (Ma, Yang et al. 1998), and dehydration is a major risk factor in kidney stone disease. It is unknown if *AQP1* variants in humans are associated with increased urine calcium excretion. Dent disease types I (*CLCN5* gene) and II (*OCRL* gene) both involve the PT and include hypercalciuria, nephrocalcinosis, and nephrolithiasis in addition to a number of defects in PT reabsorption (low molecular weight proteinuria, aminoaciduria, glucosuria, and phosphaturia) (Hoopes, Shrimpton et al. 2005). Figure 1-2 depicts transport mechanisms believed to be involved in the passive transport of calcium in the PT.

In the TAL, many defects are known to lead to nephrocalcinosis and nephrolithiasis. Bartter syndrome is a grouping of rare disorders of TAL sodium transport resulting in hypercalciuria and increased risk of kidney stones, as well as hypotension, hypokalemia, and metabolic alkalosis (Hebert 2003). Causative mutations in Bartter syndrome have so far been identified in five genes: loss-of-function mutations in *SLC12A1* (coding for the Na^+-K^+-$2Cl^-$ cotransporter 2, or NKCC2), *KCNJ1* (coding for the renal outer medullary potassium channel also known as ROMK or Kir1.1), *CLCNKB* (coding for the chloride channel Kb, or CLC-Kb), and *BSND* (coding for Barttin, a β-subunit of ClC-K channels required for correct trafficking of chloride

channels to the basolateral plasma membrane), as well as gain-of-function mutations in the *CASR* gene (Hebert 2003). In addition, patients with FHHNC have an increased risk of kidney stones in addition to hypercalciuria and nephrocalcinosis (Sayer 2017). Figure 1-5A depicts calcium transport mechanisms in the TAL.

Finally, in the DCT calcium transport occurs across the apical membrane via the transient receptor potential cation channel V5 (TRPV5), and a rare coding variant has been identified in the *TRPV5* gene that greatly increases kidney stone risk (Oddsson, Sulem et al. 2015). In addition to TRPV5, DCT calcium transport is believed to be facilitated by the cytoplasmic shuttle protein calbindin-D28k and transported out of the cell by several potential basolateral transport proteins (Hoenderop, Nilius et al. 2005). Figure 1-5B depicts the purported mechanisms of calcium transport in the DCT, which will be discussed in more detail in chapter 3.

1.6 Overall Hypothesis of Dissertation: Claudin-2 mediates PT calcium transport

My overall hypothesis is that claudin-2 mediates calcium reabsorption in the PT, and loss or reduction of claudin-2 increases nephrolithiasis risk. There is abundant evidence that PT reabsorption plays a major role in the pathogenesis of idiopathic hypercalciuria and calcium stone formation. Calcium stone formers respond abnormally to diuretic administration in a pattern suggestive of defective PT sodium reabsorption (Sutton and Walker 1980). This is particularly true for patients with fasting hypercalciuria (Sutton and Walker 1980, Sakhaee, Nicar et al. 1985). More recently, larger studies of idiopathic hypercalciuric stone formers have measured lithium clearance, a well-established surrogate of PT sodium reabsorption, and confirmed that decreased PT reabsorption is common among these patients (Worcester, Coe et al. 2008, Ko, Bergsland et al. 2015). Despite defective PT sodium reabsorption, these patients have normal fractional sodium excretion due to compensatory transport mechanisms in the downstream nephron (Worcester, Coe et al. 2008). Our lab and others have found similar defective PT sodium reabsorption in mice with deletion of claudin-2 (Muto, Hata et al. 2010, Pei, Solis et al. 2016).

Given that PT calcium transport is inextricably linked to PT sodium reabsorption (Alexander, Rievaj et al. 2014), the above findings suggest that defective PT calcium reabsorption is a common intrarenal cause of idiopathic hypercalciuria and thus calcium stone formation. Current evidence suggests that PT calcium reabsorption is primarily passive and likely to be paracellular (Figure 1-2B). Of the claudin isoforms highly expressed in the PT, only claudin-2 is cation-permeable. In addition, claudin-2 knockout mice have increased urine calcium excretion (Muto, Hata et al. 2010). In chapter 2, I explore my hypothesis by testing the electrophysiological and calcium permeability properties of PT claudin isoforms in combination, *in vitro*. In chapter 3, I use an *in vivo* mouse model with deletion of claudin-2 to test the hypothesis that 1) these animals are defective in PT calcium reabsorption and 2) they develop characteristics common to human kidney stone disease. Finally, I will consider the potential limitations, as well as future directions, of this work.

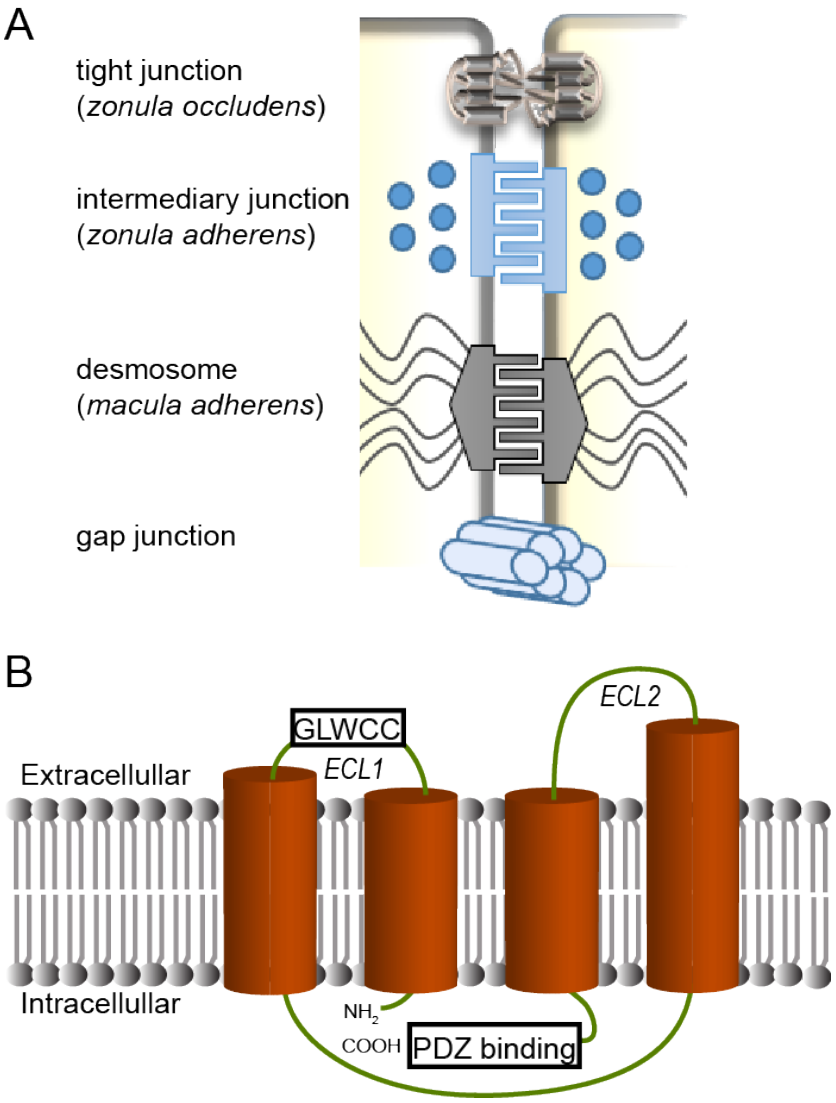

Figure 1-1. The junctional complex and claudin family of proteins

(A) The junctional complex helps to maintain the integrity of an epithelial cell barrier. *Zonula occludens* is the most apical component of the junctional complex and is composed in part by claudin proteins, followed by the *zonula adherens* and *macula adherens*. Gap junctions are also components of the junctional complex and allow direct communication between adjacent cells. (B) All members of the claudin family have 4 transmembrane domains, 2 extracellular loops (ECL1 and ECL2), and cytoplasmic N- and C-termini. The first extracellular loop, ECL1, contains the residues that confer charge selectivity to pore-forming claudins. All claudins have a characteristic GLWCC motif on ECL1, as well. In addition, a PDZ binding domain is located in the C-terminal domain of claudin family members.

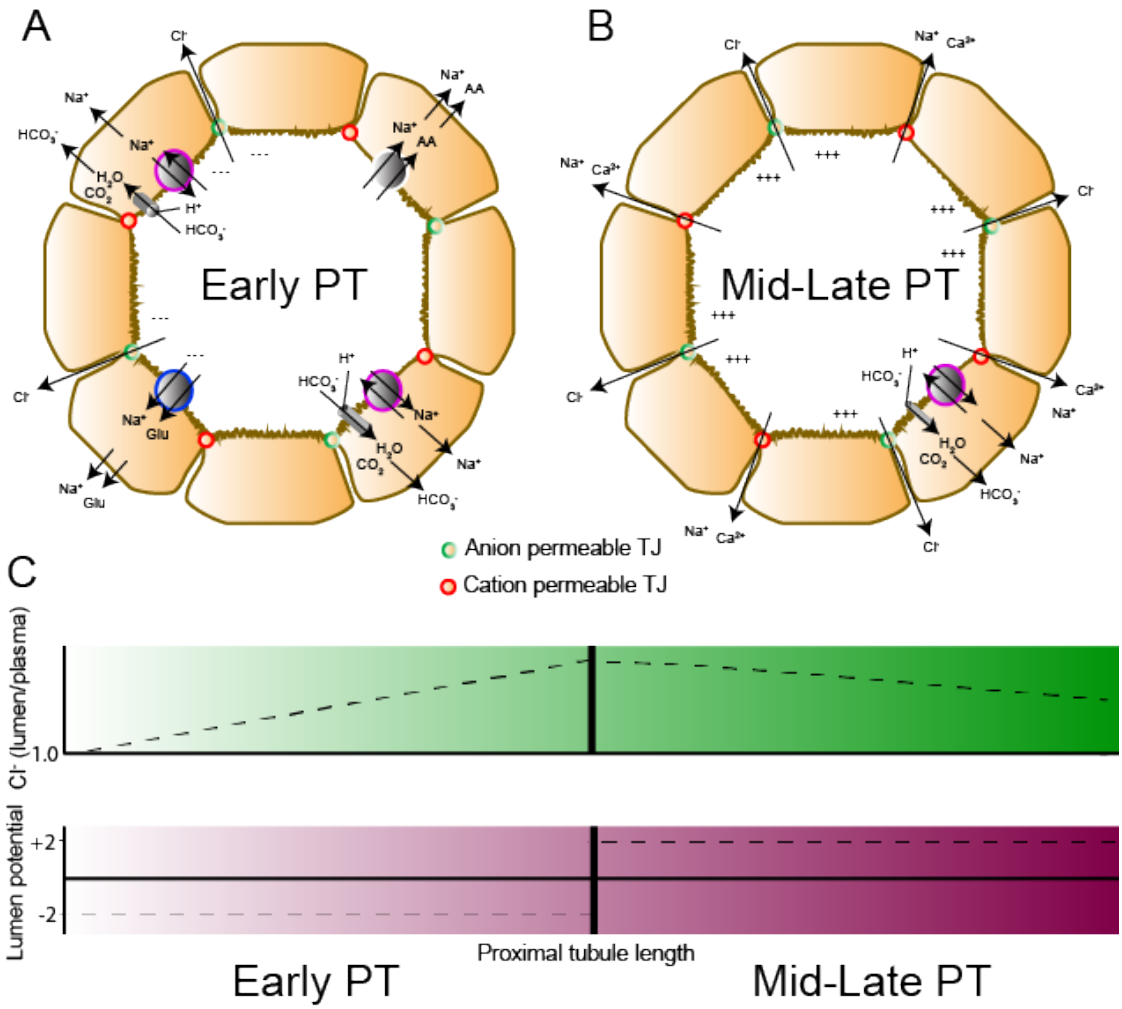

Figure 1-2. Proximal tubule paracellular transport

(A) The early portion of the proximal tubule (PT) is the major site of sodium-coupled cotransport of solutes such as amino acids and glucose. This transport drives the paracellular transport of chloride. (B) In the mid-late PT, paracellular calcium transport is driven by small electrochemical gradients. (C) Transport of sodium is electrogenic in the early PT, thus generating a slightly negative lumen potential (~ -2mV). In addition, bicarbonate and water are reabsorbed secondary to the action of the sodium-hydrogen exchanger, increasing the intraluminal chloride concentration slightly above that of plasma. The chloride concentration gradient leads to paracellular chloride reabsorption, which generates a slightly positive lumen potential in the mid-late PT (~ +2mV). This lumen potential then is believed to drive passive paracellular transport of sodium and calcium (Rector 1983, Taal, Brenner et al. 2012).

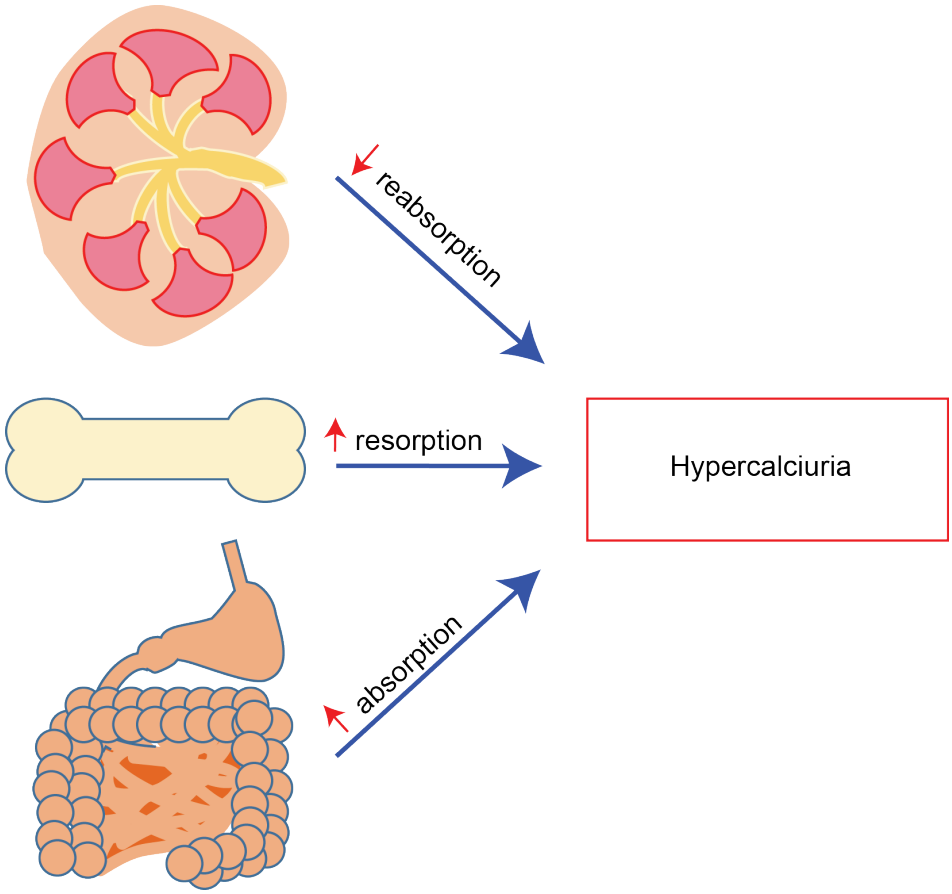

Figure 1-3. General mechanisms of hypercalciuria

Hypercalciuria may be caused by reduced renal reabsorption of calcium, increased bone resorption of calcium, or increased absorption of calcium in the gastrointestinal tract.

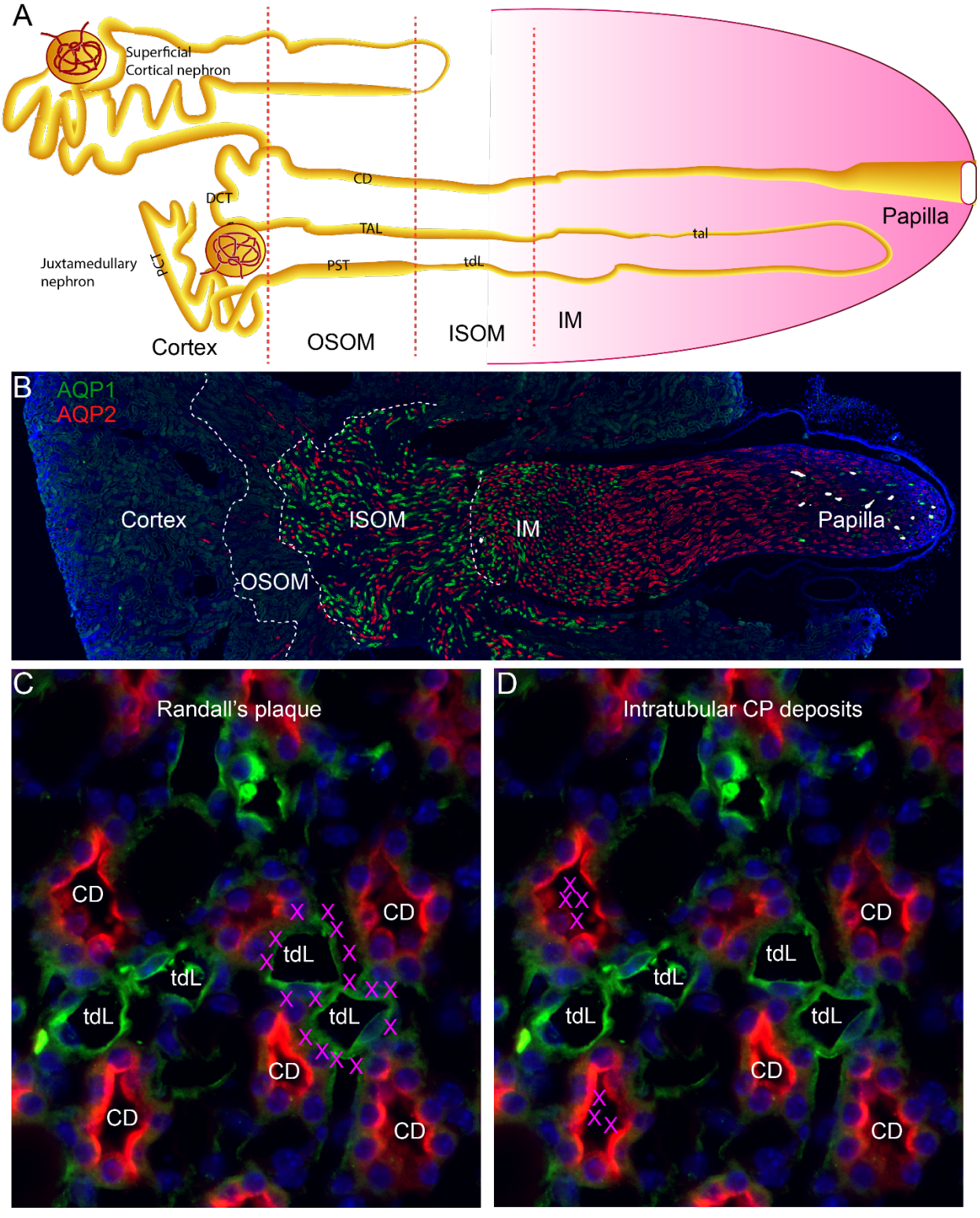
A
Superficial
Cortical nephron
CD
DCT
TAL
Papilla
tal
Juxtamedullary
nephron
PCT
PST
tdL
Cortex
OSOM
ISOM
IM
B
AQP1
AQP2
Cortex
ISOM
IM
Papilla
OSOM
C
Randall's plaque
CD
tdL
D
Intratubular CP deposits

Figure 1-4. Renal architecture and anatomical location of stone-associated nephrocalcinosis

(A) Illustration of the structure of superficial and juxtamedullary nephrons in association with overall renal architecture. Superficial nephrons have relatively short loops of Henle, whereas juxtamedullary nephrons have loops of Henle which descend into the inner medulla and papillary regions of the kidney. (B) Section from a *Cldn2*$^{-/y}$ mouse stained for markers of PT and thin descending limb (tdL) of the loops of Henle (AQP1, green) and collecting duct (CD) principal cells (AQP2, red). Von Kossa calcium staining is pseudocolored white. Mouse kidneys contain a single papilla. (C) Calcium deposition is expected to occur at the basement membranes of the thin descending limbs if nephrocalcinosis resembles Randall's plaques (magenta Xs). (D) Calcium deposition is expected to occur within the inner medullary collecting ducts if nephrocalcinosis resembles calcium phosphate stone formers (magenta Xs). PCT= proximal convoluted tubule; PST= proximal straight tubule; taL= thin ascending limb; TAL= thick ascending limb; DCT= distal convoluted tubule; CD= collecting duct; OSOM= outer stripe of the outer medulla; ISOM= inner stripe of the outer medulla; IM= inner medulla.

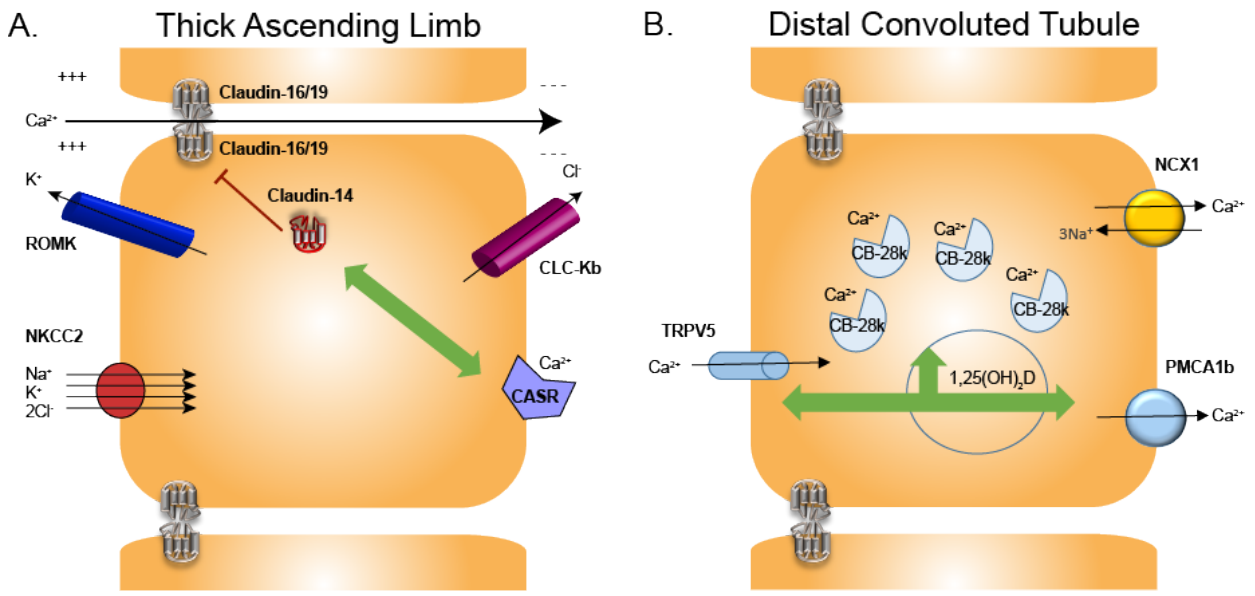

Figure 1-5. Calcium transport in the thick ascending limb and distal convoluted tubule

(A) In the thick ascending limb, a large lumen positive potential drives paracellular calcium transport. This potential is generated by the activity of the Na^+-K^+-$2Cl^-$ cotransporter (NKCC2), and subsequent efflux of apical K^+ through the renal outer medullary potassium channel (ROMK) and basolateral Cl^- through the chloride channel Kb (CLC-Kb). Paracellular mediators of calcium transport are claudins-16 and -19. Activation of the calcium-sensing receptor (CASR) leads to upregulation of claudin-14, which is a barrier claudin, thereby reducing paracellular calcium transport. (B) In the distal convoluted tubule, apical calcium is transported via the transient receptor potential cation channel subfamily V member 5 (TRPV5). Cytoplasmic calcium shuttle protein calbindinD-28k (CB-28k) is believed to facilitate intracellular calcium movement to the basolateral membrane, where it is extruded by plasma membrane calcium ATPase (PMCA1b) and the Na^+-Ca^{2+} exchanger (NCX1). TRPV5, CB28k, and PMCA1b expression are regulated by $1,25(OH)_2$-vitamin D_3. Transport in both segments is regulated in part by parathyroid hormone (not shown) (Taal, Brenner et al. 2012).

Chapter 2: Co-expression of PT claudins leads to distinctive permeability properties

2.1 Abstract

The permeability of the paracellular pathway is determined by the apical TJ, which forms a seal between epithelial cells and can either form a tight barrier or pores that allow permeation of small ions across the intercellular space. Claudins are TJ proteins that in part determine the paracellular permeability of epithelia. The PT is characterized by a highly conductive paracellular pathway, which is believed to contribute to a significant amount of solute and water reabsorption by the kidney. I sought to identify the expression pattern of the major claudins expressed in the PT and found that claudin-2 and claudin-10 are expressed throughout the PT, whereas claudin-3 is strongly expressed within the late PST. Additionally, claudin-2 and claudin-3 are expressed exclusively within the descending thin limbs of long loop and short loop nephrons, respectively. I next developed a novel dual-claudin induction cell model with which to characterize the net effect of PT claudin expression, *in vitro*. In keeping with previous studies, I found that claudin-2 increases cation permeability in MDCK I cells while claudin-10a increases anion selectivity. However, claudin-3 expression had a negligible effect on all measures of our electrophysiological characterization, with or without claudin-2 expression. Co-expression of claudins-2 and -10a led to a high conductance monolayer with essentially unbiased ion selectivity. Utilizing the titrability of this cell system and a claudin-2 mutant in which the pore can be blocked with thiol-reactive reagents, I explored this reduction in permselectivity further and determined that claudins-2 and -10a form paracellular channels in parallel, rather than participating in heteromeric hybrid channel formation.

2.2 Introduction

The PT is a ‘leaky’ epithelium with low TER and high conductance of both sodium and chloride through the paracellular shunt pathway (Rector 1983). This segment is responsible for the reabsorption of approximately 60% of sodium and chloride filtered by the glomerulus (Suki

1979, Berry and Rector 1991). Small electrochemical gradients are established early in the PT, largely via energy-consuming sodium-coupled cotransport of nutrient osmolytes such as glucose and amino acids and the selective transcellular reabsorption of sodium and bicarbonate (Rector 1983). The paracellular shunt pathway is more permeable to chloride than bicarbonate, facilitating paracellular chloride reabsorption as the luminal chloride concentration increases relative to plasma (Rector 1983, Berry and Rector 1991). Passive chloride reabsorption in turn generates a small lumen positive potential that drives passive reabsorption of cations (Berry and Rector 1991). Additionally, convective forces could potentially contribute to sodium, chloride, and calcium reabsorption due to the relatively low reflection coefficient for these ions compared with that of reabsorbed bicarbonate, sugars, and amino acids (Berry and Rector 1991).

Claudins were first discovered in 1998 by Furuse et al. as four-pass transmembrane proteins within TJ subcellular fractions (Furuse, Fujita et al. 1998). There are ≥ 24 different isoforms of claudins, some of which reduce the conductance of an epithelial layer, while other isoforms increase transepithelial conductance with charge specificity, acting as paracellular pores (Hou, Rajagopal et al. 2013). Most tissues express multiple claudin isoforms in a cell-type specific pattern, including the kidney (Kiuchi-Saishin, Gotoh et al. 2002). Claudin proteins have been demonstrated to interact within the same cell (*cis*) and across adjacent cells (*trans*) (Furuse, Sasaki et al. 1999). The importance of claudin interactions are underlined by the inability of claudin-16 to traffic to the TJ in the absence of claudin-19, *in vivo, (Hou, Renigunta et al. 2009)* and of claudin-4 to traffic to the TJ of renal epithelial cells following knockdown of claudin-8 (Hou, Renigunta et al. 2010). The most consistent data across species indicate that the major claudins expressed in the PT are claudin-2, claudin-3, and claudin-10 (Gunzel, Stuiver et al. 2009, Kirk, Campbell et al. 2010, Lee, Chou et al. 2015).

Claudin-2 has been shown to be expressed in the PT and thin descending limb of the kidney (Enck, Berger et al. 2001, Kiuchi-Saishin, Gotoh et al. 2002). *In vitro* claudin-2 overexpression MDCK I with high TER decreases the TER primarily by increasing paracellular

cation permeability (Furuse, Furuse et al. 2001, Amasheh, Meiri et al. 2002, Yu, Cheng et al. 2009). Interestingly, the related cell line, MDCK II, has high endogenous claudin-2 expression and low TER; genetic deletion of claudin-2 in MDCK II results in a striking increase in TER and decrease in cation permeability (Tokuda and Furuse 2015). *In vivo*, knockout of claudin-2 results in a reduction in the P_{Na} of isolated PTs (Muto, Hata et al. 2010). In addition to increasing cation permeability, claudin-2 also functions as a paracellular water channel, facilitated through the same extracellular pore residues that confer cation selectivity (Rosenthal, Milatz et al. 2010, Rosenthal, Gunzel et al. 2017).

In the mouse kidney, claudin-3 was first described in the thin ascending limb and TAL of the loops of Henle and more distal segments of the nephron (Kiuchi-Saishin, Gotoh et al. 2002). More recently, deep sequencing of microdissected rat kidney tubule segments suggests that claudin-3 is also highly expressed within the final segment of the PT (S3) and the short descending thin limbs (Lee, Chou et al. 2015). Immunohistochemical analyses of human cortical kidney sections has confirmed the expression of claudin-3 within the distal tubules, as well as weak basolateral staining within PTs; this study did not analyze claudin expression within the medullary regions of human kidney (Kirk, Campbell et al. 2010). Overexpression of claudin-3 in MDCK II cells was previously shown to lead to increased TER and a reduction in cation permeability, suggesting that it functions as a barrier claudin at the TJ (Milatz, Krug et al. 2010).

In the kidney, claudin-10 is expressed as multiple transcripts via alternative splicing (Van Itallie, Rogan et al. 2006, Gunzel, Stuiver et al. 2009). These alternative splicing events result in two major isoforms of claudin-10, claudins-10a and -10b, which differ in the amino acid sequence of the N-terminal cytoplasmic tail, first transmembrane domain, and most of ECL1 (Van Itallie, Rogan et al. 2006). As ECL1 contains the amino acid determinants for charge selectivity in pore-forming claudins (Colegio, Van Itallie et al. 2002), the functional difference between these spliceoforms was further explored. *In vitro* overexpression studies in MDCK II cells and LLC-PK1 porcine kidney cells showed that claudin-10a increases anion selectivity, whereas claudin-10b

increases cation selectivity (Van Itallie, Rogan et al. 2006). *In situ* hybridization found that claudin-10a is expressed primarily in the kidney cortex (Van Itallie, Rogan et al. 2006), and subsequent RT-PCR of microdissected tubule segments showed that this isoform is expressed more specifically in proximal convoluted tubule (PCT) and cortical collecting duct (CCD) (Gunzel, Stuiver et al. 2009). Claudin-10a mRNA expression was also detected in the medullary TAL, accompanied by claudin-10b expression (Gunzel, Stuiver et al. 2009).

To date, there has not been detailed analysis of the physiological effects of co-expression of the major claudins in the PT. Thus, I aimed to determine the expression pattern of these three claudins in mouse tissue and analyze the effect of co-expression of these claudins, *in vitro*, using a novel dual induction overexpression model in high resistance MDCK I cells.

2.3 Methods

2.3.1 Tissue immunohistochemistry

Animal experiments were carried out in accordance with NIH guidelines on the use of laboratory animals and were approved by the IACUC of the University of Kansas Medical Center. Animal tissues were fixed by intracardiac perfusion of 4% paraformaldehyde (PFA) and kidneys were either (A) cryoprotected overnight with 30% sucrose in PBS, embedded in Tissue-Tek OCT, and frozen or (B) fixed in 4% PFA overnight at 4ºC and embedded in paraffin. In either case, 5µm sections were prepared. Sections were blocked in 1% bovine serum albumin and 5% normal goat serum in PBS prior to incubation with primary antibodies. Antibodies and dilutions were as follows: mouse anti-claudin-2 (Invitrogen, 1:500), rabbit anti-claudin-3 (Spring Biosciences, 1:500), rabbit claudin-10 (Invitrogen, 1:500), rabbit anti-UT-A2 (a generous gift from Dr. Jeff Sands, 1:500), and mouse anti-AQP1 (Abcam, 1:500). Slides were coverslipped with ProLong Gold Antifade Mountant with DAPI (ThermoFisher Sci.) and images captured with a Nikon80i upright microscope. Confocal images were captured with a Leica TCS SPE Confocal Microscope.

2.3.2 Co-immunoprecipitation experiments

Sub-confluent HEK293 cells were transiently transfected (Lipofectamine 2000, ThermoFisher Sci.) with pcDNA3.1 claudin expression vectors and lysed in immunoprecipitation (i.p.) lysis buffer (50mM Tris-HCl, 150mM NaCl, 1% Triton-X100). Cells were mechanically homogenized with a syringe and 23G needle 7-10 times and centrifuged to sediment insoluble material (16,000G x 15min.). Cell lysates, pre-cleared with Protein G-Sepharose, were incubated with primary antibody overnight at 4ºC followed by Protein G-Sepharose beads. Immunoprecipitated beads were washed (50mM Tris-HCl, 150mM NaCl) and denatured by heating at 95ºC for 10 min prior to SDS-PAGE. Antibodies used were as follows: mouse anti-claudin-2 (Invitrogen, 1:500), rabbit anti-claudin-3 (Invitrogen, 1:500), and rabbit anti-claudin-10 (Invitrogen, 1:250).

2.3.3 Generation of double-claudin inducible cell lines

Basal medium for culture of MDCK I cells was DMEM with 5% fetal bovine serum. Retrovirus containing Tet-responsive human claudin-2 or mouse claudin-2 S68C was produced in the viral packaging line, PT67, and transduced into the MDCK I TetOff cell line, as described previously (Angelow and Yu 2009). Stable clones were selected in hygromycin using cloning cylinders, and subsequently transfected (Lipofectamine 2000, ThermoFisher Sci.) with PiggyBac transposase and PiggyBac cumate switch-inducible vectors (System Biosciences) containing either human claudin-3 or human claudin-10a. Stable double-inducible clones were selected in puromycin using cloning cylinders. Doxycycline (20ng/ml) was omitted from the medium in order to induce claudin-2 expression. Unless otherwise specified, cumate was used at 3x concentration (90µg/ml) for induction of claudin expression. Expression and localization of selected clones was tested by immunoblotting and immunofluorescence, as described below. Human claudin-10a was amplified from human kidney cDNA, and the sequence was confirmed with 100% identity to the NCBI reference sequence (NM_182848.3).

2.3.4 Immunoblotting

Cells were grown to confluence on tissue culture plates. Cells were washed and scraped into a lysis buffer containing 0.25M sucrose, 30mM histidine, and 1mM EDTA at pH 7 with protease inhibitors (cOmplete Mini, Roche Diagnostics). Mechanical lysis of confluent cells was achieved using a 25G needle, and lysates were centrifuged at 16,000G for 10min. at 4ºC. Lysates were heated at 95°C for 10min. in reducing SDS-PAGE buffer and loaded into a polyacrylamide gel. Protein was then transferred to a polyvinylidene difluoride (PVDF) membrane and blocked using 5% nonfat-dry milk. Primary antibody incubation was performed overnight at 4ºC using the following antibodies: mouse anti-claudin-2 (Invitrogen, 1:500), rabbit anti-claudin-3 (Invitrogen, 1:500), rabbit anti-claudin-10 (Invitrogen, 1:500), and rabbit anti-claudin-10 (Abcam, 1:500). Horseradish peroxidase conjugated secondary antibodies were incubated at a concentration of 1:5000 (GE Healthcare Bio-Sciences) and bands detected using chemiluminesence (Pierce).

2.3.5 Immunofluorescence

Cells were grown to confluence on permeable polycarbonate membrane filters (Corning) under conditions described above for induction of claudin expression. Cells were fixed in methanol at -20ºC for 20 min. Membranes were blocked in 1% bovine serum albumin and 5% normal goat serum in PBS with 0.05% Triton-X100 prior to incubation with primary antibodies. Antibodies and dilutions were as follows: mouse anti-claudin-2 (Invitrogen, 1:500), rabbit anti-claudin-3 (Invitrogen, 1:500), rabbit anti-claudin-10 (Invitrogen, 1:250), and rabbit anti-claudin-10 (Abcam, 1:500). Fluorophore conjugated secondary antibodies from goat were added at a concentration of 1:1000 (Life Technologies). Slides were cover-slipped with ProLong Gold Antfade Mountant with DAPI (ThermoFisher Sci.) and images captured with a Nikon80i upright microscope.

2.3.6 Electrophysiological characterization

For initial characterization of clones, cells were plated at a confluent density (0.8×10^5 cells/well) onto Snapwell filters (Corning). Initial experiments using claudin-2/10a inducible cell clones more monitored in a CellZScope (nanoAnalytics). On day 5, doxycyline and cumate were

added to designated wells. On Day 8-9, TER was stable in all induction conditions and cells were loaded into Ussing chambers for electrophysiological studies. Current-passing electrodes of Ag wire and voltage-sensing electrodes made of Ag/AgCl pellets were introduced to Ussing chambers via agar bridges prepared with 3M KCl and 3% agar. Ussing chambers were bubbled continuously with gas lifts and maintained at 37ºC throughout experiments. Electrodes were connected through single channel input modules (DM-MC6) to a multichannel voltage/current clamp (VCC-MC6) controlled by a computer, with data acquired at 1s intervals using Acquire and Analyze software (Physiologic Instruments, San Diego, CA). Baseline TER for each condition is from averages of 24 data points, whereas the remainder of data is the average of 3 data points immediately before and after medium exchange.

Standard Ringer's solution contained 150mM NaCl, 10mM glucose, 2mM $CaCl_2$, 1mM $MgCl_2$, and 10mM Tris-HEPES at pH 7.4. For NaCl dilution potential measurements, medium in the basolateral compartment was replaced by isosmotic Ringer's solution with 75mM NaCl and 150mM mannitol. For alkali metal bi-ionic potentials and organic cation diffusion potentials, the basolateral medium was switched to a Ringer's solution with 150mM or 75mM, respectively, of the cation-chloride salt replacing NaCl. Liquid junction potentials were estimated with blank filters as described previously (Yu, Cheng et al. 2009). The Goldman-Hodgkin-Katz constant field voltage equation was used to calculate ion permeabilities, as described in detail by Yu (Yu 2011). This equation can be simplified to the following:

$$\beta = \frac{\alpha - x}{\alpha x - 1},$$

where $x = e^{-(\frac{VF}{RT})}$

V is the diffusion potential corrected for liquid junction potentials as described by Yu et al. (Yu, Cheng et al. 2009). β is the ratio of permeabilities to sodium and chloride, P_{Cl}/P_{Na}. At 37ºC, RT/F is 26.71mV. The ratio of activity, α, is 1.89 because the activity coefficients for NaCl at 150mM and 75mM are 0.752 and 0.797, respectively.

P_{Na} and P_{Cl} were calculated and derived using the method of Kimizuka and Koketsu (Kimizuka and Koketsu 1964). The equation for calculation is as follows:

$$P_{Na} = \frac{RT}{F^2} \times \frac{G_M}{\alpha(1+\beta)}$$

$$P_{Cl} = \beta \times P_{Na}$$

The permeability ratio of a given cation, X^+, relative to P_{Na} (γ) was also calculated using the Goldman-Hodgkin-Katz equation and it was assumed that the activity coefficients of NaCl and XCl were identical, as described previously (Yu 2011). The equation for γ for exchange with 150mM XCl was:

$$\gamma = (1+\beta) \times e^{V/26.71} - \beta$$

The equation for γ for exchange with 75mM XCl (α again is equal to 1.89) was:

$$\gamma = 1.89(1+\beta) \times e^{V/26.71} - 1.89\beta - 1$$

For experiments with the claudin-2 S68C mutant cell lines, 2-aminoethyl methanethiosulfonate (MTSEA) was prepared as a 100x stock solution (250mM) immediately prior to beginning each set of cells due to its extremely short half-life in aqueous solution. MTSEA was added to both apical and basolateral compartments of Ussing chambers and several minutes were allowed for blocking of the claudin-2 pore prior to NaCl dilution potential measurements.

2.3.7 Calcium flux experiments

Unidirectional calcium flux was measured in cells grown on Transwells (Corning) under conditions identical to those described for Ussing chamber experiments. Basal medium contained 1.8mM $CaCl_2$, and radiotracer (hot) medium was prepared by the addition of $^{45}CaCl_2$ to obtain a specific activity of 2Ci/mol. Hot medium was added to the apical compartment of cells, and "cold" basal medium was added to the basolateral compartment. Samples of basolateral medium was taken at multiple time points. Background was subtracted from all CPM counts, and the counting efficiency of the liquid scintillation counter was determined by the calculated/expected counts in

a sample of 2Ci/mol hot medium. The amount of calcium transported per well was calculated as follows:

$$Ca^{2+}\,(mol) = CPM \div Counting\ efficiency\ \times \left(\frac{total\ basal\ volume}{sample\ volume}\right) \div 2.22\ \times 10^{12}\,\frac{dpm}{Ci} \div \frac{2Ci}{mol}$$

Calcium flux is expected to be linear, and thus flux was calculated as the slope of the best fit line of calcium transported at all time points, divided by the surface area. Calcium permeability can be calculated from this as the calcium flux divided by the calcium concentration, and expressed in units of 10^{-6} cm/s.

2.4 Results

2.4.1 Claudin-2 and claudin-10 are both expressed along the PT

I analyzed kidney sections of adult mice by confocal microscopy and found that claudin-2 and claudin-10 are co-expressed in PT segments (Figure 2-1A). The intensity of claudin-10 staining appeared consistent throughout both PCTs and PSTs (not shown). In addition, intense basolateral staining of claudin-10 was found in nearby TAL segments (Figure 2-1A). All claudin antibodies used in these studies were generated against the C-terminal portion of the proteins, making it impossible to differentiate between claudin-10a and claudin-10b spliceoforms in the present study.

2.4.2 Claudin-3 is expressed in the PST and short loop populations of thin descending limbs

In mouse cortex, faint claudin-3 staining was occasionally detected within claudin-2-positive PCTs (Figure 2-1B). In addition, strong claudin-3 expression was observed in the CCD (Figure 2-1B). At the corticomedullary boundary, where PCTs transition into PSTs, I observed strong claudin-3 expression that was continuous throughout the outer medulla (Figure 2-1C-D). The depth of claudin-2 positive basolateral invaginations is less within PSTs than the PCTs (Figure 2-1C), in keeping with morphologic analyses comparing the basolateral membranes of the differing segments of PT epithelia (Faarup, Holstein-Rathlou et al. 2011).

Interestingly, at the boundary of the outer and inner stripes of the outer medulla, where PSTs transition into thin descending limbs, I observed populations of thin limbs which exclusively expressed either claudin-2 or claudin-3 (Figure 2-1D). In order to determine whether these populations were specific to short or long loop segments, I immunostained kidney sections with aquaporin-1 (AQP1), a marker of thin descending limbs of long loop nephrons (Zhai, Fenton et al. 2007). Like claudin-2, I found that AQP1 stained a distinct population of thin limbs from claudin-3 (Figure 2-2), suggesting that the claudin-3 positive tubules are not long loop descending thin limbs but rather short and/or intermediate descending thin limb segments (Kim, Lee et al. 2016). These thin limbs were dispersed throughout the inner stripe of the outer medulla.

2.4.3 Claudin-3 overexpression does not alter the electrophysiological properties of MDCK I cells

Co-immunoprecipitation experiments show that claudin-2 and claudin-3 interact, *in vitro* (Figure 2-3). I therefore generated a double-inducible cell line in which claudin-2 expression is repressed in the presence of doxycycline (Tet-Off) and claudin-3 expression is induced in the presence of cumate. While endogenous claudin-3 is generally high in MDCK I cells, I identified a stable clone with particularly low endogenous expression by Western blotting and confirmed TJ localization by immunofluorescence (Figure 2-4A-B). My results show no difference in TER upon overexpression of claudin-3 (Figure 2-4C). Similarly, I detected no change in the P_{Na}, P_{Na}/P_{Cl}, or unidirectional calcium flux upon overexpression of claudin-3 in MDCK I cells (Figure 2-4D-F). Moreover, induction of claudin-3 overexpression did not alter the permeability properties of claudin-2.

2.4.4 Co-expression of claudins-2 and -10a reduces the permselectivity of MDCK I cells

In an analogous set of experiments to those above, I generated claudin-2 Tet-Off cells with cumate-inducible claudin-10a expression and confirmed localization of claudin isoforms at the TJ (Figure 2-5A-B). Claudin-10a reduced TER to the same degree as claudin-2 (Figure 2-5C). Similar to findings from previous studies, claudin-10a increased P_{Cl} ($p<0.0001$) without affecting

P_{Na} (Figure 2-5D), whereas claudin-2 increased P_{Na} ($p<0.0001$, Figure 2-5D) without affecting P_{Cl}. However, I found a significant reduction in both the P_{Na} and P_{Cl} in cells expressing both claudins compared with expression of claudin-2 or claudin-10a alone, respectively (Figure 2-5D-E). Interesting, the P_{Na}/P_{Cl} of claudin-2/10a dual-expressing cells was not different compared with MDCK I cells without induction of claudin expression, indicating that the net effect of the combination of the two claudins was a lack of charge selectivity (Figure 2-5E).

Upon measuring unidirectional calcium flux of this cell model, I found that claudin-10a reduced the permeability to calcium to a similar degree as sodium (Figure 2-5F). My major findings were confirmed in another clone (Figure 2-6). However, calcium flux did not differ between cells expressing claudin-2 and both claudins in this clone (Figure 2-6F). In a PT epithelial cell line, it has been shown that an osmotic gradient can increase unidirectional calcium flux (Pan, Borovac et al. 2012). Additionally, it has been demonstrated that claudin-2 permeates water as well as cations (Rosenthal, Milatz et al. 2010, Rosenthal, Gunzel et al. 2017), and osmotic water flux increases ^{22}Na flux in high resistance MDCK cells (Rosenthal, Milatz et al. 2010). I hypothesized that conditions inducing water transport across the claudin-2 pore would also increase calcium flux via convective forces, or “solvent drag”. Thus, I induced water flux using a basolateral mannitol gradient, with and without osmotic compensation, and reduced water flux with an apical sodium gradient (Figure 2-7B). However, no effect of claudin-2 or claudin-10a was observed on the osmotic unidirectional flux of calcium (Figure 2-7A).

2.4.5 Titratable expression of claudins in the dual induction system

Co-expression of claudin-2 and claudin-10a led to reduced P_{Na} and P_{Cl} compared with the permeability of the isoforms alone, respectively. I hypothesized that these claudins may form extracellular pores in 2 possible ways. First, pores may be formed in parallel along the TJ. In this parallel model, homomeric claudin-2 and claudin-10a channels are inserted into the TJ, and we would expect their respective permeabilities to be additive (Figure 2-8A) and described by the following equations:

$$P_{Na(total)} = P_{Na(Cldn2)} + P_{Na(Cldn10a)}$$

$$P_{Cl(total)} = P_{Cl(Cldn2)} + P_{Cl(Cldn10a)}$$

Assuming a linear relationship between the protein expression of each protein at the TJ and its permeability properties, then P_{Na} or P_{Cl} should also have a linear relationship to induction of protein expression.

$$P_{Na}/P_{Cl} = \left[(P_{Na(Cldn2)} + P_{Na(Cldn10a)})/(P_{Cl(Cldn2)} + P_{Cl(Cldn10a)})\right]$$

If we assume that the P_{Na} of claudin-10a and the P_{Cl} of claudin-2 are very low, we can simplify this to:

$$P_{Na}/P_{Cl} \sim \left[P_{Na(Cldn2)}/P_{Cl(Cldn10a)}\right]$$

The second possibility is that these claudins form heteromeric extracellular pores (Figure 2-8B). If claudins-2 and -10a form hybrid pores, the proportional expression of claudin isoforms would have a non-linear relationship with ion permeability. If the pore has novel permeability properties, then we might expect these properties to be most evident when the ratio of claudin-2: claudin-10a is 1:1. However, the results would be indistinguishable from the parallel model of pore formation if the properties of a claudin-2/-10a hybrid pore are intermediate between the properties to of either isoform alone. I sought to test this by using the titratability of our cell expression system. Our findings in two clonal cell populations suggest that expression of claudin-2 has a linear relationship with P_{Na} regardless of the level of claudin-10a expression. Therefore, the two claudins are unlikely to form a pore with novel properties (Figure 2-9).

Claudin-2 only contains two extracellular cysteine residues which together form a disulfide bond, thereby rendering them inaccessible to soluble thiol-reactive reagents such as MTSEA (Li, Angelow et al. 2013). As a result, cysteine-scanning mutagenesis, followed by covalent modification of cysteine residues with thiol reactive reagents, has proven useful for mapping the pore-lining residues of claudin-2 (Li, Zhuo et al. 2014). Of all of the putative pore-lining residues, mutagenesis of a serine residue in ECL1, claudin-2 S68C, resulted in a functional claudin-2 pore

with the greatest inhibition of conductance (>60%) following the addition of MTSEA (Li, Zhuo et al. 2014). In order to investigate the hypothesis that claudin-2 and claudin-10a form heterotypic extracellular channels, I utilized our double-inducible system with overexpression of this mutant, claudin-2 S68C, in addition to claudin-10a. If a hybrid pore with intermediate properties explains the reduced permselectivity of the dual induction condition, we would expect that blockage of claudin-2 would interfere with the pore and reduce P_{Cl} to a greater proportion than expected (based on the claudin-2 only induction condition). Similar to the wild type cell lines, I found that P_{Na} and P_{Cl} are less than expected with dual induction. However, our findings showed that blockage of claudin-2 reduces P_{Cl} to a similar extent in claudin-2 and claudin-2/10a induction conditions (claudin-2/10a 0.20 vs claudin-2 0.24, Table 2-1). This suggests that claudin-2 and claudin-10a insert into the TJ via the parallel model (Figure 2-8A).

2.5 Discussion

The work presented here shows the expression pattern of the predominant claudin isoforms within the PT and thin descending limb of the loops of Henle. In addition, I generated a novel inducible dual-claudin expression model to study the effects of claudin co-expression *in vitro*. Specifically, I investigated the net effect of overexpression of claudin-2 with the other predominant claudin isoforms within the PT, claudin-10a and claudin-3.

My present work showed that the expression of claudin-2 is strong throughout the PCT and PST, while claudin-10 was weakly expressed compared with expression in the TAL (Figure 2-1). It should be noted that our claudin-10 antibody is directed towards the C-terminus of the protein, which does not differ between claudin-10a and claudin-10b isoforms. Previously, microdissection experiments did not collect PST segments for detection of claudin-10a (Gunzel, Stuiver et al. 2009), and, conversely, deep sequencing of microdissected PST segments did not distinguish between the two isoforms of claudin-10 (Lee, Chou et al. 2015). Thus, I am unable to distinguish between the isoforms myself, and I am working under the assumption that claudin-10a is also the dominant isoform within the PST. I am assuming this in part because *in situ* hybridization studies

grossly suggest that the claudin-10a isoform predominates in the cortex and outer stripe of the outer medulla, where PSTs are numerous (Van Itallie, Rogan et al. 2006). In contrast, claudin-10b is relatively scarce in the outer stripe but highly concentrated in the inner stripe of the outer medulla, where TALs are abundant (Van Itallie, Rogan et al. 2006).

In MDCK I cells, overexpressed claudin-2 and claudin-10a formed cation-selective and anion-selective pores, respectively, and co-expression reduced ion permselectivity to P_{Na} and P_{Cl} (Figure 2-5). While heteromeric biochemical interactions between different claudin isoforms have been well described, there have been no studies that distinguished whether these interactions produced functionally heteromeric paracellular channels with novel functional properties. Here I used a novel double-inducible and titratable expression system to show that the claudin-2 and -10a pores function independently and in parallel, as opposed to forming a heterotypic hybrid channel.

As discussed in the introduction, the driving forces for passive sodium and water transport in the PT are small osmotic gradients and positive lumen potentials created secondary to passive chloride movement along its concentration gradient. These driving forces may result in a substantial amount of isosmotic fluid reabsorption along the PT due to the high permeability of the nephron segment, *in vivo*. An epithelium with high permeability to chloride, sodium, and water is key to large amounts of reabsorption occurring in this segment. I speculate that chloride movement occurs across the TJ mediated by claudin-10a, and claudin-2 provides the paracellular shunt pathway for sodium and water to follow.

In contrast to claudin-2 and claudin-10a, claudin-3 was found only within the PSTs of the outer stripe of the outer medulla (Figure 2-1). According to micro-perfusion experiments in rabbits, P_{Na}/P_{Cl} is higher in juxtamedullary PT segments compared with superficial segments (Kawamura, Imai et al. 1975, Jacobson and Kokko 1976, Warnock and Burg 1977, Berry, Warnock et al. 1978). In addition, studies in rabbits have shown that water permeability of the juxtamedullary straight PT segments is approximately double that of other PT segments (Van Der Goot and Corman

1991), and water permeability in the PST is in large part mediated by the paracellular pathway (Carpi-Medina and Whittembury 1988). While the contribution of claudins to paracellular permeability is well established, it is not clear how claudin-3 expression would contribute to the physiological properties observed in these experiments. It is established that cation and water permeation through claudin-2 are both mediated by the same pore lining residues (Rosenthal, Gunzel et al. 2017). Interestingly, overexpression of claudin-3 in MDCK II cells, which have high endogenous claudin-2 expression, did not alter water permeability despite a marked reduction in TER (Milatz, Krug et al. 2010).

I discovered separate populations of thin descending limbs of Henle with claudin-2 or claudin-3 expression, and further identified the claudin-3 positive segments as thin descending limbs of a distinct population from those of long loop nephrons (Figure 2-2). This expression pattern of claudins may reflect the opposing permeability properties in long and short loop nephrons. The upper segments of descending thin limbs of long loop nephrons have a high P_{Na}, which is likely related to the high expression of claudin-2 in these segments (Imai and Yoshitomi 1990). In contrast, short descending limbs have much lower P_{Na}, P_{Cl} (Imai and Yoshitomi 1990) and P_{Na}/P_{Cl} (Imai 1984) than the upper descending thin limb segments of long loop nephrons. Short loop nephrons also have a high permeability to urea compared with long loop nephrons (Imai and Yoshitomi 1990). This high urea permeability is suggested to facilitate urea recycling from ascending vasa recta, which carry a large amount of urea from the inner medulla (Jamison 1987). Urea recycling also occurs in the PSTs, with urea flowing from the cortical TALs of long loop nephrons (Jamison 1987). While it is unclear what claudin-3 contributes to urea recycling, it is interesting to note the high expression of claudin-3 in these segments. Our dual-claudin induction model may be utilized in future studies to investigate the effect of claudin-3 overexpression on urea permeability.

My findings indicate that overexpression of claudin-3 results in negligible effects on ion selectivity and TER, with or without the expression of claudin-2. This differs from previous findings

in MDCK II cells, mentioned above. As our model is based on the high TER cell line, MDCK I, and both human claudin isoforms are overexpressed in these cells, the results of the two studies are not necessarily interchangeable. A common concern of overexpression studies for studying claudin biology is the presence of endogenous claudins, which may affect the observed results (Gunzel and Yu 2013). Indeed, MDCK I cells have endogenous canine claudin-3 expression, and I attempted to mitigate these effects by carefully selecting a clonal cell line with low expression levels, by both immunoblotting and immunofluorescence (Figure 2-4). Future studies could utilize genomic editing techniques such as transcription activator-like effector nucleases (TALENs) in order to genetically knockout the endogenous claudin-3 gene in MDCK I cells, as was recently described by Tokuda (Tokuda and Furuse 2015). It will be interesting to explore the effects of these PT claudins further, especially given the strong co-expression of claudins-2, -3, and -10 within juxtamedullary PSTs.

The claudin-2 isoform was previously shown to increase unidirectional calcium flux in renal epithelial cells, but calcium flux had heretofore not been measured in overexpression studies of claudin-3 and claudin-10a. My findings suggest that only claudin-2 increases the cation and calcium permeability of MDCK I cells, while claudin-10a modulates permeability by reducing the paracellular permeability to cations. I have also shown that claudin-2 and claudin-10a form independent pores when inserted into the TJ rather than a hybrid pore. In cells inducible for claudin-3 and claudin-2, no difference was observed in calcium permeability or TER. While previous studies in low resistance cell lines have shown that claudin-3 increases TER (Milatz, Krug et al. 2010), my results suggest that this effect is counteracted by overexpression of claudin-2. My major findings strengthen the evidence for claudin-2 as the putative paracellular calcium pore in the PT, responsible for a significant fraction of renal calcium reabsorption.

Table 2-1. Effect of claudin-2 pore blockage in cells with dual inducibility of claudin-2 S68C and claudin-10a

Claudin induction	None	MTSEA			None	MTSEA			None	MTSEA
	$P_{Na(total)}$	$P_{Na(total)}$	$P_{Na(Cldn2\text{-}MTSEA)}$	$P_{Na(Cldn2\text{-}MTSEA)}/P_{Na(total)}$	$P_{Cl(total)}$	$P_{Cl(total)}$	$P_{Cl(Cldn2\text{-}MTSEA)}$	$P_{Cl(Cldn2\text{-}MTSEA)}/P_{Cl(total)}$	P_{Na}/P_{Cl}	P_{Na}/P_{Cl}
None	0.60	0.67			0.79	0.92			0.76	0.72
Cldn2	6.54	2.59	3.95	0.60	1.73	1.34	0.39	0.24	3.91	2.04
Cldn10a	0.63	0.64			4.06	3.96	0.10	0.02	0.16	0.16
Cldn2/10a expected*	7.17	3.23	3.94		5.79	5.31	0.48		1.24	0.61
Cldn2/10a observed	5.10	2.02	3.08	0.60	2.76	2.21	0.55	0.20	1.89	0.94

Ussing experiments in cells inducible for expression of claudin-2 S68C (cldn2) and claudin-10a (cldn10a). Unknown values or values less than zero are left blank

$P_{X(Cldn2\text{-}MTSEA)}$ is the permeability of X that is attributable to cldn2 prior to blockage of pore with MTSEA

**Expected values of cldn2/cldn10a dual induction conditions. P_X values are sum of single claudin induction experiments, whereas expected P_{Na}/P_{Cl} is calculated as discussed in the text above.*

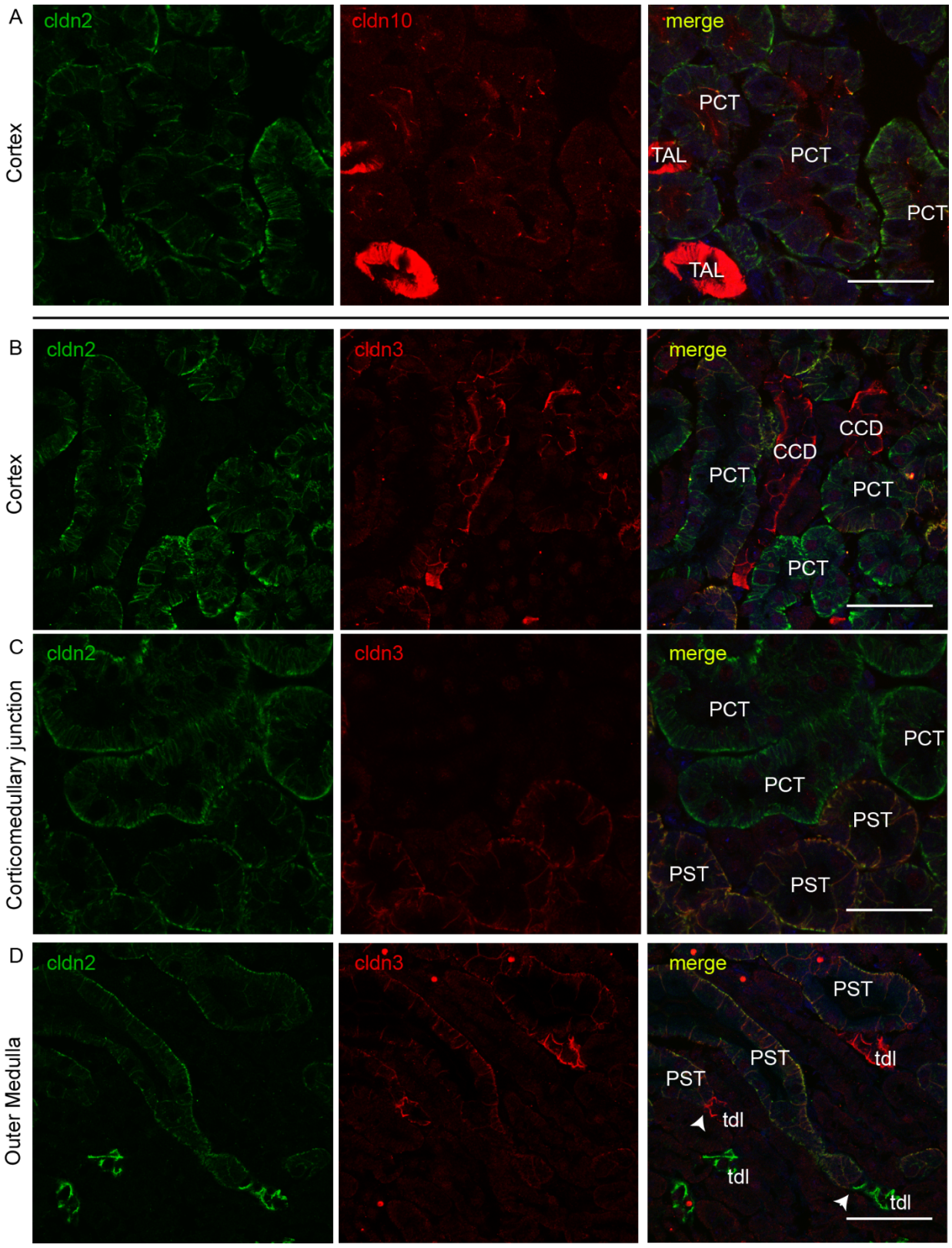
A
Cortex
cldn2
cldn10
merge
PCT
TAL
PCT
PCT
TAL
B
Cortex
cldn2
cldn3
merge
CCD
CCD
PCT
PCT
PCT
C
Corticomedullary junction
cldn2
cldn3
merge
PCT
PCT
PCT
PST
PST
PST
D
Outer Medulla
cldn2
cldn3
merge
PST
PST
tdl
PST
tdl
tdl
tdl

Figure 2-2. Colocalization of PT claudins in adult mice

(A) Tight junction colocalization of claudin-2 (cldn2) and claudin-10 (cldn10) in the kidney was detected throughout the proximal convoluted tubule (PCT). Strong basolateral claudin-10 staining was also detected in the thick ascending limb (TAL) and the straight proximal tubule segments of the outer medulla (not shown). (B-D) Colocalization of claudin-2 and claudin-3 in the PCT (B,C), proximal straight tubules (PST) (C,D), and thin descending limbs (tdl) (D). Claudin-2 and -3 colocalize to both tight junction and basolateral membrane throughout the PST (C,D). At points where PSTs transition to tdls, some populations of tdl only express claudin-2, whereas others only express claudin-3 (D, arrowheads). Claudin-3 was also expressed in cortical collecting duct (CCD). Scale bars = 50μm.

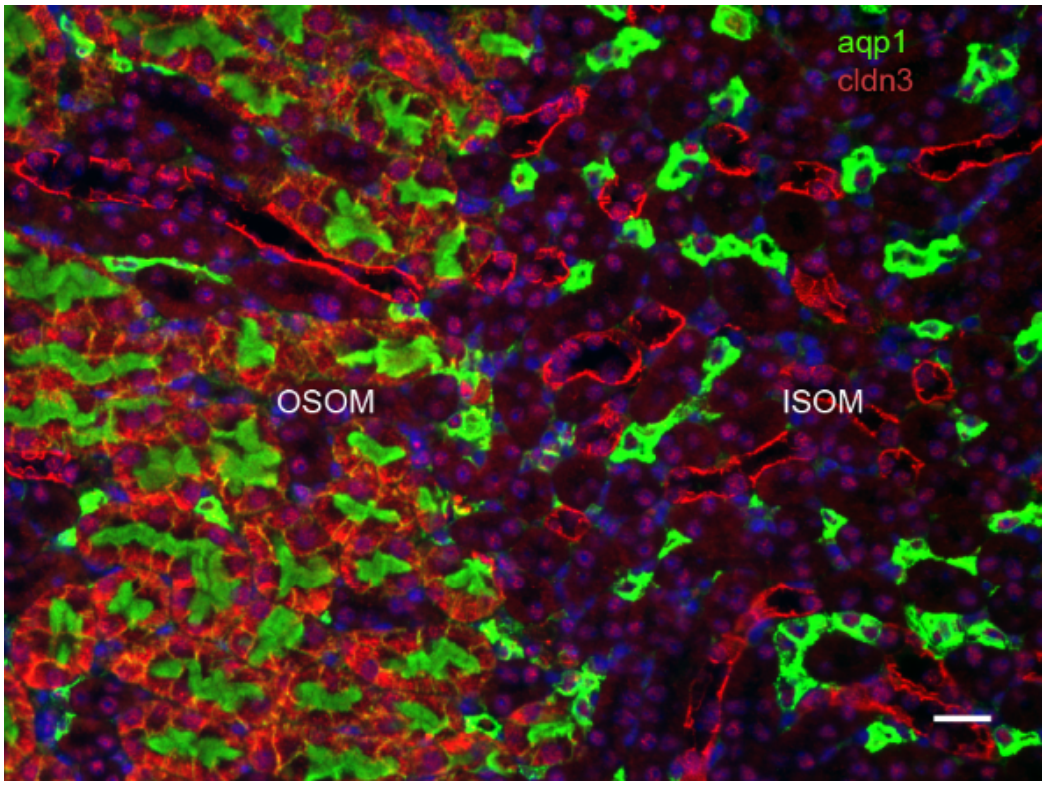

Figure 2-3. Localization of claudin-3 within short loop nephrons

Claudin-3 (cldn3, red) expression is not found in long loop descending thin limb tubules, which express aquaporin-1 (aqp1, green).. Scale bars = 50μm. OSOM= outer stripe of the outer medulla; ISOM= inner stripe of the outer medulla.

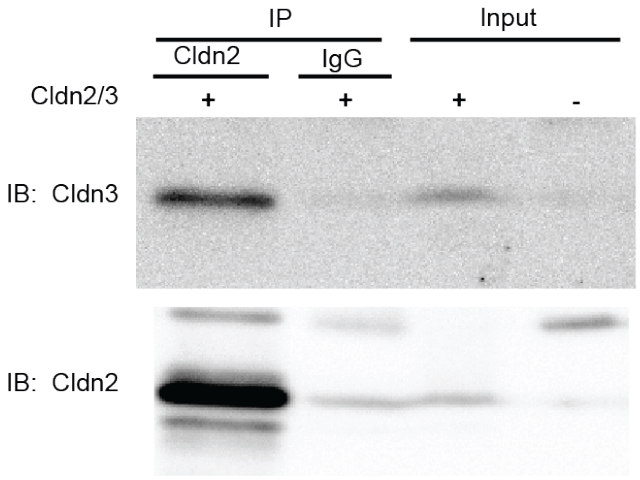

Figure 2-3. Co-immunoprecipitation of claudin-2 and claudin-3

Human embryonic kidney cells (Hek293) were transiently transfected with claudin-2 (cldn2) and claudin-3 (cldn3), and sub-confluent cell lysates were collected. Input shows expression of both claudins in whole cell lysates. Cldn3 co-immunoprecipitated with cldn2, but neither was precipitated with negative control, IgG.

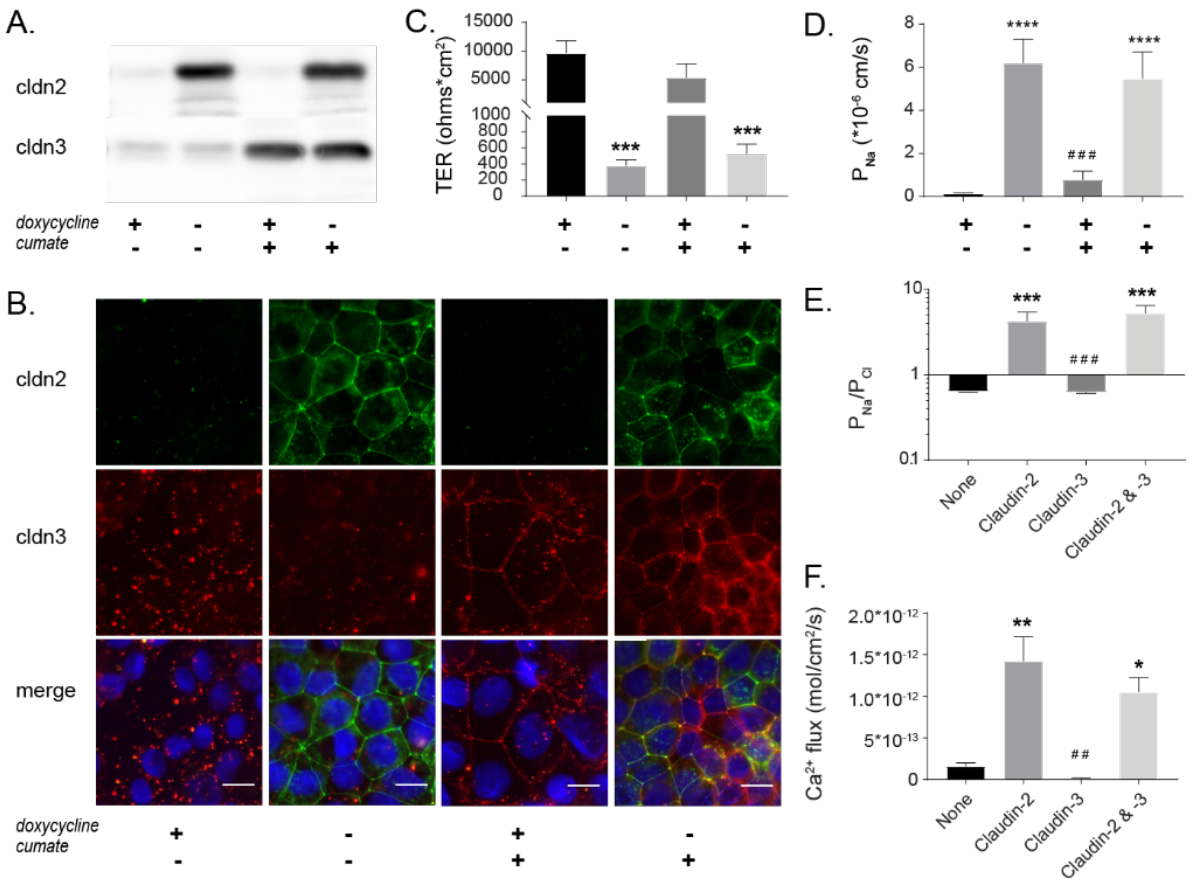

Figure 2-4. Claudin-3 expression has minimal effect on the electrophysiological properties of MDCK I cells

MDCK I TetOff cells stably transfected with wild type human claudin-2 and claudin-3 under control of the tetracycline-controlled transactivator and cumate switch, respectively. Cells were grown in the presence (+) or absence (-) of doxycycline and cumate. (A) Representative immunoblots of clone with low endogenous claudin-3 expression used for electrophysiological characterization. (B) Immunolocalization of claudin-2 and claudin-3 in cells grown in the presence (+) or absence (-) of doxycycline and cumate. Scale bars = 25μm. (C) Cells were loaded into Ussing chambers for measurement of transepithelial resistance (TER) (n=6). (D) Permeability to sodium (P_{Na}) was determined in dilution potential experiments. (E) Ratio of sodium and chloride permeability (P_{Na}/P_{Cl}) (n=6). Data were $\log_{10}$ transformed prior to analysis. (F) Calcium (Ca^{2+}) permeability was determined by unidirectional radiotracer flux assay (n=3). Data were analyzed by two-way ANOVA with Tukey's correction for multiple comparisons and presented as Mean ± SEM. Significant differences compared with no claudin induction are represented by: *, P<0.05; **, P<0.01; ***, P<0.001; ****, P<0.0001. Significant differences compared with claudin-2 expression only are represented by: ##, P<0.01; ###, P<0.001.

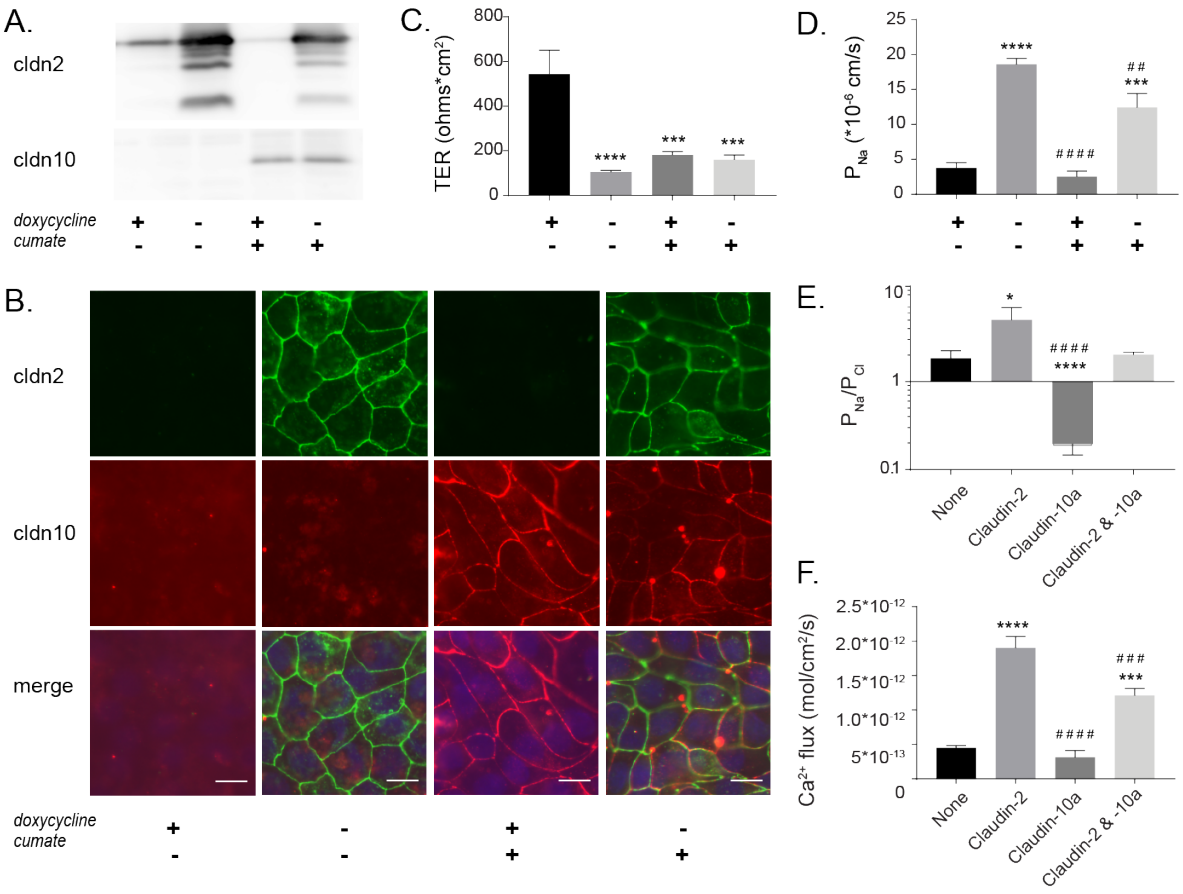

Figure 2-5. Co-expression of claudin-2 and claudin-10a leads to a reduction in permselectivity of MDCK I cell monolayers

MDCK I TetOff cells stably transfected with wild type human claudin-2 and claudin-10a under control of the tetracycline-controlled transactivator and cumate switch, respectively. Cells were grown in the presence (+) or absence (-) of doxycycline and cumate. (A) Representative immunoblots of single clone (clone 9) used for subsequent electrophysiological characterization. (B) Immunolocalization of claudin-2 and claudin-10a in cells grown in the presence (+) or absence (-) of doxycycline and cumate. Scale bars = 25µm. (C) Cells were loaded into Ussing chambers for measurement of transepithelial resistance (TER) (n=9). (D) Permeability to sodium (P_{Na}) was determined in dilution potential experiments. (E) Ratio of sodium and chloride permeability (P_{Na}/P_{Cl}) (n=9). Data were $\log_{10}$ transformed prior to analysis. (F) Calcium (Ca^{2+}) permeability was determined by unidirectional radiotracer flux assay (n=3). Data were analyzed by two-way ANOVA with Tukey's correction for multiple comparisons and presented as Mean ± SEM. Significant differences compared with no claudin induction are represented by: *, P<0.05; **, P<0.01; ***, P<0.001; ****, P<0.0001. Significant differences compared with claudin-2 expression only are represented by: ##, P<0.01; ###, P<0.001; ####, P<0.0001.

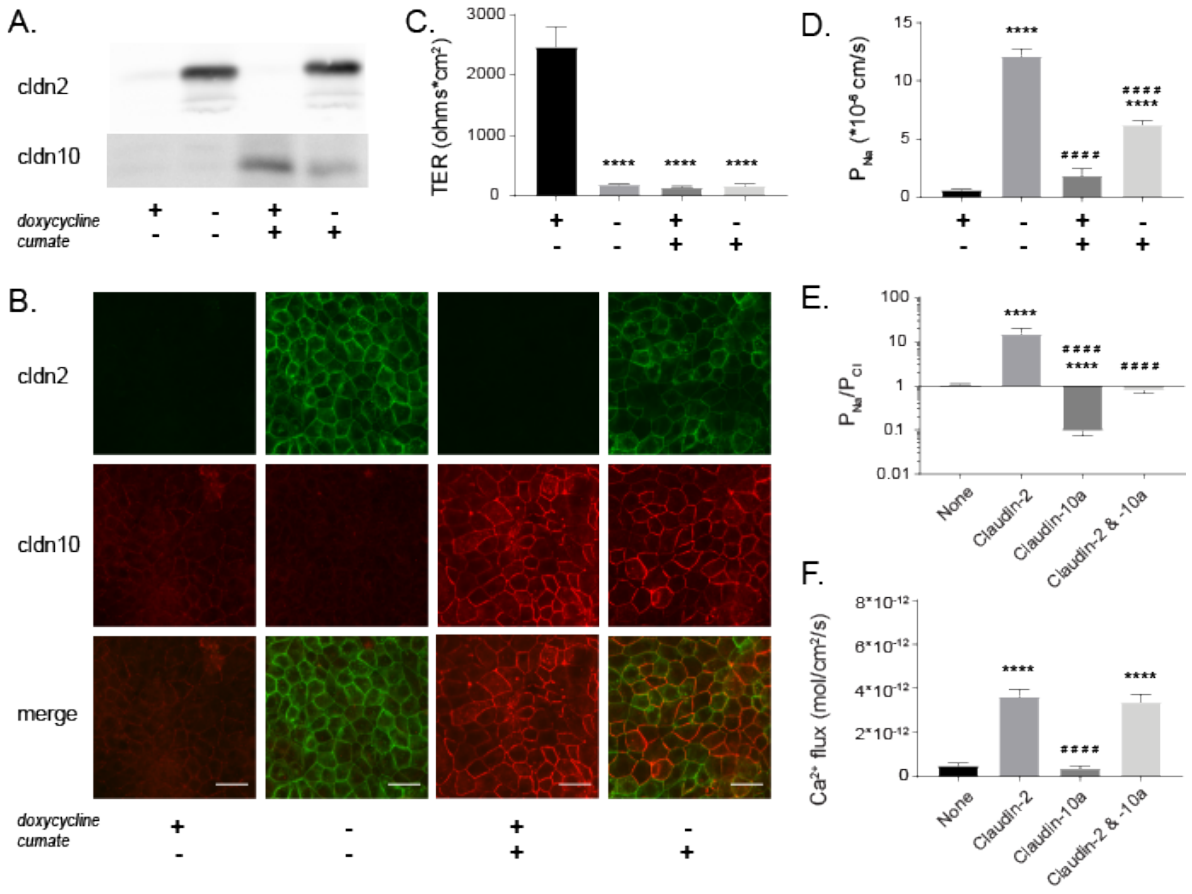

Figure 2-6. Results repeated in another clone co-expressing claudin-2 and claudin-10a

MDCK I TetOff cells stably transfected with wild type human claudin-2 and claudin-10a under control of the tetracycline-controlled transactivator and cumate switch, respectively. Cells were grown in the presence (+) or absence (-) of doxycycline and cumate. (A) Representative immunoblots of single clone (clone 1) used for subsequent electrophysiological characterization. (B) Immunolocalization of claudin-2 and claudin-10a in cells grown in the presence (+) or absence (-) of doxycycline and cumate. Scale bars = 25µm. (C) Cells were loaded into Ussing chambers for measurement of transepithelial resistance (TER) (n=9). (D) Permeability to sodium (P_{Na}) was determined in dilution potential experiments. (E) Ratio of sodium and chloride permeability (P_{Na}/P_{Cl}) (n=9). Data were $\log_{10}$ transformed prior to analysis. (F) Calcium (Ca^{2+}) permeability was determined by unidirectional radiotracer flux assay (n=3). Data were analyzed by two-way ANOVA with Tukey's correction for multiple comparisons and presented as Mean ± SEM. Significant differences compared with no claudin induction are represented by: ****, P<0.0001. Significant differences compared with claudin-2 expression only are represented by: ####, P<0.0001.

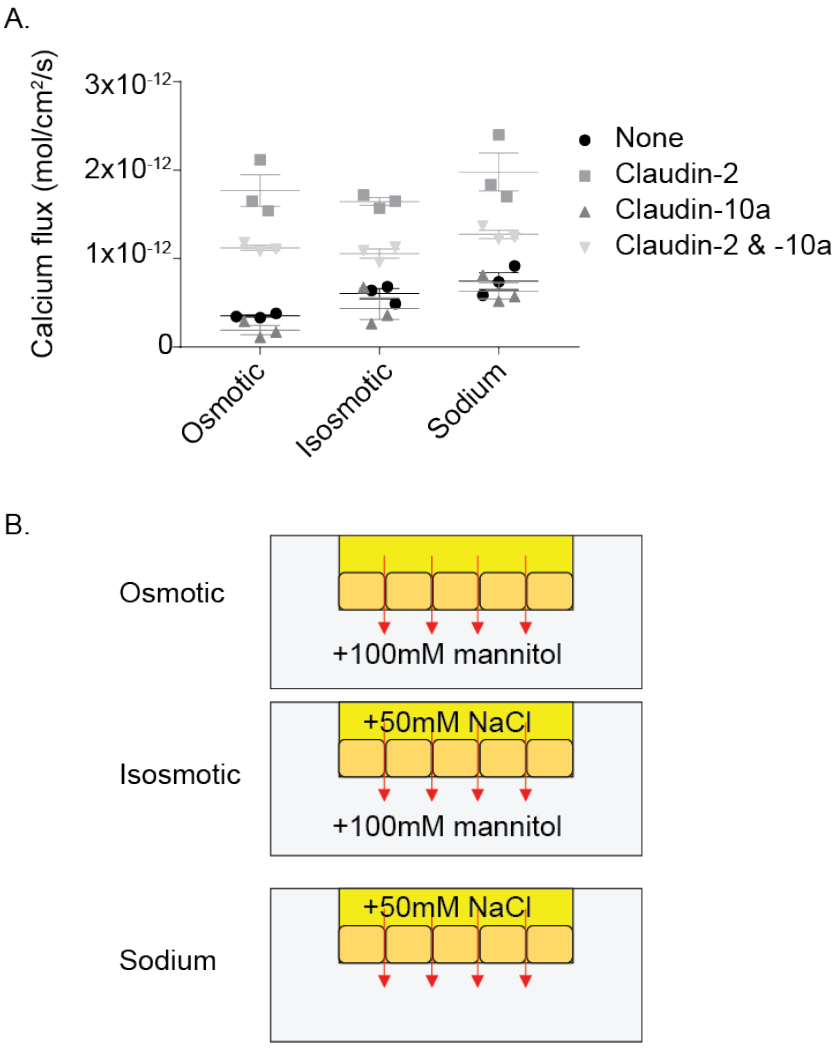

Figure 2-7. Claudin-2 mediated calcium flux is not increased by osmotic "solvent drag"

Unidirectional radiotracer calcium flux experiments were performed on claudin-2/-10a dual induction cells (clone 9) under hyperosmotic conditions. (A) Results of calcium flux in 3 separate conditions revealed no significant effect of claudin-2 on calcium flux. No significant differences between control data were detected. Data were analyzed by two-way ANOVA with Tukey's correction for multiple comparisons and individual values shown. Bars are Mean ± SEM (n=3). (B) Experimental conditions for the three gradient experiments are shown. Radiotracer calcium is added to apical chamber, as described in the methods. Mannitol was added to basolateral medium and sodium chloride (NaCl) to apical medium in the amounts shown.

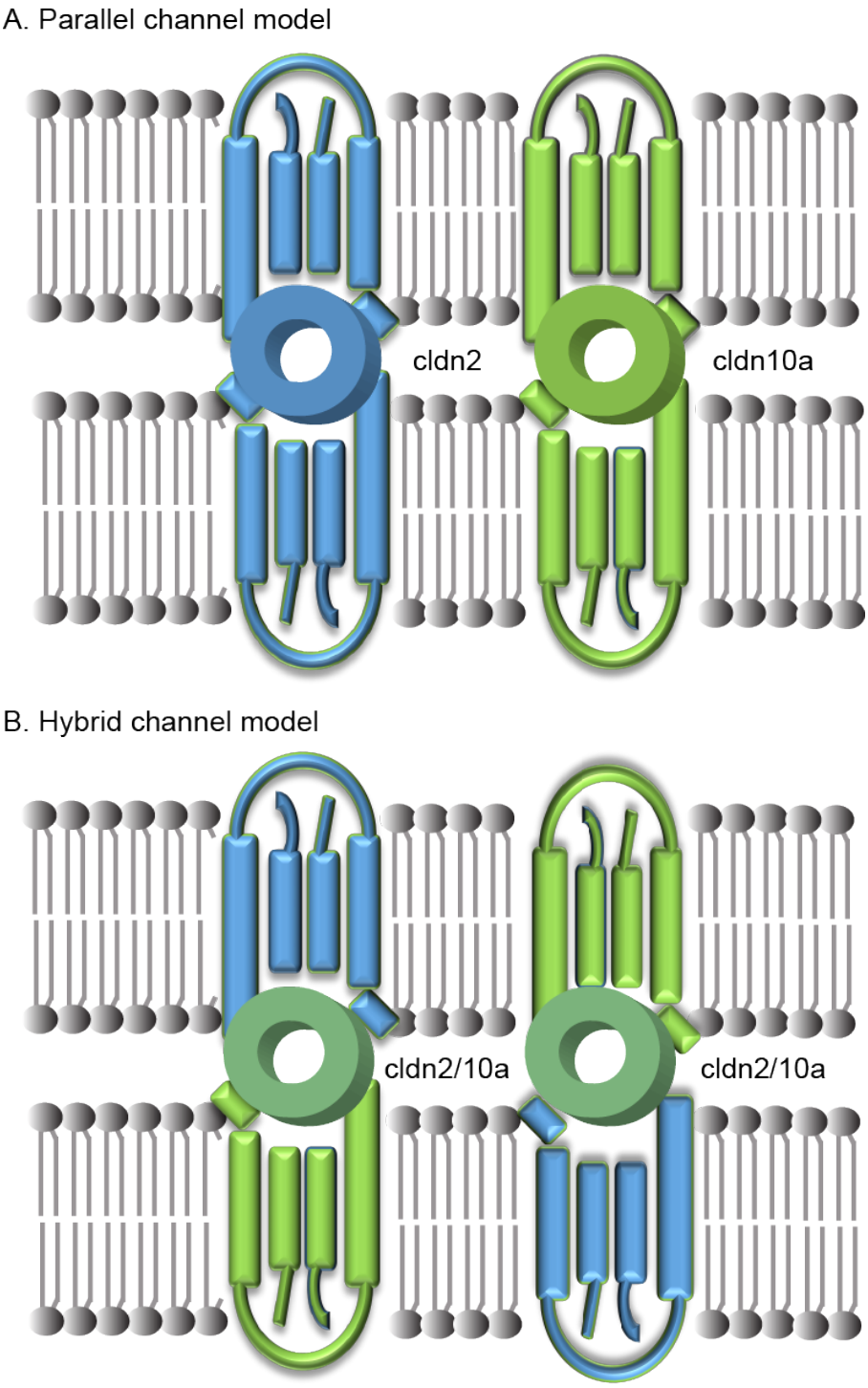

Figure 2-8. Two models of extracellular claudin pore formation with co-expression of PT claudins in MDCK I cells

(A) In the parallel model of claudin pore formation, claudin-2 (cldn2) and claudin-10a (cldn10a) each insert in parallel into an otherwise poorly permeably tight junction strand. (B) An alternative model is that the combination of cldn2 and cldn10a expression leads to the formation of a hybrid channel with novel properties (i.e. heterophilic or heteromeric claudin-2/-10a channel).

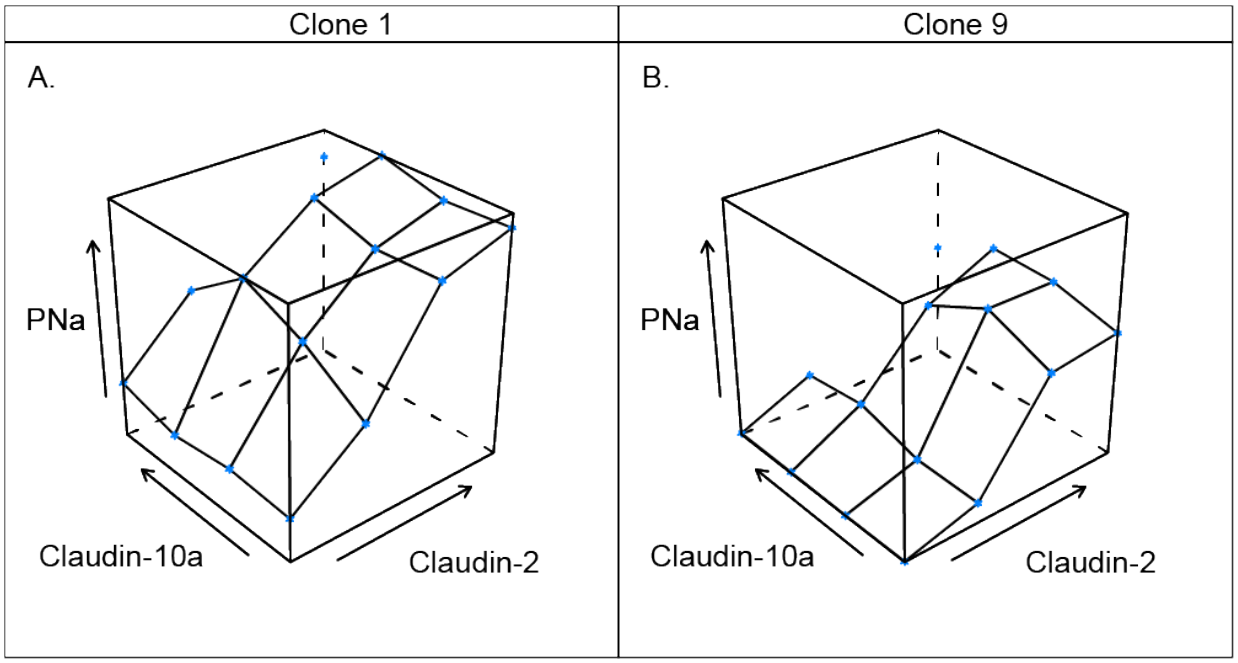

Figure 2-9. Expression of claudins in relation to sodium permeability

XYZ plot of P_{Na} plotted against induction level of claudin-2 and claudin-10a. We induced varying levels of claudin-2 (doxycycline 0, 0.01, 0.1, and 20ng/µl) and claudin-10a (cumate 0, 30, 60, and 90ng/µL) in our claudin-2/claudin-10a dual induction clones and performed dilution potential experiments. Clones show a direct relationship between claudin-2 expression and P_{Na} regardless of claudin-10a induction, suggesting that these claudins form extracellular pores via the parallel model.

Chapter 3: Claudin-2 deletion causes nephrocalcinosis in mice and common *CLDN2* variants associate with human kidney stone disease

3.1 Abstract

Hypercalciuria and nephrocalcinosis are frequent findings in patients with recurrent kidney stone disease. Hypercalciuria is often idiopathic and related to unknown defects in intestinal or renal calcium transport. In the kidney, the majority of filtered calcium is reabsorbed in the PT by an unknown pathway. Claudin-2 is a calcium-permeable TJ protein highly expressed in the PT. I hypothesized that global deletion of the *Cldn2* gene in mice would lead to defective renal calcium reabsorption and nephrocalcinosis. I first confirmed that *Cldn2*$^{-/y}$ mice exhibit increased urinary calcium excretion. Histological analyses revealed extensive intratubular calcium deposits in the loops of Henle of *Cldn2*$^{-/y}$ mice. Micro-CT analysis showed that deposits form between 4.5-6 months of age, and micro-Fourier transform infrared spectroscopy (micro-FTIR) analysis determined the composition as primarily hydroxyapatite. Surprisingly, metabolic balance studies revealed that *Cldn2*$^{-/y}$ mice have a positive calcium balance compared with wild type animals. When placed on a calcium deficient diet, calcium excretion in *Cldn2*$^{-/y}$ mice was reduced to a much greater extent than in wild type mice but remained approximately double that of wild type mice on the calcium deficient diet. These results suggest that *Cldn2*$^{-/y}$ mice exhibit both intestinal hyperabsorption and defective renal reabsorption of calcium. Utilizing genotype association analysis including the X chromosome, our collaborators identified several SNPs in the *CLDN2* locus that associate with nephrolithiasis in the Japanese population. eQTL analysis revealed a strong correlation between risk variants and reduced claudin-2 mRNA expression. I conclude that claudin-2 is an important mediator of calcium transport in both kidney and the intestinal tract, and common *CLDN2* variants are likely to contribute to the pathogenesis of kidney stone formation in the general population.

3.2 Introduction

Kidney stone disease is common, with a lifetime risk in the U.S. of about 10% *(De, Liu et al. 2014).* Health care expenditures for care related to nephrolithiasis is estimated to be more than $2 billion annually (Pearle, Calhoun et al. 2005). Studies of families (Resnick, Pridgen et al. 1968), twin concordance (Goldfarb, Fischer et al. 2005), and genome wide association (Thorleifsson, Holm et al. 2009, Gudbjartsson, Holm et al. 2010, Urabe, Tanikawa et al. 2012) have revealed a significant role for polygenic inheritance in the pathogenesis of the disease. The vast majority of stones are composed of calcium crystals, primarily calcium phosphate or CaOx (Walker, Stansbridge et al. 2013, Evan, Lingeman et al. 2014), and the major risk factor is an elevation in urine calcium, which is termed idiopathic hypercalciuria (Worcester and Coe 2010). Additional risk factors for kidney stone formation include low urine volume, hyperoxaluria, and hypocitraturia (Worcester and Coe 2010). The common causative factor in these metabolic abnormalities is supersaturation of calcium salts leading to precipitation and crystal growth (Worcester and Coe 2010).

The pathogenesis of stone formation in patients with idiopathic hypercalciuria varies depending on the composition of the stone but the majority are believed to begin with deposition of calcium within the renal papilla, or papillary nephrocalcinosis (Evan, Lingeman et al. 2014). For patients with urinary stones composed of primarily CaOx, the precursor lesions are known as Randall's plaques and are characterized by deposition of calcium phosphate within the interstitial space surrounding the basement membranes of the thin limbs of loops of Henle (Evan, Lingeman et al. 2003). By contrast, patients with predominately calcium phosphate urinary stones often have early intratubular calcium phosphate deposits in inner medullary collecting ducts, as well as interstitial aggregates of calcium phosphate termed NIPS that have microscopic features distinct from Randall's plaques (Evan, Lingeman et al. 2014). All of these forms of intrarenal deposits are believed to eventually rupture through the papillary surface and thereby form a nidus for the growth of urinary stones.

The etiology of idiopathic hypercalciuria is incompletely understood, but can generally be ascribed to increased bone resorption, intestinal hyperabsorption, and/or reduced renal reabsorption of calcium (Moe 2006). Studies of diuretic response and lithium clearance in patients with idiopathic hypercalciuria suggest that they have a specific defect in PT calcium reabsorption (Sutton and Walker 1980, Worcester, Coe et al. 2008). The PT reabsorbs approximately 60% of calcium filtered by the glomerulus (Suki 1979). It is highly permeable to calcium and the tubule fluid/plasma concentration ratio is about 1.1, suggesting that transport of calcium follows that of sodium and water (Suki 1979, Alpern, Hebert et al. 2008). In isolated perfused PTs, net calcium transport is zero in the absence of osmotic or potential differences, and reabsorption can be induced by applying a lumen positive potential difference (Ng, Rouse et al. 1984). This suggests that calcium reabsorption in the PT is passive and likely occurs by paracellular diffusion.

Paracellular transport is mediated by a family of tetraspanning membrane proteins known as claudins that are found at the TJ between epithelial cells. These proteins act as charge-selective channels or barriers regulating the movement of solutes across epithelial layers (Hou, Rajagopal et al. 2013). Claudin-2 is a cation-selective isoform (Furuse, Furuse et al. 2001, Amasheh, Meiri et al. 2002) that is permeable to both sodium and calcium (Amasheh, Meiri et al. 2002, Yu, Cheng et al. 2009) and is highly expressed in the PT and the descending thin limb of the loop of Henle (Enck, Berger et al. 2001). Isolated PTs from claudin-2 knockout mice have increased TER and reduced P_{Na}, and these animals exhibit a three-fold increase in the fractional excretion of calcium ($FECa^{2+}$) (Muto, Hata et al. 2010), suggesting that claudin-2 mediates paracellular calcium reabsorption in the PT.

In this study I tested the hypothesis that loss of claudin-2 predisposes mice to nephrocalcinosis and nephrolithiasis, mimicking the pathogenesis of human kidney stone disease. We explored the underlying mechanism and tested whether common polymorphisms in the claudin-2 gene are associated with human kidney stone disease.

3.3 Methods

3.3.1 Animal studies

The null allele of *Cldn2*$^{tm1Lex/Mmcd}$ mice was originally generated by targeted deletion of the coding exon of *Cldn2* and backcrossed into the C57BL/6J background, as described previously (Pei, Solis et al. 2016). All studies used male mice due to the location of the *Cldn2* gene on the X-chromosome, which precludes generation of wild type and knockout female littermates. Baseline measurements of urine and serum parameters were performed on 15-17 week-old mice fed standard lab chow (Teklad Rodent Diet 8604, Envigo). Urine was collected on Parafilm. Mice were then anesthetized with a xylazine (15 mg/kg i.p.) and ketamine (150 mg/kg) cocktail (1x) and blood was collected by cardiac exsanguination. To avoid possible interference of ketamine with PTH measurements, blood for this assay was collected from the submandibular vein of unanaesthetized 16 week-old mice into EDTA plasma tubes.

3.3.2 qRT-PCR

Tissue RNA was extracted with TRI Reagent (Sigma-Aldrich). First-strand cDNA iScript Reverse Transcription Supermix for RT-qPCR (Bio-Rad) was used for first-strand cDNA synthesis. qRT-PCR primers are listed in Table 3-1. A CFX96 Touch Real-Time PCR Detection System and iTaq Universal SYBR Green Supermix (Bio-Rad) were used for quantitative PCR. Expression levels were normalized to housekeeping genes β-actin (kidney) or GAPDH (intestine).

3.3.3 Immunoblotting

Kidney tissue was homogenized by .009RD single edge blade (American Safety Razor Co.), and collected in protein isolation buffer composed of 20mM HEPES pH 7.4, 10mM KCl, 2mM $MgCl_2$, 1mM EDTA, and 1mM EGTA with protease inhibitors (cOmplete Mini, Roche Diagnostics). Each sample was homogenized for 15s increments every minute for 5 minutes at a low-speed setting with an Ultra-Turrax T25 (IKA-Labortechnik) and then centrifuged at 1800 x g for 10 minutes. Lysates were heated at 95ºC for 10min in reducing SDS-PAGE buffer and loaded into a polyacrylamide gel. Protein was then transferred to a polyvinylidene difluoride (PVDF)

membrane and blocked using 5% nonfat-dry milk. Primary antibody incubation was performed overnight at 4ºC using the following antibodies: mouse anti-calbindin-D28k (Swant, 1:1000), mouse anti-claudin-2 (Invitrogen, 1:500), and mouse anti-β-actin (Sigma-Aldrich, 1:1000). Horseradish peroxidase conjugated secondary antibodies were incubated at a concentration of 1:5000 (GE Healthcare Bio-Sciences) and bands detected using chemiluminesence (Pierce). Quantitation of densitometry was achieved using ImageJ (NIH) and normalized to β-actin.

3.3.4 Metabolic balance studies

All metabolic balance studies were performed using mice between 14-18 weeks of age. Control (0.6% Ca^{2+}, TD.97191) and calcium deficient (≤ 0.01% Ca^{2+}, TD.95027) diet was purchased in powdered form (Envigo, Madison, WI) and prepared as a soft agar diet using 1% Difco Noble agar (BD Biosciences, San Jose, CA) in a ratio of 5:8 w/v diet to water.

Mice were first acclimated in metabolic cages (MMC100, Hatteras Instruments, Cary, NC) for 48 hours with free access to food and water. Control diet was started at this time (Day -4). At Day -2, mice were returned to conventional housing for 2 days of recovery. At Day 0, mice were returned to metabolic cages for collection of urine and feces. Food weight, water weight, and urine volume were recorded each day, and mice were removed for approximately 10 minutes each day during collection of urine, feces, and cleaning of cages. At Day 5, a subset of mice was switched to the low calcium diet. At the completion of the study, serum was collected by cardiac exsanguination.

3.3.5 Serum, urine, and fecal analysis

Feces were collected in glass vials and calcium was extracted by wet ashing. Briefly, 2:1 nitric: perchloric acid was added to each sample (3mL total) and heated at 95ºC until dissolved completely (~7 hours). Samples were serially diluted to a total volume of 400mL.

Urine was collected in 2 separate tubes. One aliquot was acidified using 12N HCl to a total concentration of 0.3N HCl. All aliquots were then spun down at 5000 x g for 1 min at RT and stored in -80°C.

Serum, urine, and fecal calcium was measured by a colorimetric assay (Quantichrom, BioAssay Systems). Urine creatinine was measured by the Jaffe reaction using a commercial kit (Cayman Chemical). Serum creatinine was measured by the University of Texas Southwestern Medical Center (UTSW) O'Brien Center Kidney Physiology Core by capillary electrophoresis. Urine was also assayed for oxalate (EnzyChrom, BioAssay Systems), citrate (EnzyChrom, BioAssay Systems), magnesium (QuantiChrom, BioAssay Systems), and inorganic phosphorus (Pointe Scientific).

3.3.6 Histological analysis

Six month-old mice fed standard lab chow were anesthetized using ketamine and xylazine and cardiac perfusion fixation was performed using 4% paraformaldehyde (PFA) in PBS. Kidneys were post-fixed in 4% PFA for 4 hours at room temperature.

Initial calcium staining was performed on paraffin-embedded sections that were deparaffinized and rehydrated. For von Kossa staining, sections were incubated in 5% aqueous silver nitrate for 1 hour under UV light, and 5% sodium thiosulfate for 1 min. For Alizarin Red S staining, tissues were placed in 2% Alizarin Red S, pH 4.3 for 1-3 min.

Immunofluorescence was performed on frozen sections. Fixed kidneys were cryoprotected in sucrose, embedded in OCT, and 5 μm sections were cut. Slides were first stained using the von Kossa technique. Antigen retrieval was then performed with 10 mM sodium citrate in a steamer for 6 min. Aldehyde quenching was accomplished by incubating in 0.3 M glycine in PBS, then slides were blocked for 1 hour in PBS with 5% normal goat serum, 1% BSA, and 0.3% Triton-X100. The primary antibodies used were: CLC-K (1:200, Alomone Labs), AQP1 (1:500, Abcam), AQP2 (1:500, a generous gift from Dr. Mark Knepper, NHLBI), MECA32 (1:100, Developmental Studies Hybridoma Bank, U. Iowa). Lipofuscin was quenched with 0.1% Sudan Black B in 70% ethanol for 15 min, before applying secondary antibodies (Alexa Fluor 488 and 555-conjugated goat anti-rabbit and anti-mouse IgG, 1:1000, Thermo-Fisher). Confocal fluorescent images were captured along with brightfield images for von Kossa stain (Leica TCS

SPE microscope). Von Kossa images were pseudocolored, then overlayed onto the fluorescent images using ImageJ (NIH).

3.3.7 Micro-CT analysis of kidneys

Kidneys from 6 month-old mice were fixed and ethanol dehydrated and then scanned with a high-resolution micro-CT scanner (μCT40; Scanco Medical, Southeastern, PA) as previously described (Zelenchuk, Hedge et al. 2015). Data were acquired at 55 KeV and 6 μm cubic resolutions. Renal calcifications were assessed with a threshold of 220.

3.3.8 Bone measurements

Dual energy X-ray absorptiometry (DEXA, Lunar PIXImus, GE Medical Systems) was used to measure bone mineral density in anesthetized mice (0.25x ketamine/xylazine cocktail) at 4.7, 6, 8, and 10 weeks of age. Two different sites were determined by adjusting the region of interest: femur and lumbar vertebrae. Some animals were fed a pelleted calcium-deficient diet (TD.95027, Envigo) at 12 weeks of age for 4 weeks. During the low calcium diet, measurements were taken at 12, 13, 14, 15, and 16 weeks of age. Micro-CT analysis was performed on femurs from 10 week-old animals as described previously (Zelenchuk, Hedge et al. 2015).

3.3.9 Transmission Electron Microscopy

Renal papillae were dissected from fresh kidneys, fixed in 3% glutaraldehyde in 0.1 M cacodylate buffer, and post-fixed in 1% osmium tetroxide in 0.1 M cacodylate buffer for 1 hour. They were then dehydrated in ethanol and propylene oxide and embedded in EMBED 812 resin. Cross-sections were cut through the papilla block at 80 nm thickness and picked up on 250 mesh copper grids. Next, blocks were sectioned 10 μm deeper and the same sectioning process was repeated twice. These thin sections were then contrasted with 3% uranyl acetate aqueous and Sato's lead stain. Grids were viewed at 100 kV in a JEOL JEM 1400 transmission electron microscope and images were captured as TIFF files with an AMT camera.

3.3.10 Micro-Fourier transform infrared spectroscopy

Kidney sections (~5 μm) were mounted on low-E glass slides (Kevley Technologies, Chesterland, Ohio) for attenuated total internal reflection (ATR) imaging analysis. A serial section stained with Yasue silver replacement was employed as a control section. Prior to infrared analysis, the control was visually examined with an Olympus white light microscope (20x objective) to determine the areas of interest. Sections for ATR-FTIR imaging were not stained. ATR infrared images were collected with a PerkinElmer Spectrum Spotlight 400 infrared imaging microscope interfaced to a Perkin Elmer FTIR spectrometer, as described previously (Evan, Lingeman et al. 2003). Each image (400 x 400 μm area) had a spatial resolution of 1.56 μm/pixel and contained 65,746 infrared spectra collected at a spectral resolution of 8 wavenumbers. Each spectrum in the image is the average of 4 individual scans. The images were further processed used using Spectrum Image software (Perkin Elmer).

3.3.11 Human DNA samples and genotyping

The characteristics of samples are shown in Table 3-2. DNA samples of 6,246 kidney stone cases (study 1), 4,884 Kidney stone cases (study 2), and 158,772 non kidney-stone controls (study 2) were obtained from Biobank Japan (Hirata, Nagai et al. 2017, Nagai, Hirata et al. 2017). 28,867 controls (study 1) were from three population-based cohorts, including the JPHC (Japan Public Health Center) -based prospective study (Tsugane and Sobue 2001), the J-MICC (Japan Multi-Institutional Collaborative Cohort) study (Hamajima and Group 2007), and ToMMo (Tohoku Medical Megabank Organization) (Matsuo, Oze et al. 2013, Kuriyama, Yaegashi et al. 2016). These samples were genotyped in previous studies by our collaborators (Kanai, Akiyama et al. 2018, Tanikawa, Kamatani et al. 2018). Genomic DNA samples were extracted from peripheral blood leukocytes and normal tissues using a standard method. All participants provided written, informed consent and the ethical committees at each institute approved the project. All samples were genotyped by Illumina Omniexpress Exome or the OmniExpress+HumanExome BeadChip (Table 3-2).

3.3.12 Imputation and Statistical analysis

SNPs were excluded that met the following criteria: MAF <0.005; Hardy-Weinberg equilibrium *P* value < 1 x 10^{-6}, Call rate =0 (study 1) or <0.01 (study 2). Imputation of the ungenotyped SNPs was conducted by MaCH (Scott, Mohlke et al. 2007) and minimac (Howie, Fuchsberger et al. 2012) using the data from the JPT/CHS/CHD subjects and using the 1000 genome project phase 1 (release 16, March 2012) as a reference. We excluded SNPs with a large allele frequency difference between the reference panel and the genome wide association study (GWAS, >0.16) as described previously (Low, Takahashi et al. 2017). We also excluded SNPs with low imputation quality score (Rsq < 0.3) and insertion/deletion polymorphisms. Finally, we selected 12 SNPs within *CLDN2* loci for association analysis. Association of these SNPs with kidney stone risk was assessed by logistic methods. Covariates used in each study are age, sex, and PC1 to PC10 (Price, Patterson et al. 2006). A meta-analysis of study 1 and study 2 was conducted by using METAL. Heterogeneity across the two stages was examined using the Cochrane's Q test (Breslow and Day 1987).

3.3.13 eQTL analysis

Single-tissue *cis*-acting eQTL analysis was performed with FastQTL using Release V7 of the GTEx dataset in the GTEx Portal. Nominal p-values were generated for each *CLDN2* gene variant by testing the alternative hypothesis that the slope of a linear regression model between genotype and claudin-2 expression, in pancreas samples from 220 individuals, deviates from 0. The normalized effect size of the eQTLs, defined as the slope of the linear regression, is computed in a normalized space where magnitude has no direct biological interpretation.

3.3.14 Study approval

All animal experiments were performed in accordance with NIH guidelines on the use of laboratory animals and were approved by the Institutional Animal Care and Use Committee at the University of Kansas Medical Center. For the GWAS, all human subjects provided written

informed consent. The study protocol conformed to the Declaration of Helsinki, and the study was approved by the ethical committee at the University of Tokyo.

3.4 Results

3.4.1 Deletion of *Cldn2* in mice results in hypercalciuria and nephrocalcinosis

Muto, et al. (2010) previously reported that claudin-2 knockout mice are hypercalciuric (Muto, Hata et al. 2010). Using an independent claudin-2 knockout mouse line (Pei, Solis et al. 2016), I confirmed that urinary calcium excretion is increased (Table 3-3). Hypercalciuria is a major risk factor for nephrocalcinosis, the precipitation of calcium deposits within the kidney parenchyma and tubules, and the formation of kidney stones (Evan, Lingeman et al. 2014). I examined 6 month-old mice for evidence of calcium deposition within the kidney. Von Kossa staining, in which ionized silver precipitates with phosphate, showed numerous deposits localized to the renal papilla of *Cldn2*$^{-/y}$ mice (Figure 3-1A). In order to empirically determine the composition of these deposits, I used Alizarin Red S staining, which is specific for calcium and stains calcium phosphate or calcium carbonate at a pH of 4.2 (Proia and Brinn 1985). This revealed a similar pattern of calcium deposition as von Kossa staining (Figure 3-1B). While CaOx cannot be stained by Alizarin Red S at this pH, both CaOx and Alizarin Red S-calcium complexes should exhibit birefringence when examined under polarized light (Wolman 1975). Only Alizarin Red S positive areas showed birefringence by polarized light microscopy, suggesting the absence of CaOx deposits (Figure 3-1C). In order to verify these findings, I performed micro-FTIR and found that the composition of mineral in *Cldn2*$^{-/y}$ mice is composed primarily of calcium phosphate in the form of hydroxyapatite (Figure 3-1D). TEM revealed large circular mineral deposits with a “tree-trunk”-like laminated appearance typical of hydroxyapatite (Figure 3-1E). These deposits appeared to be surrounded by a basement membrane, although no intact epithelium could be identified in the sections. I performed a time course to determine the onset of nephrocalcinosis as measured by X-ray micro-CT. There was scant mineral in wild type kidneys at all age groups examined. In contrast, none of the *Cldn2*$^{-/y}$ mice had papillary deposits at 4.5 months but all had

developed papillary deposition at 6 months and 1 year (Figures 3-1F & 3-1G). *Cldn2*$^{-/-}$ female mice also had extensive nephrocalcinosis at 1 year (data not shown).

I used a combination of von Kossa and immunofluorescence staining to localize these deposits within the renal papilla in 6 month-old mice. No deposits were found within inner medullary collecting ducts or the vasa recta (Figures 3-2A & 3-2C). Occasionally, mineral was located within the lumen of aquaporin-1 (AQP1)-positive descending thin limbs or kidney-specific chloride channel (CLC-K) positive ascending thin limbs of the loops of Henle (Figures 3-2A and 3-2B, arrows). However, the vast majority of deposits did not associate with any epithelial markers so I was unable to distinguish between intratubular deposits with denuded or damaged tubular epithelium and interstitial aggregates of mineral in the majority of deposits analyzed. To detect earlier deposits, I examined the papillae of 5 month-old *Cldn2*$^{-/y}$ mice by TEM. Calcium deposits in these mice were detected within lumina of intact tubules with type 4 cells of ascending thin limbs of the loops of Henle, identifiable by their extensive lateral interdigitations (Figure 3-2D), as well as type 3 cells of descending thin limbs of the loops of Henle, characterized by infrequent TJ strands (Pannabecker 2012) (Figure 3-2E). This indicates that deposits form in the loops of Henle throughout the papillary region. In support of this, the diameter of calcium deposits in 6 month-old *Cldn2*$^{-/y}$ mice on histological cross-sections and micro-CT reconstructions was approximately 20 µm (Figure 3-3), similar to that reported for thin limbs of the loops of Henle (Pannabecker 2012).

3.4.2 Hypercalciuria in *Cldn2*$^{-/y}$ mice is due to defective renal tubular calcium reabsorption

$FECa^{2+}$ was increased in *Cldn2*$^{-/y}$ mice compared with their wild type littermates (Table 3-3). There was no significant difference in serum calcium levels (Table 3-3), and we previously showed that GFR is unchanged in *Cldn2*$^{-/y}$ mice (Pei, Solis et al. 2016). Hence, the filtered load of calcium is unchanged. This suggests that renal tubule calcium reabsorption is decreased in *Cldn2*$^{-/y}$ mice. As claudin-2 is predominantly expressed in the PT and is permeable to calcium

(Yu, Cheng et al. 2009), it is likely that *Cldn2*$^{-/y}$ mice are hypercalciuric due to impaired PT paracellular calcium transport.

Urine calcium excretion in *Cldn2*$^{-/y}$ mice might also be affected by changes in expression of calcium transporters in more distal segments of the kidney. We previously showed that expression of thick ascending limb (TAL) calcium transporters, such as claudin-16 and -19 and the electroneutral NKCC2 are not different between *Cldn2*$^{-/y}$ and wild type mice (Pei, Solis et al. 2016). I found that protein expression of calbindin-D28k, a cytosolic calcium carrier protein known to be upregulated by 1,25$(OH)_2$ vitamin D_3 (Hoenderop, Nilius et al. 2005), is unchanged in *Cldn2*$^{-/y}$ mice (Figure 3-4A-B). I also measured mRNA expression of claudin-14, a negative regulator of TAL paracellular calcium transport, and found no difference (Figure 3-4C). Similarly, I found no difference in mRNA expression of genes involved in active, transcellular calcium transport in the DCT and CNT, including TRPV5, calbindin-D28k, and the Na^+-Ca^{2+} exchanger (NCX1) (Figure 3-4C). Thus, changes in distal calcium transport proteins do not contribute to the hypercalciuria in *Cldn2*$^{-/y}$ mice, nor do they compensate for it.

3.4.3 Concurrent intestinal hyperabsorption of calcium in *Cldn2*$^{-/y}$ mice

If the hypercalciuria in *Cldn2*$^{-/y}$ mice is due to primary renal calcium wasting, we would expect them to be in negative calcium balance and hence to exhibit a compensatory increase in the calciotropic hormones, PTH and 1,25$(OH)_2$ vitamin D_3 (Hoenderop, Nilius et al. 2005). However, there were no significant differences in the levels of these hormones (Table 3-3). We would also expect *Cldn2*$^{-/y}$ mice to have calcium loss from bone, leading to reduced bone mineral density (BMD) and volume. To test this, I utilized DEXA analysis to measure BMD at 4.7, 6, 8, and 10 weeks of age. I found no detectable difference in either total or lumbar BMD in *Cldn2*$^{-/y}$ mice (Figures 3-5A & 3-5B). I analyzed femurs from 10 week-old mice using micro-CT and again found no difference in the density or quality of the bone between genotypes (Table 3-4). It is possible that *Cldn2*$^{-/y}$ mice could adequately compensate for calcium loss on a normal calcium diet. Thus, I switched a subset of animals to a low calcium diet at 12 weeks and measured BMD

weekly over the next 4 weeks. Again, there was no difference in BMD between wild type and *Cldn2*$^{-/y}$ mice (Figures 3-5A & 3-5B). Figure 3-5C shows representative micro-CT reconstructions of femurs from 10 week-old mice, which do not show any gross differences in cortical or trabecular bone in *Cldn2*$^{-/y}$ mice. Another group of mice was aged to one year and confirmed that *Cldn2*$^{-/y}$ mice BMD remained similar to wild type mice on a normal calcium diet (Figures 3-5D & 3-5E).

The finding that there was no change in the levels of PTH, 1,25$(OH)_2$ vitamin D_3 and BMD in *Cldn2*$^{-/y}$ mice despite marked hypercalciuria suggests that they may have concurrent intestinal hyperabsorption of calcium. Indeed, concurrent renal calcium wasting and intestinal hyperabsorption of calcium is typical of idiopathic hypercalciuria in patients with kidney stones and in hypercalciuric rats (Kim, Sessler et al. 1993, Moe 2006). Moreover, claudin-2 is known to be expressed in the intestinal tract. To test the hypothesis that there is also primary intestinal hyperabsorption of calcium in *Cldn2*$^{-/y}$ mice, I determined whether the hypercalciuria was attenuated by a reduction in dietary calcium content. I placed animals in metabolic cages on a control diet (0.6% Ca^{2+}), and after 5 days switched half of them to a calcium-deficient (<0.01% Ca^{2+}) diet (Figure 3-6A). I found that urinary calcium excretion in *Cldn2*$^{-/y}$ mice is highly sensitive to dietary calcium intake (Figure 3-6A). On the control diet, $FECa^{2+}$ in *Cldn2*$^{-/y}$ mice was approximately five times higher than in wild type mice (0.69% vs. 0.14%, Figure 3-6B). In contrast, the $FECa^{2+}$ of *Cldn2*$^{-/y}$ mice on the Ca^{2+}-deficient diet was only twice that of wild type mice (0.22% vs. 0.11%) (Figure 3-6B). No differences in serum calcium were found between the groups (Figure 3-6C).

These results suggest that hypercalciuria in *Cldn2*$^{-/y}$ mice is due to intestinal hyperabsorption of calcium, in addition to a primary renal calcium leak. To confirm this, I performed metabolic balance studies over a 3-day period on the control diet (0.6% Ca^{2+}). As expected, renal calcium excretion was increased in *Cldn2*$^{-/y}$ mice (Figure 3-7A). Intestinal calcium absorption, determined from the difference between dietary calcium intake and fecal calcium content, was greater in *Cldn2*$^{-/y}$ mice than in wild type mice (Figure 3-7B). Net calcium balance

was slightly positive in *Cldn2*$^{-/y}$ mice and greater than in wild type mice (Figure 3-7C). I measured intestinal expression of TRPV6, calbindin-D9k, and the plasma membrane calcium ATPase (PMCA1) and found no difference between genotypes (Figure 3-8).

3.4.4 Variants in the *CLDN2* gene are associated with nephrolithiasis in the general population

Because claudin-2 knockout in mice caused hypercalciuria and nephrocalcinosis, we hypothesized that genetic variants in *CLDN2* might be associated with the risk of kidney stones in humans. To date, several GWAS of nephrolithiasis have been performed in the general population (Thorleifsson, Holm et al. 2009, Urabe, Tanikawa et al. 2012, Oddsson, Sulem et al. 2015), but none of these studies have included the X chromosome in their analyses. To evaluate the role of *CLDN2* in human kidney stones, we examined the association of 12 SNPs in the *CLDN2* locus with disease risk. In this analysis, a total of 11,130 kidney stone cases and 187,639 controls were analyzed (Tables 3-2 & 3-5). As a result, 9 SNPs showed significant association with disease risk with p-values of 0.0462-0.0055 (Table 3-6). Three of these SNPs, rs7057398, rs12008279, and rs5917027, were previously shown to be associated with chronic pancreatitis (Whitcomb, LaRusch et al. 2012).

My hypothesis predicts that causal variants for nephrolithiasis in *CLDN2* should decrease claudin-2 tissue expression. I performed an analysis for *cis*-acting eQTL in *CLDN2* using the dataset from the Genotype-Tissue Expression (GTEx) project. Seven of the SNPs associated with nephrolithiasis were genotyped in GTEx, and in all 7 cases, the nephrolithiasis risk allele was strongly associated with decreased claudin-2 expression in pancreatic tissue (Table 3-6). At this time, there are insufficient number of kidney cortex samples in GTEx to perform eQTL analysis of kidney expression. However, we know that *CLDN2* has three alternative first exons and hence three alternative promoters. In the GTEx expression data, human kidney cortex and pancreas both exclusively express the same transcript (ENST00000540876.1) and therefore use the same

promoter. Thus, it is highly likely that transcriptional regulation by *cis*-acting eQTLs in these 2 tissues is identical.

Interestingly, the alleles in *CLDN2* that are associated with increased risk of pancreatitis (Whitcomb, LaRusch et al. 2012) are all associated with increased claudin-2 expression in the pancreas, and with decreased risk for nephrolithiasis (Figures 3-9 & 3-10). The strong reciprocal relationship between risk variants for these two diseases and tissue expression levels increases the likelihood that these represent true causal disease associations.

3.5 Discussion

PT calcium reabsorption is passive and follows sodium and water reabsorption. It was previously shown by Muto et al. (2010) that deletion of claudin-2, which is highly expressed in the PT, causes a reduction in TER and P_{Na} in PTs *ex vivo* (Muto, Hata et al. 2010). My work adds to this by determining that *Cldn2*$^{-/y}$ mice have a large decrease in renal calcium reabsorption that cannot be explained by reduced expression of calcium transporters in the TAL or DCT / connecting tubule. Additionally, I found that *Cldn2*$^{-/y}$ mice remain hypercalciuric after 5 days on a calcium deficient diet. This suggests that, although these mice are able to conserve sodium similar to wild type animals on a normal and low sodium diet (Pei, Solis et al. 2016), they are unable to fully compensate for a proximal renal leak of calcium regardless of dietary calcium content. This evidence suggests that *Cldn2*$^{-/y}$ mice are deficient in PT calcium transport, implicating claudin-2 as the mediator of paracellular calcium reabsorption in the PT. Ultimately, micropuncture experiments are needed to confirm a PT-specific calcium leak in *Cldn2*$^{-/y}$ mice.

In addition, I found a slightly positive calcium balance and a pronounced effect of dietary calcium on urinary excretion in *Cldn2*$^{-/y}$ mice. These data suggest that, in addition to reduction in renal calcium reabsorption, altered calcium absorption or secretion in the gastrointestinal tract also occurs as a consequence of global claudin-2 deletion. Similar to *Cldn2*$^{-/y}$ mice, recurrent kidney stone formers often exhibit both intestinal hyperabsorption of calcium and reduced renal calcium reabsorption (Worcester, Coe et al. 2008). Whether common mechanisms of idiopathic

hypercalciuria originate from intestinal hyperabsorption, reduced renal reabsorption, or primary defects in both tissues remains an open debate. However, given the calcium permeating properties of claudin-2, its low expression and highly restricted localization to intestinal crypts in adult mammals (Rahner, Mitic et al. 2001), and its regulation by $1,25(OH)_2$ vitamin D_3 (Zhang, Wu et al. 2015), I find the hypothesis that loss of claudin-2 in the intestine directly causes increased paracellular calcium absorption unlikely. It should be noted that infection of *Cldn2*$^{-/y}$ mice with the enteropathogenic bacteria *C. rodentium* increases the permeability of the small intestine via the "leak pathway," which allows the passage of solutes and larger molecules secondary to intestinal damage (Tsai, Zhang et al. 2017). However, loss of claudin-2 does not affect colonic histology and there is no difference in the baseline characteristics of fecal sodium and water excretion (Tsai, Zhang et al. 2017), suggesting that the "leak pathway" is not increased in healthy *Cldn2*$^{-/y}$ mice. As such, it is difficult to see how loss of claudin-2 would contribute to intestinal calcium permeability. Additionally, experiments by Tamura show that the small intestines of claudin-2 knockout animals have reduced P_{Na} (Tamura, Hayashi et al. 2011). Given the properties of claudin-2 as both a sodium and a calcium permeable pore, we would expect that calcium permeability is reduced as well. An intriguing possibility is that claudin-2 mediates intestinal losses of calcium. However, it is not clear what role, if any, dietary calcium plays in the regulation of intestinal calcium secretion so this may not explain the strong relationship between dietary calcium and urinary calcium excretion.

The relevance of the present study is underlined by findings that the majority of recurrent kidney stone formers have hypercalciuria and reduced calcium reabsorption in the PT (Worcester, Coe et al. 2008). Another important similarity between *Cldn2*$^{-/y}$ mice and recurrent kidney stone formers is the presence of calcium deposits in the renal papilla. My work suggests that claudin-2 deletion and the subsequent increase in delivery of calcium to the loops of Henle leads to papillary nephrocalcinosis in mice. In humans, nephrocalcinosis is appreciable on CT scan in approximately one sixth of CaOx stone formers and three quarters of hydroxyapatite stone

formers (Bhojani, Paonessa et al. 2015). It is well established that Randall's plaques are a precursor to the most common stones, composed of CaOx, as residual plaque is found in approximately one third of intact stones (Letavernier, Vandermeersch et al. 2015). On endoscopic examination, 74% of stone formers have Randall's plaques identified on the papillary epithelium surface, compared with 43% of non-stone forming patients (Low and Stoller 1997). Expressed as a percentage, increased coverage of plaque on the papillary epithelium is associated with CaOx stones as well as high urine calcium and low urine volume (Kuo, Lingeman et al. 2003). Unfortunately, no animal models have yet been identified which recapitulate the deposition of calcium phosphate within the basement membranes of the loops of Henle (Wu 2015). One potential reason for the failure to reproduce Randall's plaques in mice is the comparative differences between mice and humans in medullary architecture (Wu 2015). Whereas the papillary epithelium of the loops of Henle is surrounded by expansive interstitial connective tissue in humans, the majority of loops of Henle in mice have sparse interstitial tissue and are closely apposed with one another and other papillary tubules.

A form of nephrocalcinosis characterized by intratubular plugs of calcium is even more common than Randall's plaques, found in the papillae of 92% of cancer patients without a history of kidney stone disease (Huguet, Le Dudal et al. 2017). The presence of medullary plugging is highly associated with Randall's plaques (Verrier, Bazin et al. 2016). Intratubular plugs are composed of calcium phosphate and located within AQP1 negative loops of Henle (Huguet, Le Dudal et al. 2017), consistent with both the lowermost portions of descending thin limbs and the ascending thin limbs (Wei, Rosen et al. 2015). Observations that intratubular plugs correlate with the presence of Randall's plaques have led to a newly proposed model of nephrocalcinosis and stone formation in humans, in which medullary plugging precedes plaque formation and subsequent stone growth (Hsi, Ramaswamy et al. 2017). Indeed, present evidence suggests that the severity and density of upstream calcium phosphate medullary plugging can predict Randall's plaque deposition (Hsi, Ramaswamy et al. 2017, Sherer, Chen et al. 2018). The nephrocalcinosis

I have identified in *Cldn2*$^{-/y}$ mice is remarkably similar to the intratubular plugs described in kidney stone patients, despite the lack of Randall's plaque-like structures.

In addition to Randall's plaque-associated CaOx stone formers, a significant proportion of stone formers develop calcium phosphate stones (Evan, Lingeman et al. 2014). This stone type is associated with intratubular plugs of calcium phosphate, rather than Randall's plaques. However, this tubule plugging is localized to the inner medullary collecting ducts in these patients (Evan, Lingeman et al. 2014). Clearly, *Cldn2*$^{-/y}$ mice share features of both types of stone formers, as they form nephrocalcinosis that is localized to the loops of Henle similar to Randall's plaques but is located within tubular lumina rather than the interstitium, mimicking calcification found in hydroxyapatite stone formers (Evan, Lingeman et al. 2014) or that which is common in the general population but has not been definitively linked to kidney stone disease.

Given the significant differences between nephrocalcinosis in stone forming humans and *Cldn2*$^{-/y}$ mice, it is useful to revisit previous mouse models of kidney stone disease. A number of mouse models have been described that share elements of human kidney stone disease. For instance, models involving distal calcium transporters such as *Trpv5*$^{-/-}$ (Hoenderop, van Leeuwen et al. 2003, Renkema, Velic et al. 2009) and *Cldn16*$^{-/-}$ (Will, Breiderhoff et al. 2010) mice have hypercalciuria but lack papillary nephrocalcinosis or nephrolithiasis under normal conditions. In each case, it has been presumed that the lack of nephrocalcinosis is due to compensatory adaptations by the kidney. Perhaps due to the fact that many adaptations occur in the distal tubule, such as acidification of the urine by the H^+-ATPase proton pump or reduced water transport via AQP2 (Renkema, Velic et al. 2009), *Cldn2*$^{-/y}$ mice are unable to prevent nephrocalcinosis within the more proximal loops of Henle. It should be noted that mild calcification was shown in the medullae of transgenic claudin-16 knockdown mice (Hou, Shan et al. 2007) and patients with loss-of-function mutations in claudins-16 and -19, causing FHHNC, develop medullary calcifications early in life (Konrad, Hou et al. 2008). This does suggest a role for distal calcium transport in renal calcification. However, FHHNC pathology is severe and distinct from

idiopathic kidney stone formers, characterized by immature glomeruli, fibrosis, glomerulosclerosis, and declining renal function (Kuwertz-Broking, Frund et al. 2001).

Additionally, several mouse models of papillary nephrocalcinosis have been described in which proteins involved in the inhibition of crystal formation are ablated, such as osteopontin (encoded by gene *Opn*) and Tamm-Horsfall protein (encoded by gene *Thp*) (Mo, Liaw et al. 2007). Only about half of *Thp*$^{-/-}$ mice were reported to have nephrocalcinosis present at 6 months of age (Liu, Mo et al. 2010), and nephrocalcinosis was reported to be even less frequent in *Opn*$^{-/-}$ mice (Mo, Liaw et al. 2007). Hypercalciuria is not present in either mouse model (Mo, Liaw et al. 2007). Dysfunctional phosphate transport in the PT, as occurs in mice with deletion of the type II sodium phosphate cotransporter (Npt2a) or sodium hydrogen exchange regulator factor-1 (NHERF1), also results in papillary nephrocalcinosis. *Npt2a*$^{-/-}$ mice, for instance, have renal phosphate wasting, hypophosphatemia, and hypercalcemia in addition to hypercalciuria, and develop nephrocalcinosis more severely within cortex than medulla (Khan and Glenton 2008). Similarly, NHERF1 loss causes reduction of Npt2a in the PT and leads to phosphate wasting, hypophosphatemia, hypercalciuria, and nephrocalcinosis (Weinman, Mohanlal et al. 2006). Contrast all of these mouse models with *Cldn2*$^{-/y}$ mice, in which urinary calcium excretion is high, serum and urinary phosphate are normal (Muto, Hata et al. 2010, Schnermann, Huang et al. 2013), and 100% of mice at 6 months and 1 year of age had clearly appreciable papillary deposition of mineral on micro-CT reconstructions. I purport that these characteristics make *Cldn2*$^{-/y}$ mice a more physiologically relevant model of human idiopathic kidney stone disease than has previously been described (Wu 2015). An important advance I have made in studying kidney stone disease is that previous models of papillary nephrocalcinosis relied solely on histological analyses to detect calcium deposition in kidneys, whereas I utilized micro-CT with a high sensitivity for detecting nephrocalcinosis in intact kidneys. This technique should aid future studies focused on nephrocalcinosis and kidney stone disease.

The striking findings of hypercalciuria and papillary nephrocalcinosis in *Cldn2*$^{-/y}$ mice led us to test the hypothesis that polymorphisms in the *CLDN2* locus associate with kidney stone disease. Our analysis identified 9 SNPs that are associated with nephrolithiasis, many of which are incredibly common in the general population. Subsequent eQTL analysis revealed that 7 of the SNPs identified share a strong association with reduced claudin-2 expression in human pancreatic tissue. Unexpectedly, the non-risk alleles of several of these SNPs have been identified previously with regards to alcohol-related pancreatitis and increased pancreatic claudin-2 expression. We hypothesize that, in addition to reducing claudin-2 expression in the pancreas, these SNPs result in lowered claudin-2 expression in the kidney. Our future studies will aim at analyzing genotype-renal gene expression association as has been described recently (Ko, Yi et al. 2017).

In conclusion, the evidence I present suggests that paracellular calcium transport in the proximal nephron is mediated at least in part by claudin-2, and deletion of claudin-2 leads to intratubular deposition of calcium in the loops of Henle. This pattern of deposition is similar to nephrocalcinosis in human subjects, and mounting evidence suggests that a direct relationship exists between the abundance and density of these deposits, Randall's plaques, and idiopathic kidney stone disease. The relevance of these findings is highlighted by our findings that common SNPs in the *CLDN2* locus associate with kidney stone disease. Importantly, these SNPs are significantly associated with reduced tissue expression of claudin-2. Conditional knockout studies are needed to determine the absolute contribution of renal claudin-2 expression to hypercalciuria in *Cldn2*$^{-/y}$ mice. Future studies will focus on potential pharmacologic strategies to increase renal claudin-2 expression, as this may be a useful strategy for the preventative treatment of recurrent kidney stone formation.

Table 3-1. Primers used for qRT-PCR

Gene	5'- Forward sequence -3'	5'- Reverse sequence -3'	Product Size (bp)
Calbindin-D28k	GTGTGTCCTCTGCTGGTTATT	CCTGACCCAAACCTGCATTA	127
Calbindin-D9k	TTCAGTCAGAGTTCCCCAGC	CCATCGCCATTCTTATCCAGC	82
Claudin-12	AGGTATTCCCGAGCGGAGCCA	CCCGGAGGCTTCAGGGAACCA	56
Claudin-14	GCAGCTGCGGCAAAGGAGTCT	ACGGCCGTCTAATGGGTCCCT	136
Claudin-2	TGGCGTCCAACTGGTGGGCT	ACCGCCGTCACAATGCTGGC	120
GAPDH	CCCAGCAAGGACACTGAGCAAGAG	GGCTCCCTAGGCCCCTCCTGTTATT	116
NCX1	AGTCTCCCACCCAATGTTTC	CTCCTGTTTCTGCCTCTGTATC	106
PMCA1	TTAGAGAAGCCAGAATCAAGAAGT	CAGCATCAGTGTCATCAATAAGG	109
TRPV5	GAGGAAGTACAAGAGCAGCTATC	CCTGGACAAAGGAGGTGTTT	102
TRPV6	ACACACACTGCAGAAAGTCCA	TCAGAGCCTGGACATCGTTT	96
β-actin	CTAAGGCCAACCGTGAAAAG	ACCAGAGGCATACAGGGACA	104

Table 3-2. Characteristics of study population

Stage	Sample type	Source	Platform	Number of samples	Female (%)	
GWAS study 1	Kidney stone	BBJ	OmniExpressExome or OmniExpress+HumanExome	6,246	1,531	(24.5%)
	Control	JPHC, J-MICC, ToMMo	OmniExpressExome	28,867	17490	(60.6%)
GWAS study 2	Kidney stone	BBJ	OmniExpressExome or OmniExpress+HumanExome	4,884	1,302	(26.7%)
	Control	BBJ	OmniExpressExome or OmniExpress+HumanExome	158,772	75207	(47.4%)

Note: BBJ:Biobank Japan, JPHC: Japan Public Health Center-based prospective study, J-MICC: Japan Multi-Institutional Collaborative Cohort study, ToMMo:Tohoku Medical Megabank Organization

Table 3-3. Serum and urinary parameters of mice on standard lab chow

Parameter	Wild type			*Cldn2*$^{-/y}$			
Serum	**Mean**	**SEM**	**n**	**Mean**	**SEM**	**n**	**P value**
Calcium (mg/dL)	10.24	0.17	9	10.74	0.43	8	0.27
1,25-dihydroxyvitamin D (pmol/L)	193	13	8	201	21	8	0.74
PTH (pg/mL)	696	158	11	699	134	10	0.99
Urine							
FECa (%)	0.11	0.01	8	0.20	0.01	7	0.0001
Phosphorus/Cr (mg/mg)	7.73	1.64	8	6.65	1.76	5	0.67
Oxalate/Cr (mg/mg)	0.09	0.01	5	0.12	0.01	4	0.22
Citrate/Cr (mg/mg)	6.79	0.58	8	7.11	0.95	5	0.76
Mg/Cr (mg/mg)	3.57	0.20	8	3.11	0.25	5	0.18

PTH, parathyroid hormone; FECa, fractional excretion of calcium; Cr, creatinine

Table 3-4. Micro-CT analysis of femurs from 10 week-old animals

		Wild type	*Cldn2*$^{-/y}$
	Sample size (n)	*5*	*4*
Epiphyseal cancellous bone	BS/BV	97.1 ± 2.4	92.6 ± 6.2
	BV/TV trabecular	0.0426 ± 0.0049	0.0507 ± 0.0083
	BV/TV cortical	0.992 ± 0.001	0.993 ± 0.000
	Tb.N (1/mm)	3.65 ± 0.41	4.01 ± 0.06
	Tb.Th (mm)	0.0305 ± 0.0025	0.0332 ± 0.0021
	Tb.Sp (mm)	0.290 ± 0.043	0.247 ± 0.005
	Connectivity (1/mm^3)	47.8 ± 13.7	74.6 ± 12.9
	SMI (1)	3.08 ± 0.09	2.82 ± 0.12
	Anisotropy (1)	1.55 ± 0.05	1.60 ± 0.08
	MOI (mm^4)	0.532 ± 0.024	0.613 ± 0.021*
	Ct.Th (mm)	0.154 ± 0.008	0.149 ± 0.011
Cortical bone	MOI (mm^4)	0.337 ± 0.035	0.378 ± 0.058
	BV (mm^3)	1.33 ± 0.09	1.51 ± 0.12
	TV_δ (mm^3)	1.32 ± 0.09	1.50 ± 0.13
	BV/TV_δ	0.988 ± 0.002	0.990 ± 0.001
	TV_α (mm^3)	2.93 ± 0.15	3.36 ± 0.21
	BV/TV_α	0.451 ± 0.008	0.447 ± 0.010
	Ct.Th (mm)	0.184 ± 0.009	0.188 ± 0.010
	BS/BV	11.5 ± 0.5	11.2 ± 0.5
	BS (mm^2)	15.1 ± 0.4	16.8 ± 0.6
	MV_ρ=TV_α-BV (mm^3)	1.60 ± 0.06	1.86 ± 0.09*
	BA (mm^2)	0.758 ± 0.050	0.798 ± 0.068
	TA (mm^2)	1.68 ± 0.08	1.78 ± 0.11
	BA/TA	0.451 ± 0.008	0.447 ± 0.010
	Periosteal circ. (mm)	4.58 ± 0.11	4.72 ± 0.15
	Endosteal circ (mm)	3.39 ± 0.06	3.51 ± 0.09

*P<0.05 vs. wild type using Student's t-test
Index: BS = bone surface; BS/BV = bone-surface/total-bone volume (1/mm); BV/TV = bone-volume/total-volume (%); Tb.N = trabecular number; Tb.Th = trabecular thickness; Tb.Sp = trabecular spacing; Connectivity = number of connected structures calculated by the Euler characteristic; SMI = structural modeling index; Anisotropy = anisotropic index of longitudinal/traverse tensile compressive force resistance; MOI = moment of inertia; Ct.Th = cortical thickness; TVδ = total tissue-volume excluding marrow-volume; BV/TVδ =bone volume/TVδ (%); MVρ = (TVα-BV) = marrow-volume of defined region of interest (ROI) of central diaphysis (mm^3) where TVα is the total tissue volume including marrow volume and TVδ (mm^3); BA = bone area; TA = total area; Periosteal circumference = bone-area; Endosteal circumference = total area.

Table 3-5. Association of *CLDN2* gene variants with nephrolithiasis in two independent GWAS

	Major allele	Minor allele	GWAS1	GWAS2	Meta-analysis of GWAS1 and GWAS2										
MarkerName			OR	OR	Effect	StdErr	P-value	Direction	HetISq	HetChiSq	HetDf	HetPVal	chrloc	gene	OR (minor/major)
rs7057398	T	C	1.032	1.027	0.0289	0.0119	0.01522	++	0	0.041	1	0.8404	106144529	*RIPPLY1*	1.029
rs55662019	A	T	0.950	0.893	-0.0862	0.0341	0.01136	--	0	0.813	1	0.3673	106144537	*RIPPLY1*	0.917
rs140960200	G	C	1.035	1.181	0.0953	0.0585	0.1035	++	21.8	1.279	1	0.258	106146239	*RIPPLY1*	1.100
rs138679347	T	A	1.089	1.257	0.1557	0.0838	0.06341	++	0	0.729	1	0.3933	106146518	*RIPPLY1*	1.168

rs76106514	C	T	1.022	0.996	0.0088	0.049	0.858	+-	0	0.068	1	0.7939	106148520	*CLDN2*	1.009
rs187570171	C	G	1.022	0.996	0.0088	0.049	0.858	+-	0	0.068	1	0.7939	106150854	*CLDN2*	1.009
rs12837024	C	T	1.035	1.026	0.0296	0.0127	0.02007	++	0	0.08	1	0.7773	106154233	*CLDN2*	1.030
rs73247968	C	A	1.046	1.024	0.0345	0.0173	0.04623	++	0	0.365	1	0.5456	106155095	*CLDN2*	1.035
rs140177585	G	T	1.087	1.255	0.154	0.0836	0.06542	++	0	0.741	1	0.3893	106159601	*CLDN2*	1.166
rs141976320	G	A	1.087	1.254	0.1539	0.0836	0.06551	++	0	0.742	1	0.389	106159716	*CLDN2*	1.166
rs12008279	G	A	0.949	0.888	-0.0886	0.0337	0.008566	--	0	0.975	1	0.3234	106160702	*CLDN2*	0.915
rs140820041	G	C	1.052	1.045	0.0473	0.067	0.4803	++	0	0.002	1	0.9657	106161787	*CLDN2*	1.048

rs5917027	C	T	0.962	0.898	-0.0772	0.0278	0.005502	--	31.7	1.463	1	0.2264	106162634	*CLDN2*	0.926
rs6523906	A	G	0.961	0.898	-0.0772	0.0278	0.005502	--	31.7	1.463	1	0.2264	106162724	*CLDN2*	0.926
rs148778547	T	C	1.015	0.993	0.0036	0.0449	0.9357	+-	0	0.058	1	0.8098	106163063	*CLDN2*	1.004
rs6622121	T	C	0.961	0.899	-0.0767	0.0278	0.005783	--	30	1.429	1	0.2319	106168101	*CLDN2*	0.926
rs147829672	C	A	0.935	0.922	-0.0754	0.0284	0.008005	--	0	0.069	1	0.7922	106173341	*CLDN2*	0.927
rs148181238	T	C	1.053	1.044	0.0473	0.0667	0.4781	++	0	0.003	1	0.9553	106175421	*CLDN2*	1.048

MarkerName, dbSNP reference SNP cluster ID
OR, odds ratio for nephrolithiasis with minor allele as the reference allele. When major allele is associated with disease risk, OR is >1
Meta-analysis of GWAS1 and GWAS2 was performed using METAL (Manning AK et al., Genet Epidemiol. 2011 Jan;35(1):11-8)
Effect and StdErr, summarized estimate and standard error of the SNP beta coefficient
Direction, study-specific direction of the effect (GWAS1, GWAS2). + means major allele is risk allele in that study.
HetChiSq, heterogeneity test statistic
HetDf, heterogeneity test statistic degrees of freedom

Table 3-6. *CLDN2* gene variants associated with nephrolithiasis

Marker Name	Major allele	Minor allele	MAF	METAL		GTEx	
				OR	P-value	Expression ratio	P-value
rs7057398	T	C	0.4848	1.029	0.0152	0.619	1.7E-15
rs55662019	A	T	0.1099	0.917	0.0113	1.139	0.059
rs12837024	C	T	0.231	1.0303	0.0200	0.638	2.8E-12
rs73247968	C	A	0.1465	1.035	0.0462	0.644	1.2E-08
rs12008279	G	A	0.3698	0.915	0.0085	1.162	5.7E-03
rs5917027	C	T	0.2477	0.925	0.0055	1.297	2.4E-06
rs6523906	A	G	0.3746	0.925	0.0055	1.234	1.0E-04
rs6622121	T	C	0.3828	0.926	0.0057		
rs147829672	C	A	0.014	0.927	0.0080		

METAL, association of variants with nephrolithiasis by meta-analysis of two independent GWAS
GTEx, association of variants with claudin-2 tissue expression in pancreas by eQTL analysis
MAF, minor allele frequency (1000 genome project)
OR, odds ratio for nephrolithiasis with minor allele as the reference allele. When major allele is associated with disease risk, OR is >1.
Expression ratio, exponential of the normalized effect size (beta), major/minor allele

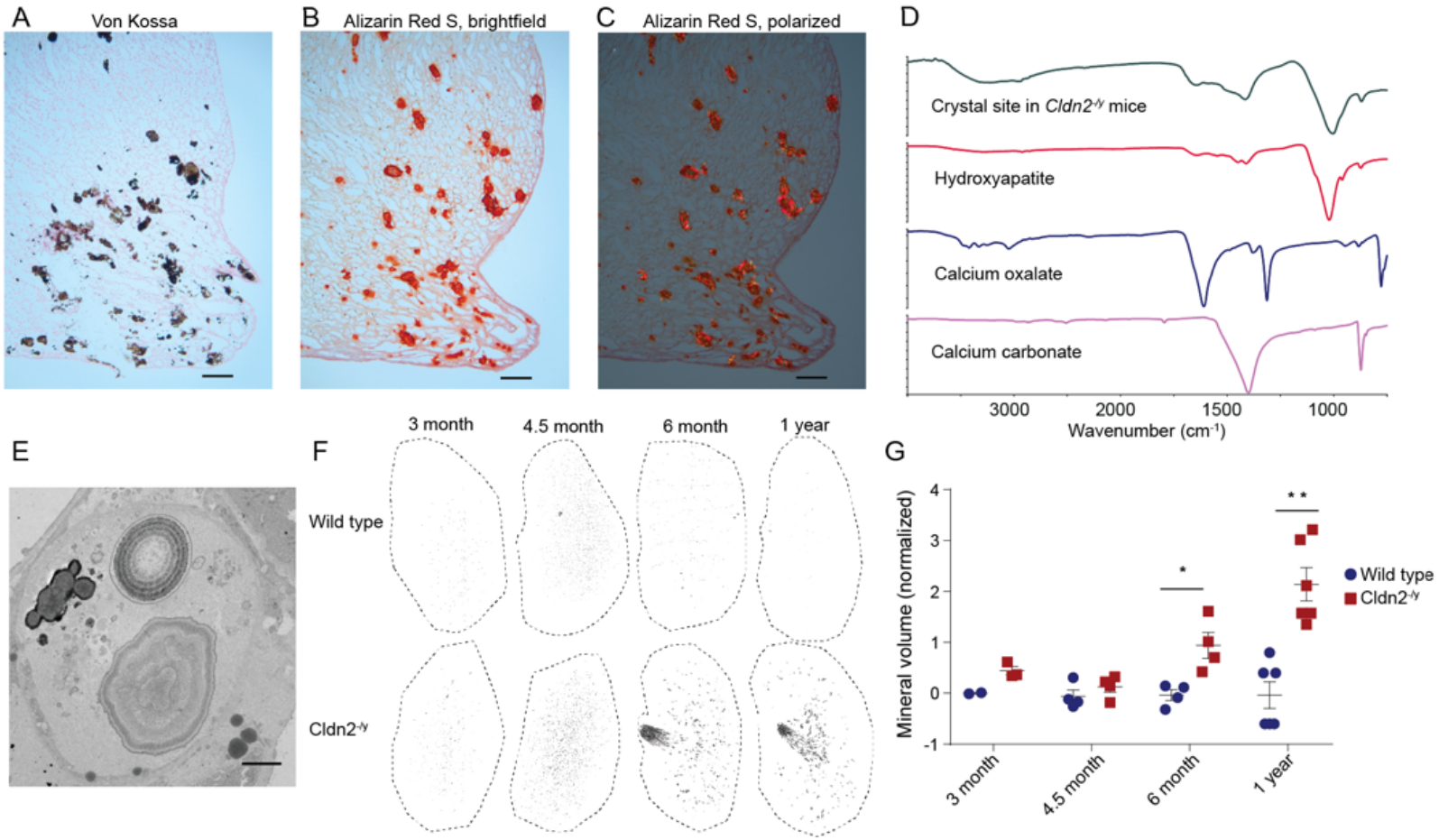

Figure 3-1. *Cldn2*$^{-/y}$ mice develop large calcium deposits within the renal papilla at 6 months of age.

A 6 month old *Cldn2*$^{-/y}$ mouse exhibits calcium deposits stained and visualized with the following methods: (A) Von Kossa (B) Alizarin Red S, pH 4.2, brightfield and (C) Alizarin Red S, pH 4.2, polarized light. Scale bars = 100 µm. (D) Micro-FTIR analysis shows that deposits are composed of primarily hydroxyapatite. TEM reveals (E) large diameter aggregates of matrix and mineral with laminated deposits characteristic of hydroxyapatite. Scale bar = 2 µm. (G) Representative 3D reconstructions of micro-CT analysis on kidneys from wild type and *Cldn2*$^{-/y}$ and (H) quantitation of the mineral volume in reconstruction analysis. Data were normalized and log transformed prior to plotting for analysis. Bars are Mean ± SEM. T-tests were performed at each time point, and corrected for multiple comparisons using the Bonferroni-Dunn method; * P>0.05; **P<0.01.

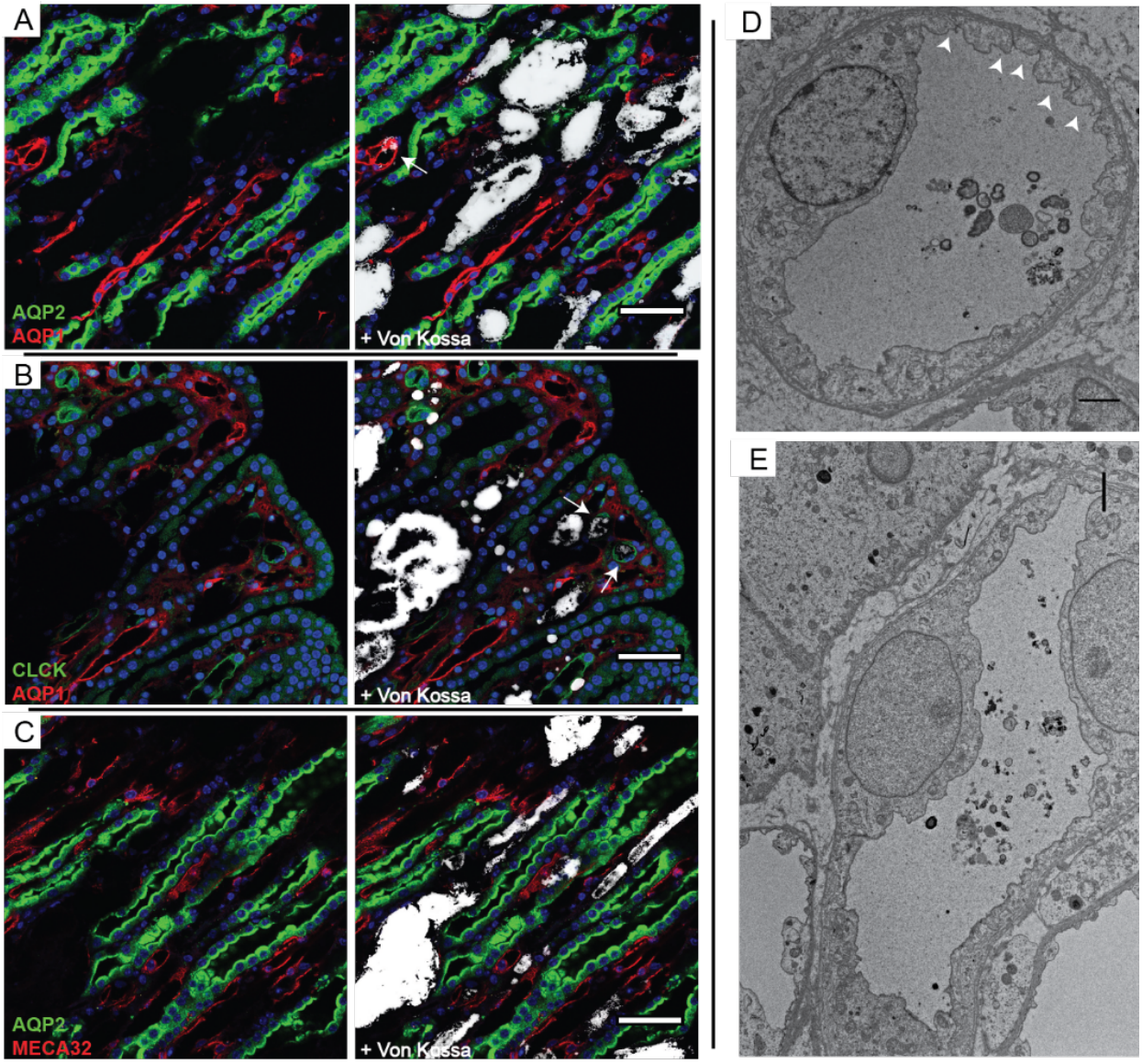

Figure 3-2. Nephrocalcinosis occurs within the loops of Henle of *Cldn2*$^{-/y}$ mice.

Confocal microscopy of papillary sections from *Cldn2*$^{-/y}$ mice shows von Kossa staining of deposits (pseudo-colored white) co-labeled with the following tubule markers: (A) Inner medullary collecting duct (AQP2) and thin descending limbs (AQP1), (B) thin descending limbs (AQP1) and thin ascending limbs (CLC-K), and (C) Inner medullary collecting ducts (AQP2) and vasa recta (MECA-32). Association of calcium deposits with tubule markers is infrequent, but instances of colocalization with AQP1 or CLC-K positive thin limbs are occasionally seen (arrows in A and B). Scale bars = 50 μm. Electron microscopy of papillae from 5 month-old *Cldn2*$^{-/y}$ mice shows small mineral deposits within (D) type 4 thin descending limb cells with frequent tight junctions (arrowheads) as well as (E) type 3 thin ascending limb cells lacking these features. Scale bars = 2μm.

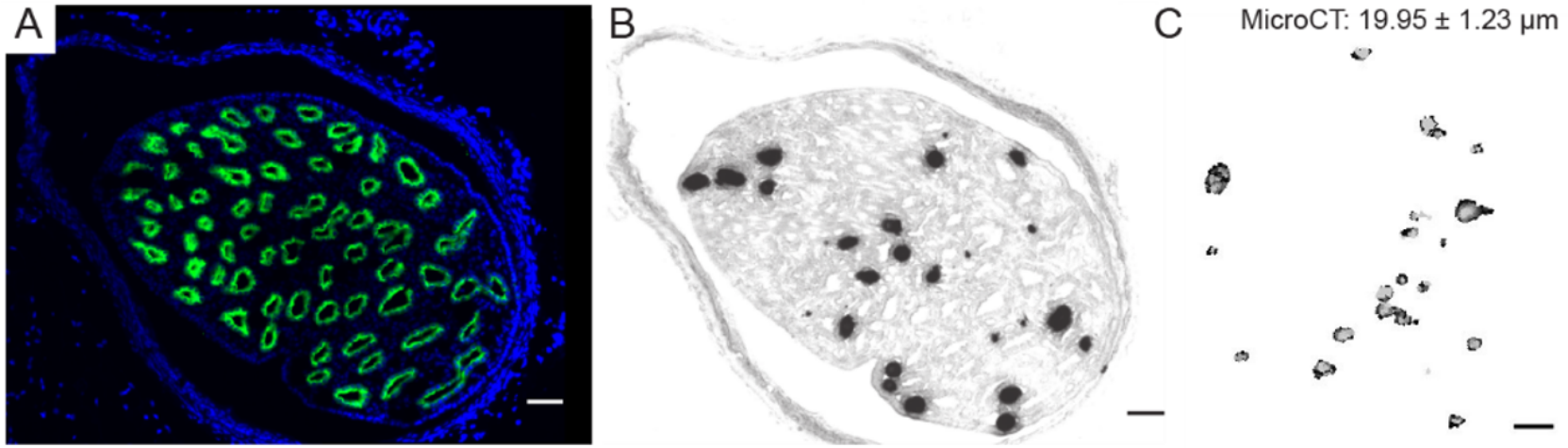

Figure 3-3. Representative cross-section images used for quantitation of Ca^{2+} deposit diameter.

Papillary tissue from a 6 month-old *Cldn2*$^{-/y}$ mouse stained with (A) AQP2 (green) and DAPI (blue) in addition to (B) von Kossa. AQP2 and von Kossa staining never overlap. Two sections from separate Cldn2$^{-/y}$ animals were used for quantitation. (C) Micro-CT reconstruction slice from a 1 year-old Cldn2$^{-/y}$ mouse papilla in cross-section. Density diameter, measured using ImageJ, is shown above the image. Scale bars = 50μm.

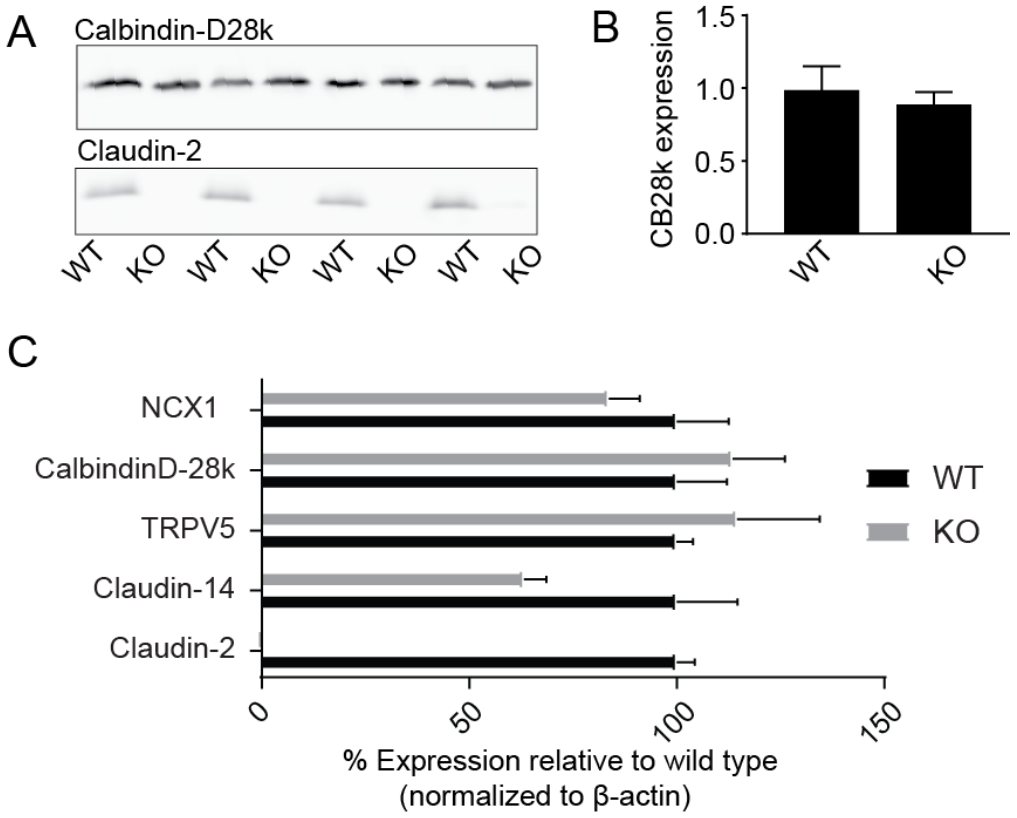

Figure 3-4. Renal expression of calcium transporters is not different in *Cldn2*$^{-/y}$ mice.

Quantitation of calcium transporters in wild type (WT) and *Cldn2*$^{-/y}$ (KO) mice. (A) Western blotting for calbindinD-28k and claudin-2 and (B) quantitation of calbindin-D28k protein expression. (C) Quantitative PCR measurements of renal calcium transporters shows no difference in mRNA expression (n=4 per group, with the exception of TRPV5 n=5). Bars are Mean ± SEM.

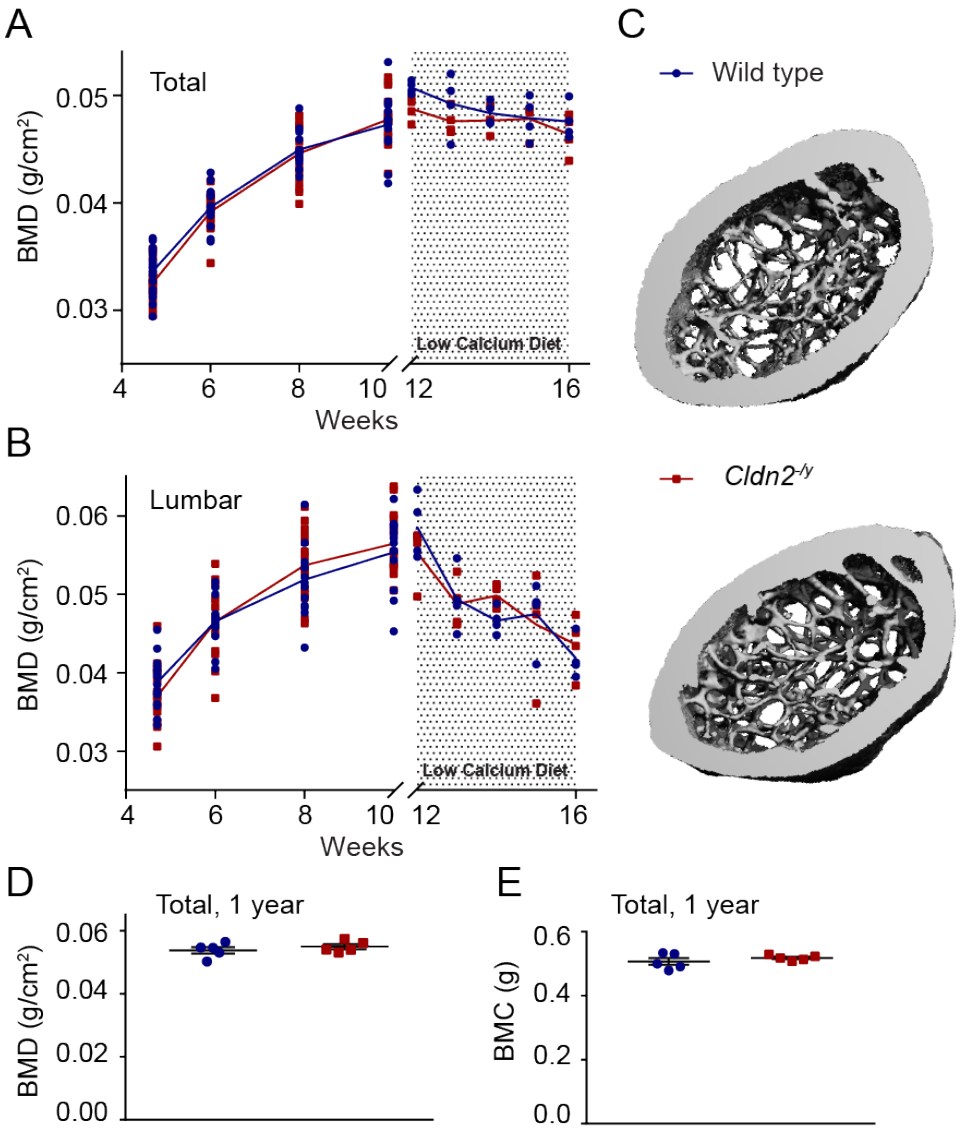

Figure 3-5. Bone mineral metabolism is not changed in *Cldn2*$^{-/y}$ mice.

Bone analysis on wild type (blue) and *Cldn2*$^{-/y}$ (red) animals on a standard chow diet. (A) Total and (B) lumbar bone mineral density (BMD) was measured using DEXA for at 4.7, 6, 8, and 10 weeks. A group of these animals was started on a low Ca^{2+} diet for 4 weeks and BMD measured weekly. (C) Representative micro-CT reconstructions of femurs showing normal cortical and trabecular bone in *Cldn2*$^{-/y}$ mice. (D) Total BMD and (E) total bone mineral content were measured on 1 year-old animals by DEXA. Bars are Mean ± SEM.

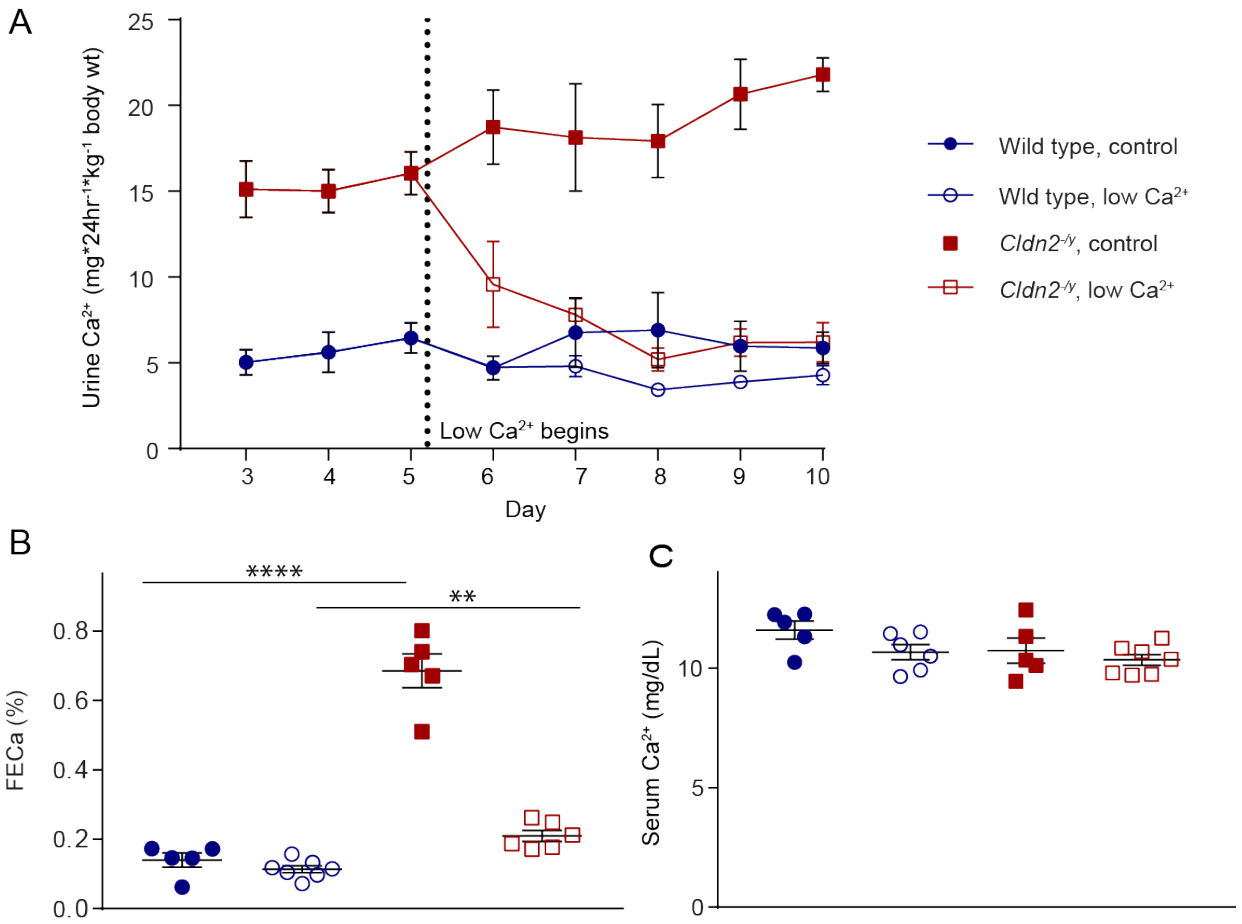

Figure 3-6. Hypercalciuria in *Cldn2*$^{-/y}$ mice is sensitive to dietary calcium intake.

(A) Metabolic cage experiments show 24 hour urine calcium (Ca^{2+}) excretion on control diet until day 5, after which half of the animals are switched to a Ca^{2+}-deficient diet (<0.01% Ca). At Day 10, the experiment was terminated and serum was collected. (B) Fractional excretion of Ca^{2+} (FECa) at day 10. Data were analyzed by two-way ANOVA with Bonferroni's correction for multiple comparisons; **P<0.01; ****P<0.0001. (C) Serum Ca^{2+} at day 10. There were no significant differences between the groups. Bars are Mean ± SEM.

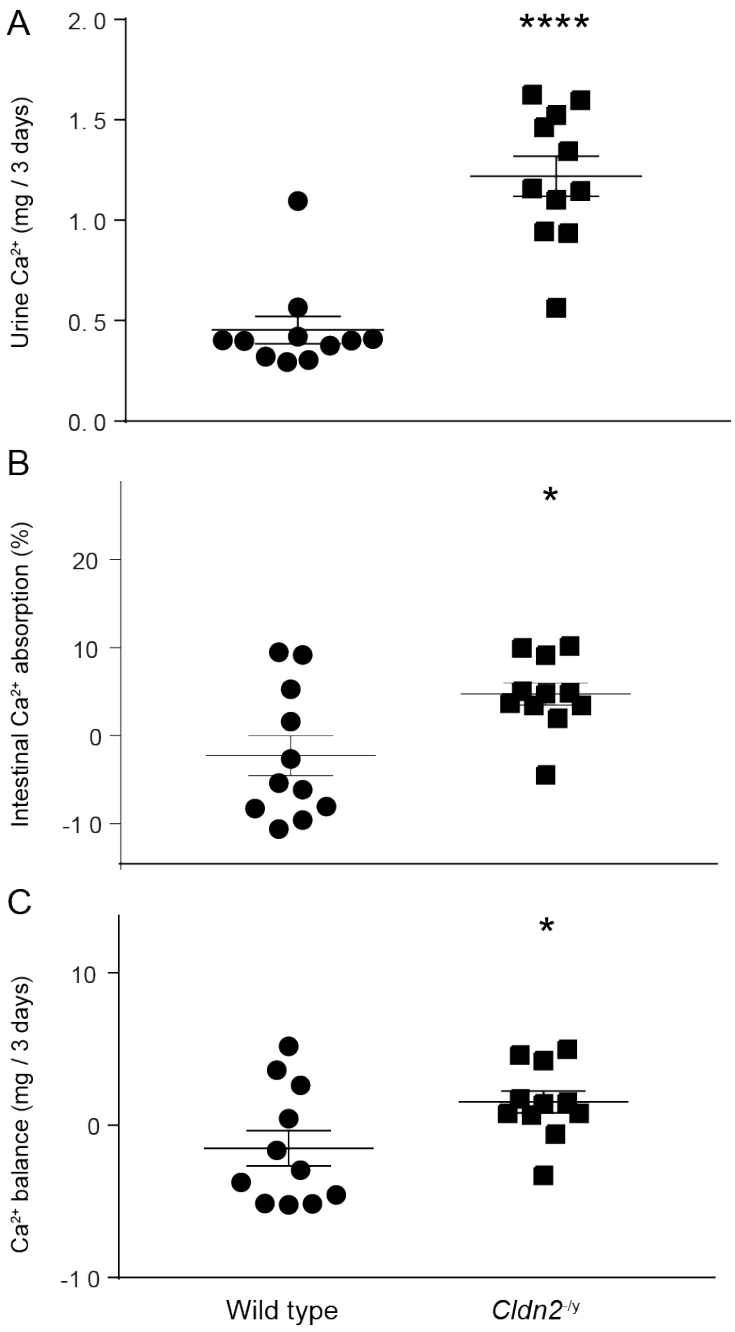

Figure 3-7. *Cldn2*$^{-/y}$ mice have a positive calcium balance.

Over the course of 3 days, urine and feces were collected for measurement of calcium (Ca^{2+}) balance. (A) Total 3 day urinary Ca^{2+} excretion. (B) Intestinal Ca^{2+} absorption, determined as the difference between dietary Ca^{2+} intake and fecal Ca^{2+}content and expressed as a percentage of dietary intake. (C) Net Ca^{2+} balance (intestinal absorption minus urinary excretion) is significantly higher in *Cldn2*$^{-/y}$ mice. Bars are Mean ± SEM. *P<0.05; ****P<0.0001 using Student's t-test.

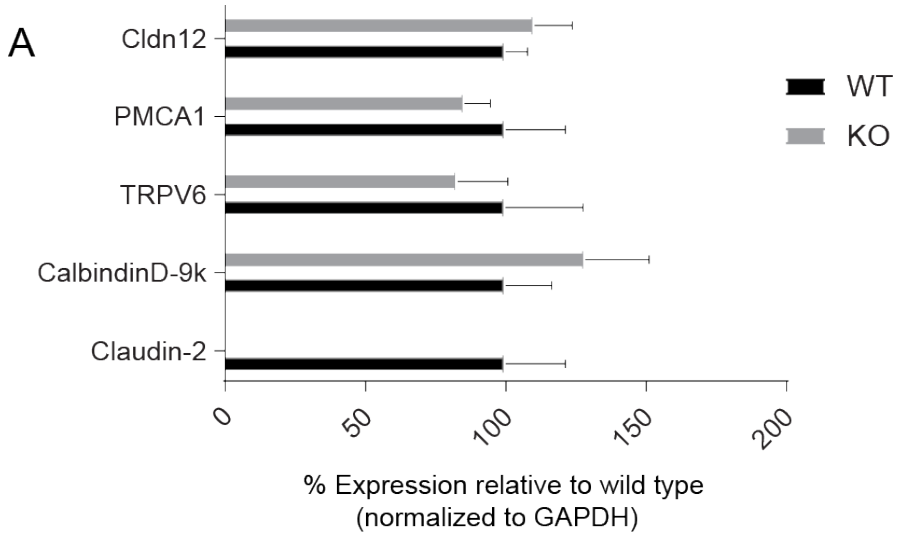

Figure 3-8. Expression of intestinal calcium transporters in *Cldn2*$^{-/y}$ mice is not different from wild type.

Quantitative-RT PCR of duodenal tissue was used to measure expression of calcium transport proteins in the intestine in wild type (WT) and *Cldn2*$^{-/y}$ (KO) mice. Fold change values were calculated relative to GAPDH expression, and then data was normalized to 100% for wild type levels. No significant differences were detected (n=5 per group). Bars are Mean ± SEM.

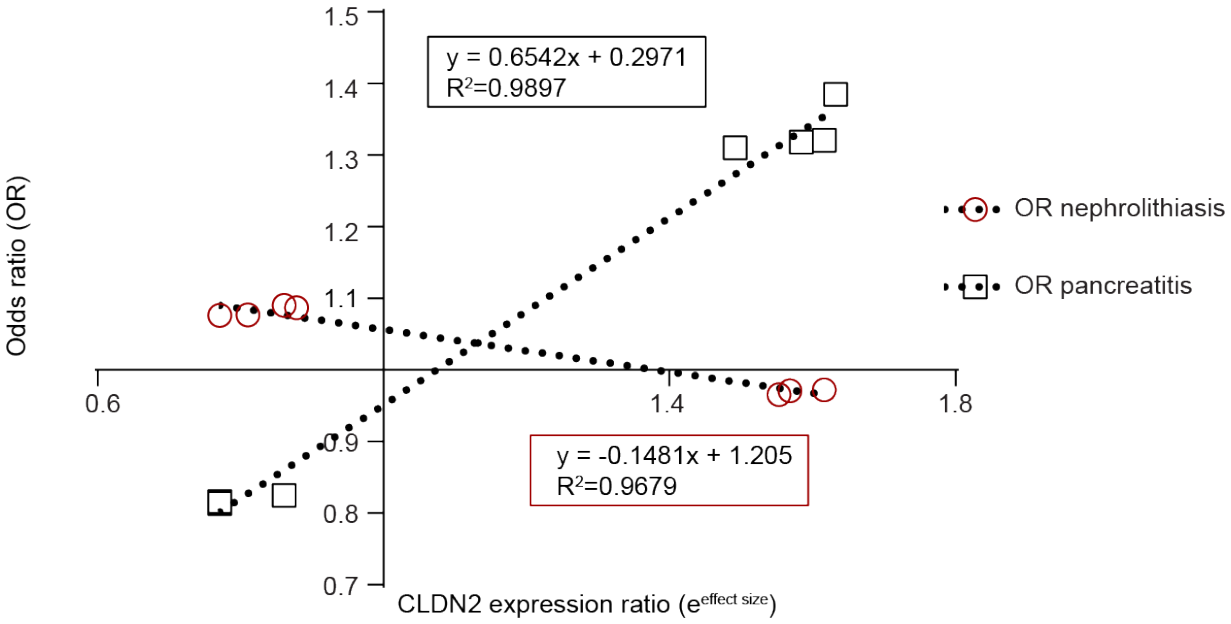

Figure 3-9. Linear regression analysis of pancreatic claudin-2 expression and disease risk.

Odd ratios of SNPs reported by Whitcomb et al. (2012) regarding alcohol-related pancreatitis and the present study of kidney stone disease are shown plotted against pancreatic claudin-2 (CLDN2) expression data (obtained from GTEx Portal). Linear regression analysis shows CLDN2 expression is highly and reciprocally correlated with disease risk for chronic pancreatitis ($p<0.0001$) and nephrolithiasis ($p<0.0001$).

Figure 3-10. Genotype - pancreatic tissue eQTL analysis.

Pancreatic claudin-2 (CLDN2) expression in three SNPs associated with both nephrolithiasis (NL) and chronic pancreatitis (CP) in the *CLDN2* locus, (A) rs5917027, (B) rs7057398, and (C) rs12008279. Note that the risk genotypes for the two diseases are different and that they are reciprocally correlated with tissue expression of CLDN2. Plots modified from GTEx Portal.

Chapter 4: Conclusion

4.1 Summary of findings

Defective PT calcium reabsorption is implicated in the pathogenesis of human kidney stone disease, and the majority of this transport is likely to be paracellular. Given that paracellular permeability is in large part determined by the claudin family of proteins, in chapter 2 I sought to establish the expression pattern of the three major claudin isoforms in the PT, claudin-2, claudin-3, and claudin-10a. Claudin-2 and claudin-10 are expressed throughout the length of the PT, but claudin-3 is restricted to the PST. I found that, while claudin-2 is expressed in thin descending limbs of long loop nephrons, claudin-3 is expressed in a distinct population of descending thin limbs. I developed stable cell lines with inducible expression of claudin-2 and either claudin-3 or claudin-10a in order to study the paracellular transport properties of these isoforms, *in vitro*. I found that, of the major PT claudin isoforms, only claudin-2 increases calcium flux *in vitro*.

In chapter 3, I investigated the mechanisms for hypercalciuria and nephrocalcinosis in *Cldn2*$^{-/y}$ mice, a novel mouse model for human kidney stone disease. I confirmed that these animals have an increase in the $FECa^{2+}$, which is a risk factor for nephrocalcinosis and kidney stone disease in humans. I next analyzed kidneys from these mice for the presence of calcium deposits within the renal parenchyma, and identified intratubular calcium phosphate deposits, in the form of hydroxyapatite, within loops of Henle of the renal papilla. Using expression and metabolic balance studies, my work shows that *Cldn2*$^{-/y}$ mice are hypercalciuric due to both defective renal calcium reabsorption and intestinal hyperabsorption of calcium. Given the striking nephrocalcinosis phenotype in *Cldn2*$^{-/y}$ mice, we tested the hypothesis that *CLDN2* polymorphisms may contribute to kidney stone risk in humans. We identified 9 SNPs in the *CLDN2* locus that had a significant association with kidney stone disease. Utilizing genotype-tissue expression analysis of human subjects (GTEx Portal), I show that these SNPs strongly associate with reduced claudin-2 expression in human pancreatic tissue. Both kidney and pancreas express

the same transcript of claudin-2, suggesting similar transcriptional regulation in these tissues. The combined results suggest that these *CLDN2* polymorphisms lead to decreased renal claudin-2 expression and a subsequent increase in nephrolithiasis risk.

4.2 Limitations

A caveat of my claudin overexpression studies is that, while all of our present knowledge points to claudin-10a as the exclusive isoform of claudin-10 expressed in the PT, isolated PSTs have not been analyzed in any studies that distinguish between claudin-10 isoforms (Gunzel, Stuiver et al. 2009, Lee, Chou et al. 2015). Due to the fact that our claudin-10 antibody is directed against the C-terminus of the protein, I am unable to distinguish between isoforms in our immunolabeling studies. While claudin-10a is an anion-selective isoform, claudin-10b exhibits cation selectivity (Van Itallie, Rogan et al. 2006). Thus, I cannot completely eliminate the possibility that claudin-10b is expressed in PST and contributes to PT calcium reabsorption. As discussed in Chapter 2, I believe that this is unlikely given the scarcity of claudin-10b expression, as detected by *in situ* hybridization, in the outer stripe of the outer medulla (Van Itallie, Rogan et al. 2006).

While our dual-claudin induction cell model can mitigate concerns in the variability in endogenous claudin expression between clonal cell populations, I cannot completely rule out an effect of endogenous claudin interactions on the calcium flux and electrophysiological studies. This is particularly true of claudin-3, which is one of the relatively abundant endogenous claudin isoforms expressed in MDCK I cells (Amasheh, Meiri et al. 2002, Yu, Cheng et al. 2009). I have taken care to select a clone with low endogenous claudin-3 expression for the claudin-3 studies, but a member of the lab has developed a TALEN-based knockout strategy for canine claudin-3 and successfully generated knockout cells for future studies in the method described in his previous work (Tokuda and Furuse 2015). Ultimately, a powerful tool for *in vitro* studies would be a renal epithelial cell model that lacks all endogenous claudin protein expression. Such a model may be achievable using CRISPR/Cas9 nuclease technology, which has been developed as a

tool for multiplex genomic editing and is capable of targeting multiple genes at once (Cong, Ran et al. 2013).

Given that the *Cldn2* gene is on the X chromosome, the majority of my animal studies were limited to male mice in order to generate wild type and knockout littermates. As such, I cannot exclude the possibility that my metabolic data is sex-specific. It should be noted that I did quantitate nephrocalcinosis in female *Cldn2* knockout animals and found that they develop nephrocalcinosis in a similar pattern and degree as their male counterparts.

Another important caveat is that our *Cldn2*$^{-/y}$ mice have a global deletion of *Cldn2*. Given the complexity of calcium homeostasis, *in vivo,* it is possible that loss of claudin-2 leads to hypercalciuria and nephrocalcinosis due to loss of claudin-2 in extra-renal, extra-intestinal tissues. Indeed, claudin-2 is expressed in a number of other tissues including the choroid plexus and pancreas (Rahner, Mitic et al. 2001). As shown in chapter 2, claudin-2 is also expressed in the kidney outside of the PT, in the thin descending limbs of long loop nephrons. Our lab is currently in the process of generating conditional (Cre-Lox) *Cldn2* knockout mice, which will allow us to delete *Cldn2* specifically within the PT. This model will ultimately be needed to determine the contribution of renal and intestinal claudin-2 to hypercalciuria and nephrocalcinosis in mice.

I was surprised to find intestinal hyperabsorption of calcium in *Cldn2*$^{-/y}$ mice, given the limited expression of claudin-2 to intestinal crypts and the decreased intestinal P_{Na} previously described in claudin-2 knockout animals (Holmes, Van Itallie et al. 2006, Tamura, Hayashi et al. 2011). The expected result was the opposite; that loss of calcium-permeable claudin-2 would *decrease* intestinal calcium permeability and thus calcium absorption. Studies are currently being completed to measure intestinal calcium transport both *in vivo*, using oral gavage of radiotracer calcium, and *ex vivo,* by measurement of unidirectional flux of calcium in ileal tissue. These studies will help to determine the mechanisms of intestinal calcium absorption in *Cldn2*$^{-/y}$ mice.

4.3 Significance and future directions

4.3.1 The dual-claudin induction model

Using the dual-claudin induction system, I found no effect of claudin-3 on TER, P_{Na}, or P_{Cl} in MDCK I cells. This begs the question of what role claudin-3 plays in the PT *in vivo*. Of particular interest to us is the role of claudin-3 in the passive movement of urea and water across the TJ, given its localization within the PST and thin descending limbs of, presumably, short loop nephrons. I speculate that claudin-3 may modulate the ratio of urea permeability to P_{Na}, *in vitro,* thereby increasing urea recycling and increasing the efficiency of the countercurrent multiplication mechanism for urinary concentration (Jamison 1987). Future studies may use this system to measure the flux of radiotracer urea, utilizing our dual-claudin induction system.

My findings show that claudin-2 and claudin-10a co-expression leads to a reduction in permselectivity in MDCK I cells. The physiological relevance of expression of both cation- and anion-selective claudin isoforms in the PT is not clear. One possibility is that co-expression of claudin-2 and claudin-10a is synergistic in the facilitation of the isosmotic movement of sodium, calcium, chloride, and water. In the absence of claudin-2, PT chloride reabsorption may be blunted by the more positive lumen potential (normally dissipated by movement of cations across the TJ). Indeed, isolated perfused PTs from claudin-2 knockout mice have reduced chloride reabsorption, in addition to reduced sodium and water reabsorption (Muto, Hata et al. 2010). These mice also have a large increase in the fractional excretion of chloride in response to hypertonic saline injection (Muto, Hata et al. 2010). I speculate that genetic deletion of claudin-10a would lead to similar findings: decreased PT sodium, calcium, and water reabsorption, in addition to defective chloride reabsorption. This relationship may be further explored using our dual-claudin induction model. It would be interesting to know if co-expression of claudin-2 and claudin-10a could increase the movement of both sodium and chloride along a concentration gradient, in spite of the overall reduction in P_{Na} and P_{Cl}. Experiments could be performed to measure the flux of sodium and chloride across the cells in the presence of a gradient, taking care

to minimize the effect of unstirred layers (Winne 1973). I speculate that there would be a greater sodium and chloride flux than expected, given the measured P_{Na} and P_{Cl}. This could be further explored utilizing our cysteine mutant cell model in order to block the claudin-2 pore and measure the difference in sodium flux. I would expect that the reduction in sodium flux following MTSEA addition would be much greater, as a percentage, in cells that express both claudin-2 S68C and claudin-10a compared with claudin-2 S68C alone.

Endogenous claudin expression can vary between clonal cell populations and complicate the interpretation of claudin overexpression *in vitro* (Gunzel and Yu 2013). Our dual-claudin induction system partially circumvents this problem for co-expression studies and provides a novel tool in the field of claudin biology. In the future, this system may be used for the rigorous evaluation of claudin mutations by allowing their direct comparison with wild type isoforms at equal expression levels and within a single clonal cell population. This system will eliminate many of the concerns of such studies to date.

4.3.2 Claudin-2 and the treatment of kidney stones

Of the major PT claudins, only claudin-2 increased calcium permeability *in vitro*. Thus, my work strengthens the hypothesis that claudin-2 is the protein mediator of paracellular calcium transport in the PT. In my analysis of *Cldn2*$^{-/y}$ mice, I described findings of nephrocalcinosis, increased calcium balance, and increased $FECa^{2+}$ upon calcium restriction. This suggests a role for claudin-2 in kidney stone formation. Following up on these findings, we subsequently identified significant genetic associations between *CLDN2* polymorphisms and human kidney stone disease. The knowledge gained from this work may help identify common mechanisms for stone formation in the general population and pave the way for improved treatments for kidney stone disease.

Recent findings linking the severity of papillary nephrocalcinosis and kidney stone disease in patients make my findings in *Cldn2*$^{-/y}$ mice particularly exciting (Verrier, Bazin et al. 2016, Hsi, Ramaswamy et al. 2017, Huguet, Le Dudal et al. 2017, Sherer, Chen et al. 2018). There are

currently no mouse models of nephrocalcinosis that form hydroxyapatite mineral around the basement membranes of the thin descending limbs, similar to Randall's plaques (Wu 2015). *Cldn2*$^{-/y}$ mice do not form hydroxyapatite mineral in this fashion, either. However, these mice develop intratubular hydroxyapatite deposits within the thin limbs. Similar intratubular mineral deposition has been identified as a risk factor for kidney stone formation (Okada, Hamamoto et al. 2018). I speculate that *Cldn2*$^{-/y}$ mice provide the best model to date for the study of nephrocalcinosis secondary to hypercalciuria. Using this model and our micro-CT method for the quantification of nephrocalcinosis will allow the testing of novel compounds that may reduce deposit formation in patients with defective PT calcium reabsorption.

Cldn2$^{-/y}$ mice as a model may also improve our understanding of the pathogenesis of nephrocalcinosis and kidney stone disease. For instance, we are unsure what contribution, if any, calcium reabsorption in the TAL and subsequent countercurrent papillary blood flow through the renal vasculature ("vas washdown") has on nephrocalcinosis (Coe, Worcester et al. 2016). Using transgenic claudin-16 knockdown mice, a model with defective TAL calcium reabsorption (Hou, Shan et al. 2007), we can test the contribution of "vas washdown" to the formation of nephrocalcinosis in *Cldn2*$^{-/y}$ mice. I would expect that, in the event of a major contribution to nephrocalcinosis by "vas washdown," knockdown of claudin-16 should reduce or prevent nephrocalcinosis in *Cldn2*$^{-/y}$ mice. In addition, given that the majority of patients with idiopathic hypercalciuria and kidney stone disease develop CaOx stones, we may be able to induce hyperoxaluria in *Cldn2*$^{-/y}$ mice and cause the formation of CaOx crystals on the surface of the papilla and/or Randall's plaques. If we are able to induce CaOx stones in *Cldn2*$^{-/y}$, the model can be further used to improve our current understanding of kidney stone pathogenesis and develop novel treatments for kidney stones.

In kidney stone formers with idiopathic hypercalciuria, reduction of urine calcium is important and necessary for prevention of stone recurrence (Borghi, Schianchi et al. 2002). While initially it was thought that restriction of dietary calcium would reduce stone recurrence, calcium

can form a complex with oxalate and prevent its absorption in the gastrointestinal tract (Borghi, Schianchi et al. 2002). As a result, calcium restriction increases oxalate absorption and will potentially exacerbate CaOx kidney stone disease. Thus, hypercalciuric stone formers must often be treated pharmacologically. A common treatment in such patients are thiazide diuretics, which reduce urine calcium in part by stimulating calcium reabsorption within the PT (Nijenhuis, Vallon et al. 2005, Worcester and Coe 2010). Unfortunately, a number of patients are unable to use these diuretics due to off-target side effects. Identification of claudin-2 as the protein mediator of PT calcium reabsorption will provide a novel drug target for the treatment of idiopathic hypercalciuria. Given that decreased claudin-2 expression in human tissues is associated with *CLDN2* risk variants, I suspect that increasing claudin-2 expression in the kidney pharmacologically would protect from kidney stone recurrence. Thus, exploring the regulatory pathways for claudin-2 expression in the PT will be an important future direction for our work.

A number of studies have identified cell signaling pathways that regulate claudin-2 expression *in vitro*. For instance, claudin-2 is regulated by numerous cytokines and growth factors such as Interleukin-6, Tumor Necrosis Factor-α and Epidermal Growth Factor through the MEK/ERK pathway (Dhawan, Ahmad et al. 2011, Suzuki, Yoshinaga et al. 2011, Amoozadeh, Dan et al. 2015). In addition, activation of the Protein Kinase C- β pathway in response to hyperosmolarity has been shown to downregulate claudin-2 expression (Ikari, Fujii et al. 2015). Finally, intestine specific deletion of Hepatocyte Nuclear Factor-4α leads to upregulation of intestinal claudin-2 (Cattin, Le Beyec et al. 2009). Identification of the pathways involved in renal claudin-2 expression *in vivo* could allow for the development of novel drugs to treat hypercalciuria in kidney stone formers.

Finally, in the emerging age of precision medicine, the identification of genetic associations may begin to help physicians make personalized decisions in disease management. For instance, the identification of kidney stone patients with common *CLDN2* risk variants may help to identify a subpopulation of stone formers whose response to treatments such as thiazide

diuretics differs from patients without these risk variants. The knowledge gained from my work may ultimately have a large impact on our understanding of the pathogenesis of nephrocalcinosis and kidney stone disease.

4.4 Concluding statement

This dissertation has explored the role of claudin-2 as the most likely protein mediator of paracellular calcium transport in the PT. Given the importance of PT calcium reabsorption in the pathogenesis of idiopathic hypercalciuria and kidney stone formation (Sutton and Walker 1980, Sakhaee, Nicar et al. 1985, Worcester, Coe et al. 2008), we were able to establish a link between claudin-2 and the development of hypercalciuria, nephrocalcinosis, and nephrolithiasis using human genome association analysis, human tissue expression analysis, and a mouse model with global deletion of *Cldn2*. My hope is that this work will lead to a better understanding of the pathogenesis of kidney stone formation and novel treatments for recurrent kidney stone formers.

References

Alberts, B. (2002). Molecular biology of the cell. New York, Garland Science.

Alexander, R. T., J. Rievaj and H. Dimke (2014). "Paracellular calcium transport across renal and intestinal epithelia." Biochem Cell Biol **92**(6): 467-480.

Alpern, R. J., S. C. Hebert, D. W. Seldin and G. H. Giebisch (2008). Seldin and Giebisch's the kidney : physiology & pathophysiology. Amsterdam ; Boston, Elsevier Inc., Academic Press.

Amasheh, S., N. Meiri, A. H. Gitter, T. Schoneberg, J. Mankertz, J. D. Schulzke and M. Fromm (2002). "Claudin-2 expression induces cation-selective channels in tight junctions of epithelial cells." J Cell Sci **115**(Pt 24): 4969-4976.

Amoozadeh, Y., Q. Dan, J. Xiao, F. Waheed and K. Szaszi (2015). "Tumor Necrosis Factor-alpha induces a biphasic change in claudin-2 expression in tubular epithelial cells: role in barrier functions." Am J Physiol Cell Physiol: ajpcell 00388 02014.

Angelow, S. and A. S. Yu (2009). "Structure-function studies of claudin extracellular domains by cysteine-scanning mutagenesis." J Biol Chem **284**(42): 29205-29217.

Barratt, L. J., F. C. Rector, Jr., J. P. Kokko and D. W. Seldin (1974). "Factors governing the transepithelial potential difference across the proximal tubule of the rat kidney." J Clin Invest **53**(2): 454-464.

Belmont, J. W., B. Reid, W. Taylor, S. S. Baker, W. H. Moore, M. C. Morriss, S. M. Podrebarac, N. Glass and I. D. Schwartz (2002). "Congenital sucrase-isomaltase deficiency presenting with failure to thrive, hypercalcemia, and nephrocalcinosis." BMC Pediatr **2**: 4.

Ben-Yosef, T., I. A. Belyantseva, T. L. Saunders, E. D. Hughes, K. Kawamoto, C. M. Van Itallie, L. A. Beyer, K. Halsey, D. J. Gardner, E. R. Wilcox, J. Rasmussen, J. M. Anderson, D. F. Dolan, A. Forge, Y. Raphael, S. A. Camper and T. B. Friedman (2003). "Claudin 14 knockout mice, a model for autosomal recessive deafness DFNB29, are deaf due to cochlear hair cell degeneration." Hum Mol Genet **12**(16): 2049-2061.

Berry, C. A. and F. C. Rector, Jr. (1991). "Mechanism of proximal NaCl reabsorption in the proximal tubule of the mammalian kidney." Semin Nephrol **11**(2): 86-97.

Berry, C. A., D. G. Warnock and F. C. Rector, Jr. (1978). "Ion selectivity and proximal salt reabsorption." Am J Physiol **235**(3): F234-245.

Bhojani, N., J. E. Paonessa, T. A. Hameed, E. M. Worcester, A. P. Evan, F. L. Coe, M. S. Borofsky and J. E. Lingeman (2015). "Nephrocalcinosis in Calcium Stone Formers Who Do Not have Systemic Disease." J Urol **194**(5): 1308-1312.

Blanchard, A., X. Jeunemaitre, P. Coudol, M. Dechaux, M. Froissart, A. May, R. Demontis, A. Fournier, M. Paillard and P. Houillier (2001). "Paracellin-1 is critical for magnesium and calcium reabsorption in the human thick ascending limb of Henle." Kidney Int **59**(6): 2206-2215.

Bongers, E., L. M. Shelton, S. Milatz, S. Verkaart, A. P. Bech, J. Schoots, E. A. M. Cornelissen, M. Bleich, J. G. J. Hoenderop, J. F. M. Wetzels, D. Lugtenberg and T. Nijenhuis (2017). "A Novel Hypokalemic-Alkalotic Salt-Losing Tubulopathy in Patients with CLDN10 Mutations." J Am Soc Nephrol **28**(10): 3118-3128.

Borghi, L., T. Schianchi, T. Meschi, A. Guerra, F. Allegri, U. Maggiore and A. Novarini (2002). "Comparison of two diets for the prevention of recurrent stones in idiopathic hypercalciuria." N Engl J Med **346**(2): 77-84.

Breslow, N. E. and N. E. Day (1987). "Statistical methods in cancer research. Volume II--The design and analysis of cohort studies." IARC Sci Publ(82): 1-406.

Bronner, F. (1998). "Calcium absorption--a paradigm for mineral absorption." J Nutr **128**(5): 917-920.

Carpi-Medina, P. and G. Whittembury (1988). "Comparison of transcellular and transepithelial water osmotic permeabilities (Pos) in the isolated proximal straight tubule (PST) of the rabbit kidney." Pflugers Arch **412**(1-2): 66-74.

Cattin, A. L., J. Le Beyec, F. Barreau, S. Saint-Just, A. Houllier, F. J. Gonzalez, S. Robine, M. Pincon-Raymond, P. Cardot, M. Lacasa and A. Ribeiro (2009). "Hepatocyte nuclear factor 4alpha, a key factor for homeostasis, cell architecture, and barrier function of the adult intestinal epithelium." Mol Cell Biol **29**(23): 6294-6308.

Coe, F. L., E. M. Worcester and A. P. Evan (2016). "Idiopathic hypercalciuria and formation of calcium renal stones." Nat Rev Nephrol **12**(9): 519-533.

Colegio, O. R., C. M. Van Itallie, H. J. McCrea, C. Rahner and J. M. Anderson (2002). "Claudins create charge-selective channels in the paracellular pathway between epithelial cells." Am J Physiol Cell Physiol **283**(1): C142-147.

Cong, L., F. A. Ran, D. Cox, S. Lin, R. Barretto, N. Habib, P. D. Hsu, X. Wu, W. Jiang, L. A. Marraffini and F. Zhang (2013). "Multiplex genome engineering using CRISPR/Cas systems." Science **339**(6121): 819-823.

De, S. K., X. Liu and M. Monga (2014). "Changing trends in the American diet and the rising prevalence of kidney stones." Urology **84**(5): 1030-1033.

Dhawan, P., R. Ahmad, R. Chaturvedi, J. J. Smith, R. Midha, M. K. Mittal, M. Krishnan, X. Chen, S. Eschrich, T. J. Yeatman, R. C. Harris, M. K. Washington, K. T. Wilson, R. D. Beauchamp and A. B. Singh (2011). "Claudin-2 expression increases tumorigenicity of colon cancer cells: role of epidermal growth factor receptor activation." Oncogene **30**(29): 3234-3247.

Enck, A. H., U. V. Berger and A. S. Yu (2001). "Claudin-2 is selectively expressed in proximal nephron in mouse kidney." Am J Physiol Renal Physiol **281**(5): F966-974.

Evan, A., J. Lingeman, F. L. Coe and E. Worcester (2006). "Randall's plaque: pathogenesis and role in calcium oxalate nephrolithiasis." Kidney Int **69**(8): 1313-1318.

Evan, A. P., J. E. Lingeman, F. L. Coe, J. H. Parks, S. B. Bledsoe, Y. Shao, A. J. Sommer, R. F. Paterson, R. L. Kuo and M. Grynpas (2003). "Randall's plaque of patients with nephrolithiasis begins in basement membranes of thin loops of Henle." J Clin Invest **111**(5): 607-616.

Evan, A. P., J. E. Lingeman, E. M. Worcester, A. J. Sommer, C. L. Phillips, J. C. Williams and F. L. Coe (2014). "Contrasting histopathology and crystal deposits in kidneys of idiopathic stone formers who produce hydroxy apatite, brushite, or calcium oxalate stones." Anat Rec (Hoboken) **297**(4): 731-748.

Faarup, P., N. H. Holstein-Rathlou, T. Norgaard, A. P. Harrison, L. Bastholm, L. Thatt, F. F. Johansen and V. Hegedus (2011). "Functionally induced changes in water transport in the proximal tubule segment of rat kidneys." Int J Nephrol Renovasc Dis **4**: 73-84.

Fanning, A. S., B. J. Jameson, L. A. Jesaitis and J. M. Anderson (1998). "The tight junction protein ZO-1 establishes a link between the transmembrane protein occludin and the actin cytoskeleton." J Biol Chem **273**(45): 29745-29753.

Farquhar, M. G. and G. E. Palade (1963). "Junctional complexes in various epithelia." J Cell Biol **17**: 375-412.

Flocks, R. H. (1939). "Calcium and phosphorus excretion in the urine: Of patients with renal or ureteral calculi." Journal of the American Medical Association **113**(16): 1466-1471.

Furuse, M., K. Fujita, T. Hiiragi, K. Fujimoto and S. Tsukita (1998). "Claudin-1 and -2: novel integral membrane proteins localizing at tight junctions with no sequence similarity to occludin." J Cell Biol **141**(7): 1539-1550.

Furuse, M., K. Furuse, H. Sasaki and S. Tsukita (2001). "Conversion of zonulae occludentes from tight to leaky strand type by introducing claudin-2 into Madin-Darby canine kidney I cells." J Cell Biol **153**(2): 263-272.

Furuse, M., M. Hata, K. Furuse, Y. Yoshida, A. Haratake, Y. Sugitani, T. Noda, A. Kubo and S. Tsukita (2002). "Claudin-based tight junctions are crucial for the mammalian epidermal barrier: a lesson from claudin-1-deficient mice." J Cell Biol **156**(6): 1099-1111.

Furuse, M., T. Hirase, M. Itoh, A. Nagafuchi, S. Yonemura, S. Tsukita and S. Tsukita (1993). "Occludin: a novel integral membrane protein localizing at tight junctions." J Cell Biol **123**(6 Pt 2): 1777-1788.

Furuse, M., H. Sasaki and S. Tsukita (1999). "Manner of interaction of heterogeneous claudin species within and between tight junction strands." J Cell Biol **147**(4): 891-903.

Gao, B., T. Yasui, Y. Itoh, Z. Li, A. Okada, K. Tozawa, Y. Hayashi and K. Kohri (2007). "Association of osteopontin gene haplotypes with nephrolithiasis." Kidney Int **72**(5): 592-598.

Goldfarb, D. S., M. E. Fischer, Y. Keich and J. Goldberg (2005). "A twin study of genetic and dietary influences on nephrolithiasis: a report from the Vietnam Era Twin (VET) Registry." Kidney Int **67**(3): 1053-1061.

Gong, Y. and J. Hou (2014). "Claudin-14 underlies Ca(+)(+)-sensing receptor-mediated Ca(+)(+) metabolism via NFAT-microRNA-based mechanisms." J Am Soc Nephrol **25**(4): 745-760.

Gong, Y., V. Renigunta, N. Himmerkus, J. Zhang, A. Renigunta, M. Bleich and J. Hou (2012). "Claudin-14 regulates renal Ca(+)(+) transport in response to CaSR signalling via a novel microRNA pathway." EMBO J **31**(8): 1999-2012.

Green, R. and G. Giebisch (1989). "Reflection coefficients and water permeability in rat proximal tubule." Am J Physiol **257**(4 Pt 2): F658-668.

Gudbjartsson, D. F., H. Holm, O. S. Indridason, G. Thorleifsson, V. Edvardsson, P. Sulem, F. de Vegt, F. C. d'Ancona, M. den Heijer, J. F. Wetzels, L. Franzson, T. Rafnar, K. Kristjansson, U. S. Bjornsdottir, G. I. Eyjolfsson, L. A. Kiemeney, A. Kong, R. Palsson, U. Thorsteinsdottir and K. Stefansson (2010). "Association of variants at UMOD with chronic kidney disease and kidney stones-role of age and comorbid diseases." PLoS Genet **6**(7): e1001039.

Gunzel, D., S. Amasheh, S. Pfaffenbach, J. F. Richter, P. J. Kausalya, W. Hunziker and M. Fromm (2009). "Claudin-16 affects transcellular Cl- secretion in MDCK cells." J Physiol **587**(Pt 15): 3777-3793.

Gunzel, D., M. Stuiver, P. J. Kausalya, L. Haisch, S. M. Krug, R. Rosenthal, I. C. Meij, W. Hunziker, M. Fromm and D. Muller (2009). "Claudin-10 exists in six alternatively spliced isoforms that exhibit distinct localization and function." J Cell Sci **122**(Pt 10): 1507-1517.

Gunzel, D. and A. S. Yu (2013). "Claudins and the modulation of tight junction permeability." Physiol Rev **93**(2): 525-569.

Hadj-Rabia, S., L. Baala, P. Vabres, D. Hamel-Teillac, E. Jacquemin, M. Fabre, S. Lyonnet, Y. De Prost, A. Munnich, M. Hadchouel and A. Smahi (2004). "Claudin-1 gene mutations in neonatal sclerosing cholangitis associated with ichthyosis: a tight junction disease." Gastroenterology **127**(5): 1386-1390.

Hadj-Rabia, S., G. Brideau, Y. Al-Sarraj, R. C. Maroun, M. L. Figueres, S. Leclerc-Mercier, E. Olinger, S. Baron, C. Chaussain, D. Nochy, R. Z. Taha, B. Knebelmann, V. Joshi, P. A. Curmi, M. Kambouris, R. Vargas-Poussou, C. Bodemer, O. Devuyst, P. Houillier and H. El-Shanti (2018). "Multiplex epithelium dysfunction due to CLDN10 mutation: the HELIX syndrome." Genet Med **20**(2): 190-201.

Halbritter, J., M. Baum, A. M. Hynes, S. J. Rice, D. T. Thwaites, Z. S. Gucev, B. Fisher, L. Spaneas, J. D. Porath, D. A. Braun, A. J. Wassner, C. P. Nelson, V. Tasic, J. A. Sayer and F. Hildebrandt (2015). "Fourteen monogenic genes account for 15% of nephrolithiasis/nephrocalcinosis." J Am Soc Nephrol **26**(3): 543-551.

Hall, J. E. and A. C. Guyton (2011). Guyton and Hall textbook of medical physiology. Philadelphia, Pa., Saunders/Elsevier.

Hamajima, N. and J. M. S. Group (2007). "The Japan Multi-Institutional Collaborative Cohort Study (J-MICC Study) to detect gene-environment interactions for cancer." Asian Pac J Cancer Prev **8**(2): 317-323.

Hebert, S. C. (2003). "Bartter syndrome." Curr Opin Nephrol Hypertens **12**(5): 527-532.

Heller, H. J., J. E. Zerwekh, F. A. Gottschalk and C. Y. Pak (2007). "Reduced bone formation and relatively increased bone resorption in absorptive hypercalciuria." Kidney Int **71**(8): 808-815.

Hirata, M., A. Nagai, Y. Kamatani, T. Ninomiya, A. Tamakoshi, Z. Yamagata, M. Kubo, K. Muto, Y. Kiyohara, T. Mushiroda, Y. Murakami, K. Yuji, Y. Furukawa, H. Zembutsu, T. Tanaka, Y. Ohnishi, Y. Nakamura, G. BioBank Japan Cooperative Hospital and K. Matsuda (2017). "Overview of BioBank Japan follow-up data in 32 diseases." J Epidemiol.

Hoenderop, J. G., B. Nilius and R. J. Bindels (2005). "Calcium absorption across epithelia." Physiol Rev **85**(1): 373-422.

Hoenderop, J. G., J. P. van Leeuwen, B. C. van der Eerden, F. F. Kersten, A. W. van der Kemp, A. M. Merillat, J. H. Waarsing, B. C. Rossier, V. Vallon, E. Hummler and R. J. Bindels (2003). "Renal Ca2+ wasting, hyperabsorption, and reduced bone thickness in mice lacking TRPV5." J Clin Invest **112**(12): 1906-1914.

Holmes, J. L., C. M. Van Itallie, J. E. Rasmussen and J. M. Anderson (2006). "Claudin profiling in the mouse during postnatal intestinal development and along the gastrointestinal tract reveals complex expression patterns." Gene Expr Patterns **6**(6): 581-588.

Hoopes, R. R., Jr., A. E. Shrimpton, S. J. Knohl, P. Hueber, B. Hoppe, J. Matyus, A. Simckes, V. Tasic, B. Toenshoff, S. F. Suchy, R. L. Nussbaum and S. J. Scheinman (2005). "Dent Disease with mutations in OCRL1." Am J Hum Genet **76**(2): 260-267.

Hou, J., D. L. Paul and D. A. Goodenough (2005). "Paracellin-1 and the modulation of ion selectivity of tight junctions." J Cell Sci **118**(Pt 21): 5109-5118.

Hou, J., M. Rajagopal and A. S. Yu (2013). "Claudins and the kidney." Annu Rev Physiol **75**: 479-501.

Hou, J., A. Renigunta, A. S. Gomes, M. Hou, D. L. Paul, S. Waldegger and D. A. Goodenough (2009). "Claudin-16 and claudin-19 interaction is required for their assembly into tight junctions and for renal reabsorption of magnesium." Proc Natl Acad Sci U S A **106**(36): 15350-15355.

Hou, J., A. Renigunta, M. Konrad, A. S. Gomes, E. E. Schneeberger, D. L. Paul, S. Waldegger and D. A. Goodenough (2008). "Claudin-16 and claudin-19 interact and form a cation-selective tight junction complex." J Clin Invest **118**(2): 619-628.

Hou, J., A. Renigunta, J. Yang and S. Waldegger (2010). "Claudin-4 forms paracellular chloride channel in the kidney and requires claudin-8 for tight junction localization." Proc Natl Acad Sci U S A **107**(42): 18010-18015.

Hou, J., Q. Shan, T. Wang, A. S. Gomes, Q. Yan, D. L. Paul, M. Bleich and D. A. Goodenough (2007). "Transgenic RNAi depletion of claudin-16 and the renal handling of magnesium." J Biol Chem **282**(23): 17114-17122.

Howie, B., C. Fuchsberger, M. Stephens, J. Marchini and G. R. Abecasis (2012). "Fast and accurate genotype imputation in genome-wide association studies through pre-phasing." Nature Genetics **44**(8): 955-959.

Hsi, R. S., K. Ramaswamy, S. P. Ho and M. L. Stoller (2017). "The origins of urinary stone disease: upstream mineral formations initiate downstream Randall's plaque." BJU Int **119**(1): 177-184.

Huguet, L., M. Le Dudal, M. Livrozet, D. Bazin, V. Frochot, J. Perez, J. P. Haymann, I. Brocheriou, M. Daudon and E. Letavernier (2017). "High frequency and wide range of human kidney papillary crystalline plugs." Urolithiasis.

Ikari, A., N. Fujii, S. Hahakabe, H. Hayashi, M. Yamaguchi, Y. Yamazaki, S. Endo, T. Matsunaga and J. Sugatani (2015). "Hyperosmolarity-Induced Down-Regulation of Claudin-2 Mediated by Decrease in PKCbeta-Dependent GATA-2 in MDCK Cells." J Cell Physiol **230**(11): 2776-2787.

Imai, M. (1984). "Functional heterogeneity of the descending limbs of Henle's loop. II. Interspecies differences among rabbits, rats, and hamsters." Pflugers Arch **402**(4): 393-401.

Imai, M. and K. Yoshitomi (1990). "Heterogeneity of the descending thin limb of Henle's loop." Kidney Int **38**(4): 687-694.

Itoh, M., M. Furuse, K. Morita, K. Kubota, M. Saitou and S. Tsukita (1999). "Direct binding of three tight junction-associated MAGUKs, ZO-1, ZO-2, and ZO-3, with the COOH termini of claudins." J Cell Biol **147**(6): 1351-1363.

Jacobson, H. R. and J. P. Kokko (1976). "Intrinsic differences in various segments of the proximal convoluted tubule." J Clin Invest **57**(4): 818-825.

Jamison, R. L. (1987). "Short and long loop nephrons." Kidney Int **31**(2): 597-605.

Kanai, M., M. Akiyama, A. Takahashi, N. Matoba, Y. Momozawa, M. Ikeda, N. Iwata, S. Ikegawa, M. Hirata, K. Matsuda, M. Kubo, Y. Okada and Y. Kamatani (2018). "Genetic analysis of quantitative traits in the Japanese population links cell types to complex human diseases." Nat Genet.

Kawamura, S., M. Imai, D. W. Seldin and J. P. Kukko (1975). "Characteristics of salt and water transport in superficial and juxtamedullary straight segments of proximal tubules." J Clin Invest **55**(6): 1269-1277.

Khan, S. R. and P. A. Glenton (2008). "Calcium oxalate crystal deposition in kidneys of hypercalciuric mice with disrupted type IIa sodium-phosphate cotransporter." Am J Physiol Renal Physiol **294**(5): F1109-1115.

Kim, M., N. E. Sessler, V. Tembe, M. J. Favus and D. A. Bushinsky (1993). "Response of genetic hypercalciuric rats to a low calcium diet." Kidney Int **43**(1): 189-196.

Kim, W. Y., H. W. Lee, K. H. Han, S. A. Nam, A. Choi, Y. K. Kim and J. Kim (2016). "Descending thin limb of the intermediate loop expresses both aquaporin 1 and urea transporter A2 in the mouse kidney." Histochem Cell Biol **146**(1): 1-12.

Kimizuka, H. and K. Koketsu (1964). "Ion transport through cell membrane." J Theor Biol **6**(2): 290-305.

Kirk, A., S. Campbell, P. Bass, J. Mason and J. Collins (2010). "Differential expression of claudin tight junction proteins in the human cortical nephron." Nephrol Dial Transplant **25**(7): 2107-2119.

Kiuchi-Saishin, Y., S. Gotoh, M. Furuse, A. Takasuga, Y. Tano and S. Tsukita (2002). "Differential expression patterns of claudins, tight junction membrane proteins, in mouse nephron segments." J Am Soc Nephrol **13**(4): 875-886.

Klar, J., J. Piontek, S. Milatz, M. Tariq, M. Jameel, T. Breiderhoff, J. Schuster, A. Fatima, M. Asif, M. Sher, K. Mabert, A. Fromm, S. M. Baig, D. Gunzel and N. Dahl (2017). "Altered paracellular cation permeability due to a rare CLDN10B variant causes anhidrosis and kidney damage." PLoS Genet **13**(7): e1006897.

Ko, B., K. J. Bergsland, D. L. Gillen, A. P. Evan, D. L. Clark, J. Baylock, F. L. Coe and E. M. Worcester (2015). "Gender Differences in Proximal and Distal Nephron Function Contribute to the Mechanism of Idiopathic Hypercalcuria in Calcium Stone Formers." Am J Physiol Regul Integr Comp Physiol: ajpregu 00071 02015.

Ko, Y. A., H. Yi, C. Qiu, S. Huang, J. Park, N. Ledo, A. Kottgen, H. Li, D. J. Rader, M. A. Pack, C. D. Brown and K. Susztak (2017). "Genetic-Variation-Driven Gene-Expression Changes Highlight Genes with Important Functions for Kidney Disease." Am J Hum Genet **100**(6): 940-953.

Konrad, M., J. Hou, S. Weber, J. Dotsch, J. A. Kari, T. Seeman, E. Kuwertz-Broking, A. Peco-Antic, V. Tasic, K. Dittrich, H. O. Alshaya, R. O. von Vigier, S. Gallati, D. A. Goodenough and A. Schaller (2008). "CLDN16 genotype predicts renal decline in familial hypomagnesemia with hypercalciuria and nephrocalcinosis." J Am Soc Nephrol **19**(1): 171-181.

Konrad, M., A. Schaller, D. Seelow, A. V. Pandey, S. Waldegger, A. Lesslauer, H. Vitzthum, Y. Suzuki, J. M. Luk, C. Becker, K. P. Schlingmann, M. Schmid, J. Rodriguez-Soriano, G. Ariceta, F. Cano, R. Enriquez, H. Juppner, S. A. Bakkaloglu, M. A. Hediger, S. Gallati, S. C. Neuhauss, P. Nurnberg and S. Weber (2006). "Mutations in the tight-junction gene claudin 19 (CLDN19) are associated with renal magnesium wasting, renal failure, and severe ocular involvement." Am J Hum Genet **79**(5): 949-957.

Kuo, R. L., J. E. Lingeman, A. P. Evan, R. F. Paterson, J. H. Parks, S. B. Bledsoe, L. C. Munch and F. L. Coe (2003). "Urine calcium and volume predict coverage of renal papilla by Randall's plaque." Kidney Int **64**(6): 2150-2154.

Kuriyama, S., N. Yaegashi, F. Nagami, T. Arai, Y. Kawaguchi, N. Osumi, M. Sakaida, Y. Suzuki, K. Nakayama, H. Hashizume, G. Tamiya, H. Kawame, K. Suzuki, A. Hozawa, N. Nakaya, M. Kikuya, H. Metoki, I. Tsuji, N. Fuse, H. Kiyomoto, J. Sugawara, A. Tsuboi, S. Egawa, K. Ito, K. Chida, T. Ishii, H. Tomita, Y. Taki, N. Minegishi, N. Ishii, J. Yasuda, K. Igarashi, R. Shimizu, M. Nagasaki, S. Koshiba, K. Kinoshita, S. Ogishima, T. Takai-Igarashi, T. Tominaga, O. Tanabe, N. Ohuchi, T. Shimosegawa, S. Kure, H. Tanaka, S. Ito, J. Hitomi, K. Tanno, M. Nakamura, K. Ogasawara, S. Kobayashi, K. Sakata, M. Satoh, A. Shimizu, M. Sasaki, R. Endo, K. Sobue, T. Tohoku Medical Megabank Project Study Group and M. Yamamoto (2016). "The Tohoku Medical Megabank Project: Design and Mission." J Epidemiol **26**(9): 493-511.

Kuwertz-Broking, E., S. Frund, M. Bulla, R. Kleta, C. August and K. Kisters (2001). "Familial hypomagnesemia-hypercalciuria in 2 siblings." Clin Nephrol **56**(2): 155-161.

Lee, J. W., C. L. Chou and M. A. Knepper (2015). "Deep Sequencing in Microdissected Renal Tubules Identifies Nephron Segment-Specific Transcriptomes." J Am Soc Nephrol.

Letavernier, E., S. Vandermeersch, O. Traxer, M. Tligui, L. Baud, P. Ronco, J. P. Haymann and M. Daudon (2015). "Demographics and characterization of 10,282 Randall plaque-related kidney stones: a new epidemic?" Medicine (Baltimore) **94**(10): e566.

Leys, S. P. and A. Riesgo (2012). "Epithelia, an evolutionary novelty of metazoans." J Exp Zool B Mol Dev Evol **318**(6): 438-447.

Li, J., S. Angelow, A. Linge, M. Zhuo and A. S. Yu (2013). "Claudin-2 pore function requires an intramolecular disulfide bond between two conserved extracellular cysteines." Am J Physiol Cell Physiol **305**(2): C190-196.

Li, J., M. Zhuo, L. Pei, M. Rajagopal and A. S. Yu (2014). "Comprehensive cysteine-scanning mutagenesis reveals Claudin-2 pore-lining residues with different intrapore locations." J Biol Chem **289**(10): 6475-6484.

Liu, F. Y. and M. G. Cogan (1984). "Axial heterogeneity in the rat proximal convoluted tubule. I. Bicarbonate, chloride, and water transport." Am J Physiol **247**(5 Pt 2): F816-821.

Liu, Y., L. Mo, D. S. Goldfarb, A. P. Evan, F. Liang, S. R. Khan, J. C. Lieske and X. R. Wu (2010). "Progressive renal papillary calcification and ureteral stone formation in mice deficient for Tamm-Horsfall protein." Am J Physiol Renal Physiol **299**(3): F469-478.

Low, R. K. and M. L. Stoller (1997). "Endoscopic mapping of renal papillae for Randall's plaques in patients with urinary stone disease." J Urol **158**(6): 2062-2064.

Low, S. K., A. Takahashi, Y. Ebana, K. Ozaki, I. E. Christophersen, P. T. Ellinor, A. F. Consortium, S. Ogishima, M. Yamamoto, M. Satoh, M. Sasaki, T. Yamaji, M. Iwasaki, S. Tsugane, K. Tanaka, M. Naito, K. Wakai, H. Tanaka, T. Furukawa, M. Kubo, K. Ito, Y. Kamatani and T. Tanaka (2017). "Identification of six new genetic loci associated with atrial fibrillation in the Japanese population." Nat Genet **49**(6): 953-958.

Ma, T., B. Yang, A. Gillespie, E. J. Carlson, C. J. Epstein and A. S. Verkman (1998). "Severely impaired urinary concentrating ability in transgenic mice lacking aquaporin-1 water channels." J Biol Chem **273**(8): 4296-4299.

Matsuo, K., I. Oze, S. Hosono, H. Ito, M. Watanabe, K. Ishioka, S. Ito, M. Tajika, Y. Yatabe, Y. Niwa, K. Yamao, S. Nakamura, K. Tajima and H. Tanaka (2013). "The aldehyde dehydrogenase 2 (ALDH2) Glu504Lys polymorphism interacts with alcohol drinking in the risk of stomach cancer." Carcinogenesis **34**(7): 1510-1515.

Milatz, S., S. M. Krug, R. Rosenthal, D. Gunzel, D. Muller, J. D. Schulzke, S. Amasheh and M. Fromm (2010). "Claudin-3 acts as a sealing component of the tight junction for ions of either charge and uncharged solutes." Biochim Biophys Acta **1798**(11): 2048-2057.

Mo, L., L. Liaw, A. P. Evan, A. J. Sommer, J. C. Lieske and X. R. Wu (2007). "Renal calcinosis and stone formation in mice lacking osteopontin, Tamm-Horsfall protein, or both." Am J Physiol Renal Physiol **293**(6): F1935-1943.

Moe, O. W. (2006). "Kidney stones: pathophysiology and medical management." Lancet **367**(9507): 333-344.

Muto, S., M. Hata, J. Taniguchi, S. Tsuruoka, K. Moriwaki, M. Saitou, K. Furuse, H. Sasaki, A. Fujimura, M. Imai, E. Kusano, S. Tsukita and M. Furuse (2010). "Claudin-2-deficient mice are defective in the leaky and cation-selective paracellular permeability properties of renal proximal tubules." Proc Natl Acad Sci U S A **107**(17): 8011-8016.

Nagai, A., M. Hirata, Y. Kamatani, K. Muto, K. Matsuda, Y. Kiyohara, T. Ninomiya, A. Tamakoshi, Z. Yamagata, T. Mushiroda, Y. Murakami, K. Yuji, Y. Furukawa, H. Zembutsu, T. Tanaka, Y. Ohnishi, Y. Nakamura, G. BioBank Japan Cooperative Hospital and M. Kubo (2017). "Overview of the BioBank Japan Project: Study design and profile." J Epidemiol.

Ng, R. C., D. Rouse and W. N. Suki (1984). "Calcium transport in the rabbit superficial proximal convoluted tubule." J Clin Invest **74**(3): 834-842.

Nijenhuis, T., V. Vallon, A. W. van der Kemp, J. Loffing, J. G. Hoenderop and R. J. Bindels (2005). "Enhanced passive Ca2+ reabsorption and reduced Mg2+ channel abundance explains thiazide-induced hypocalciuria and hypomagnesemia." J Clin Invest **115**(6): 1651-1658.

Oddsson, A., P. Sulem, H. Helgason, V. O. Edvardsson, G. Thorleifsson, G. Sveinbjornsson, E. Haraldsdottir, G. I. Eyjolfsson, O. Sigurdardottir, I. Olafsson, G. Masson, H. Holm, D. F. Gudbjartsson, U. Thorsteinsdottir, O. S. Indridason, R. Palsson and K. Stefansson (2015). "Common and rare variants associated with kidney stones and biochemical traits." Nat Commun **6**: 7975.

Okada, A., S. Hamamoto, K. Taguchi, R. Unno, T. Sugino, R. Ando, K. Mizuno, K. Tozawa, K. Kohri and T. Yasui (2018). "Kidney stone formers have more renal parenchymal crystals than non-stone formers, particularly in the papilla region." BMC Urol **18**(1): 19.

Pahari, A., P. J. Milla and W. G. van't Hoff (2003). "Neonatal nephrocalcinosis in association with glucose-galactose malabsorption." Pediatr Nephrol **18**(7): 700-702.

Pak, C. Y. (1979). "Physiological basis for absorptive and renal hypercalciurias." Am J Physiol **237**(6): F415-423.

Pak, C. Y., R. Kaplan, H. Bone, J. Townsend and O. Waters (1975). "A simple test for the diagnosis of absorptive, resorptive and renal hypercalciurias." N Engl J Med **292**(10): 497-500.

Pan, W., J. Borovac, Z. Spicer, J. G. Hoenderop, R. J. Bindels, G. E. Shull, M. R. Doschak, E. Cordat and R. T. Alexander (2012). "The epithelial sodium/proton exchanger, NHE3, is necessary for renal and intestinal calcium (re)absorption." Am J Physiol Renal Physiol **302**(8): F943-956.

Pannabecker, T. L. (2012). "Structure and function of the thin limbs of the loop of Henle." Compr Physiol **2**(3): 2063-2086.

Pearle, M. S., E. A. Calhoun, G. C. Curhan and P. Urologic Diseases of America (2005). "Urologic diseases in America project: urolithiasis." J Urol **173**(3): 848-857.

Pei, L., G. Solis, M. T. Nguyen, N. Kamat, L. Magenheimer, M. Zhuo, J. Li, J. Curry, A. A. McDonough, T. A. Fields, W. J. Welch and A. S. Yu (2016). "Paracellular epithelial sodium transport maximizes energy efficiency in the kidney." J Clin Invest.

Price, A. L., N. J. Patterson, R. M. Plenge, M. E. Weinblatt, N. A. Shadick and D. Reich (2006). "Principal components analysis corrects for stratification in genome-wide association studies." Nat Genet **38**(8): 904-909.

Proia, A. D. and N. T. Brinn (1985). "Identification of calcium oxalate crystals using alizarin red S stain." Arch Pathol Lab Med **109**(2): 186-189.

Rahner, C., L. L. Mitic and J. M. Anderson (2001). "Heterogeneity in expression and subcellular localization of claudins 2, 3, 4, and 5 in the rat liver, pancreas, and gut." Gastroenterology **120**(2): 411-422.

Randall, A. (1937). "The Origin and Growth of Renal Calculi." Ann Surg **105**(6): 1009-1027.

Rector, F. C., Jr. (1983). "Sodium, bicarbonate, and chloride absorption by the proximal tubule." Am J Physiol **244**(5): F461-471.

Reed, B. Y., H. J. Heller, W. L. Gitomer and C. Y. Pak (1999). "Mapping a gene defect in absorptive hypercalciuria to chromosome 1q23.3-q24." J Clin Endocrinol Metab **84**(11): 3907-3913.

Renkema, K. Y., A. Velic, H. B. Dijkman, S. Verkaart, A. W. van der Kemp, M. Nowik, K. Timmermans, A. Doucet, C. A. Wagner, R. J. Bindels and J. G. Hoenderop (2009). "The calcium-sensing receptor promotes urinary acidification to prevent nephrolithiasis." J Am Soc Nephrol **20**(8): 1705-1713.

Resnick, M., D. B. Pridgen and H. O. Goodman (1968). "Genetic predisposition to formation of calcium oxalate renal calculi." N Engl J Med **278**(24): 1313-1318.

Rosenthal, R., D. Gunzel, S. M. Krug, J. D. Schulzke, M. Fromm and A. S. Yu (2017). "Claudin-2-mediated cation and water transport share a common pore." Acta Physiol (Oxf) **219**(2): 521-536.

Rosenthal, R., S. Milatz, S. M. Krug, B. Oelrich, J. D. Schulzke, S. Amasheh, D. Gunzel and M. Fromm (2010). "Claudin-2, a component of the tight junction, forms a paracellular water channel." J Cell Sci **123**(Pt 11): 1913-1921.

Sakhaee, K., M. J. Nicar, D. C. Brater and C. Y. Pak (1985). "Exaggerated natriuretic and calciuric responses to hydrochlorothiazide in renal hypercalciuria but not in absorptive hypercalciuria." J Clin Endocrinol Metab **61**(5): 825-829.

Sayer, J. A. (2017). "Progress in Understanding the Genetics of Calcium-Containing Nephrolithiasis." J Am Soc Nephrol **28**(3): 748-759.

Scales, C. D., Jr., A. C. Smith, J. M. Hanley, C. S. Saigal and P. Urologic Diseases in America (2012). "Prevalence of kidney stones in the United States." Eur Urol **62**(1): 160-165.

Schnermann, J., Y. Huang and D. Mizel (2013). "Fluid reabsorption in proximal convoluted tubules of mice with gene deletions of claudin-2 and/or aquaporin1." Am J Physiol Renal Physiol **305**(9): F1352-1364.

Scott, L. J., K. L. Mohlke, L. L. Bonnycastle, C. J. Willer, Y. Li, W. L. Duren, M. R. Erdos, H. M. Stringham, P. S. Chines, A. U. Jackson, L. Prokunina-Olsson, C. J. Ding, A. J. Swift, N. Narisu, T. Hu, R. Pruim, R. Xiao, X. Y. Li, K. N. Conneely, N. L. Riebow, A. G. Sprau, M. Tong, P. P. White, K. N. Hetrick, M. W. Barnhart, C. W. Bark, J. L. Goldstein, L. Watkins, F. Xiang, J. Saramies, T. A. Buchanan, R. M. Watanabe, T. T. Valle, L. Kinnunen, G. R.

Abecasis, E. W. Pugh, K. F. Doheny, R. N. Bergman, J. Tuomilehto, F. S. Collins and M. Boehnke (2007). "A genome-wide association study of type 2 diabetes in Finns detects multiple susceptibility variants." Science **316**(5829): 1341-1345.

Sherer, B. A., L. Chen, M. Kang, A. R. Shimotake, V. W. S, T. Chi, M. L. Stoller and S. P. Ho (2018). "A Continuum of Mineralization from Human Renal Pyramid to Stones on Stems." Acta Biomater.

Simon, D. B., Y. Lu, K. A. Choate, H. Velazquez, E. Al-Sabban, M. Praga, G. Casari, A. Bettinelli, G. Colussi, J. Rodriguez-Soriano, D. McCredie, D. Milford, S. Sanjad and R. P. Lifton (1999). "Paracellin-1, a renal tight junction protein required for paracellular Mg2+ resorption." Science **285**(5424): 103-106.

Stamatelou, K. K., M. E. Francis, C. A. Jones, L. M. Nyberg and G. C. Curhan (2003). "Time trends in reported prevalence of kidney stones in the United States: 1976-1994." Kidney Int **63**(5): 1817-1823.

Stevenson, B. R., J. D. Siliciano, M. S. Mooseker and D. A. Goodenough (1986). "Identification of ZO-1: a high molecular weight polypeptide associated with the tight junction (zonula occludens) in a variety of epithelia." J Cell Biol **103**(3): 755-766.

Stewart, A. F., M. Adler, C. M. Byers, G. V. Segre and A. E. Broadus (1982). "Calcium homeostasis in immobilization: an example of resorptive hypercalciuria." N Engl J Med **306**(19): 1136-1140.

Suki, W. N. (1979). "Calcium transport in the nephron." Am J Physiol **237**(1): F1-6.

Sutton, R. A. and V. R. Walker (1980). "Responses to hydrochlorothiazide and acetazolamide in patients with calcium stones. Evidence suggesting a defect in renal tubular function." N Engl J Med **302**(13): 709-713.

Suzuki, H., T. Nishizawa, K. Tani, Y. Yamazaki, A. Tamura, R. Ishitani, N. Dohmae, S. Tsukita, O. Nureki and Y. Fujiyoshi (2014). "Crystal structure of a claudin provides insight into the architecture of tight junctions." Science **344**(6181): 304-307.

Suzuki, T., N. Yoshinaga and S. Tanabe (2011). "Interleukin-6 (IL-6) regulates claudin-2 expression and tight junction permeability in intestinal epithelium." J Biol Chem **286**(36): 31263-31271.

Suzuki, Y., A. Pasch, O. Bonny, M. G. Mohaupt, M. A. Hediger and F. J. Frey (2008). "Gain-of-function haplotype in the epithelial calcium channel TRPV6 is a risk factor for renal calcium stone formation." Hum Mol Genet **17**(11): 1613-1618.

Taal, M. W., B. M. Brenner and F. C. Rector (2012). Brenner & Rector's the kidney. Philadelphia, PA, Elsevier/Saunders.

Tamura, A., H. Hayashi, M. Imasato, Y. Yamazaki, A. Hagiwara, M. Wada, T. Noda, M. Watanabe, Y. Suzuki and S. Tsukita (2011). "Loss of claudin-15, but not claudin-2, causes Na+ deficiency and glucose malabsorption in mouse small intestine." Gastroenterology **140**(3): 913-923.

Tanikawa, C., Y. Kamatani, A. Takahashi, Y. Momozawa, K. Leveque, S. Nagayama, K. Mimori, M. Mori, H. Ishii, J. Inazawa, J. Yasuda, A. Tsuboi, A. Shimizu, M. Sasaki, T. Yamaji, N. Sawada, M. Iwasaki, S. Tsugane, M. Naito, K. Wakai, T. Koyama, T. Takezaki, K. Yuji, Y. Murakami, Y. Nakamura, M. Kubo and K. Matsuda (2018). "GWAS Identifies Two Novel Colorectal Cancer Loci at 16q24.1 and 20q13.12." Carcinogenesis.

Tefekli, A. and F. Cezayirli (2013). "The history of urinary stones: in parallel with civilization." ScientificWorldJournal **2013**: 423964.

Thorleifsson, G., H. Holm, V. Edvardsson, G. B. Walters, U. Styrkarsdottir, D. F. Gudbjartsson, P. Sulem, B. V. Halldorsson, F. de Vegt, F. C. d'Ancona, M. den Heijer, L. Franzson, C. Christiansen, P. Alexandersen, T. Rafnar, K. Kristjansson, G. Sigurdsson, L. A. Kiemeney, M. Bodvarsson, O. S. Indridason, R. Palsson, A. Kong, U. Thorsteinsdottir and K. Stefansson (2009). "Sequence variants in the CLDN14 gene associate with kidney stones and bone mineral density." Nat Genet **41**(8): 926-930.

Tokuda, S. and M. Furuse (2015). "Claudin-2 knockout by TALEN-mediated gene targeting in MDCK cells: claudin-2 independently determines the leaky property of tight junctions in MDCK cells." PLoS One **10**(3): e0119869.

Tsai, P. Y., B. Zhang, W. Q. He, J. M. Zha, M. A. Odenwald, G. Singh, A. Tamura, L. Shen, A. Sailer, S. Yeruva, W. T. Kuo, Y. X. Fu, S. Tsukita and J. R. Turner (2017). "IL-22 Upregulates Epithelial Claudin-2 to Drive Diarrhea and Enteric Pathogen Clearance." Cell Host Microbe **21**(6): 671-681 e674.

Tsugane, S. and T. Sobue (2001). "Baseline survey of JPHC study--design and participation rate. Japan Public Health Center-based Prospective Study on Cancer and Cardiovascular Diseases." J Epidemiol **11**(6 Suppl): S24-29.

Urabe, Y., C. Tanikawa, A. Takahashi, Y. Okada, T. Morizono, T. Tsunoda, N. Kamatani, K. Kohri, K. Chayama, M. Kubo, Y. Nakamura and K. Matsuda (2012). "A genome-wide association study of nephrolithiasis in the Japanese population identifies novel susceptible Loci at 5q35.3, 7p14.3, and 13q14.1." PLoS Genet **8**(3): e1002541.

Van Der Goot, F. and B. Corman (1991). "Axial heterogeneity of apical water permeability along rabbit kidney proximal tubule." Am J Physiol **260**(1 Pt 2): R186-191.

Van Itallie, C. M., S. Rogan, A. Yu, L. S. Vidal, J. Holmes and J. M. Anderson (2006). "Two splice variants of claudin-10 in the kidney create paracellular pores with different ion selectivities." Am J Physiol Renal Physiol **291**(6): F1288-1299.

Verrier, C., D. Bazin, L. Huguet, O. Stephan, A. Gloter, M. C. Verpont, V. Frochot, J. P. Haymann, I. Brocheriou, O. Traxer, M. Daudon and E. Letavernier (2016). "Topography, Composition and Structure of Incipient Randall Plaque at the Nanoscale Level." J Urol **196**(5): 1566-1574.

Walker, V., E. M. Stansbridge and D. G. Griffin (2013). "Demography and biochemistry of 2800 patients from a renal stones clinic." Ann Clin Biochem **50**(Pt 2): 127-139.

Warnock, D. G. and M. B. Burg (1977). "Urinary acidification: CO2 transport by the rabbit proximal straight tubule." Am J Physiol **232**(1): F20-25.

Weber, S., L. Schneider, M. Peters, J. Misselwitz, G. Ronnefarth, M. Boswald, K. E. Bonzel, T. Seeman, T. Sulakova, E. Kuwertz-Broking, A. Gregoric, J. B. Palcoux, V. Tasic, F. Manz, K. Scharer, H. W. Seyberth and M. Konrad (2001). "Novel paracellin-1 mutations in 25 families with familial hypomagnesemia with hypercalciuria and nephrocalcinosis." J Am Soc Nephrol **12**(9): 1872-1881.

Wei, G., S. Rosen, W. H. Dantzler and T. L. Pannabecker (2015). "Architecture of the human renal inner medulla and functional implications." Am J Physiol Renal Physiol **309**(7): F627-637.

Weinman, E. J., V. Mohanlal, N. Stoycheff, F. Wang, D. Steplock, S. Shenolikar and R. Cunningham (2006). "Longitudinal study of urinary excretion of phosphate, calcium, and uric acid in mutant NHERF-1 null mice." Am J Physiol Renal Physiol **290**(4): F838-843.

Whitcomb, D. C., J. LaRusch, A. M. Krasinskas, L. Klei, J. P. Smith, R. E. Brand, J. P. Neoptolemos, M. M. Lerch, M. Tector, B. S. Sandhu, N. M. Guda, L. Orlichenko, C. Alzheimer's Disease Genetics, S. Alkaade, S. T. Amann, M. A. Anderson, J. Baillie, P. A. Banks, D. Conwell, G. A. Cote, P. B. Cotton, J. DiSario, L. A. Farrer, C. E. Forsmark, M. Johnstone, T. B. Gardner, A. Gelrud, W. Greenhalf, J. L. Haines, D. J. Hartman, R. A. Hawes, C. Lawrence, M. Lewis, J. Mayerle, R. Mayeux, N. M. Melhem, M. E. Money, T. Muniraj, G. I. Papachristou, M. A. Pericak-Vance, J. Romagnuolo, G. D. Schellenberg, S. Sherman, P. Simon, V. P. Singh, A. Slivka, D. Stolz, R. Sutton, F. U. Weiss, C. M. Wilcox, N. O. Zarnescu, S. R. Wisniewski, M. R. O'Connell, M. L. Kienholz, K. Roeder, M. M. Barmada, D. Yadav and B. Devlin (2012). "Common genetic variants in the CLDN2 and PRSS1-PRSS2 loci alter risk for alcohol-related and sporadic pancreatitis." Nat Genet **44**(12): 1349-1354.

Wilcox, E. R., Q. L. Burton, S. Naz, S. Riazuddin, T. N. Smith, B. Ploplis, I. Belyantseva, T. Ben-Yosef, N. A. Liburd, R. J. Morell, B. Kachar, D. K. Wu, A. J. Griffith, S. Riazuddin and T. B. Friedman (2001). "Mutations in the gene encoding tight junction claudin-14 cause autosomal recessive deafness DFNB29." Cell **104**(1): 165-172.

Will, C., T. Breiderhoff, J. Thumfart, M. Stuiver, K. Kopplin, K. Sommer, D. Gunzel, U. Querfeld, I. C. Meij, Q. Shan, M. Bleich, T. E. Willnow and D. Muller (2010). "Targeted deletion of murine Cldn16 identifies extra- and intrarenal compensatory mechanisms of Ca2+ and Mg2+ wasting." Am J Physiol Renal Physiol **298**(5): F1152-1161.

Winne, D. (1973). "Unstirred layer, source of biased Michaelis constant in membrane transport." Biochim Biophys Acta **298**(1): 27-31.

Wolman, M. (1975). "Polarized light microscopy as a tool of diagnostic pathology." J Histochem Cytochem **23**(1): 21-50.

Worcester, E. M. and F. L. Coe (2008). "New insights into the pathogenesis of idiopathic hypercalciuria." Semin Nephrol **28**(2): 120-132.

Worcester, E. M. and F. L. Coe (2010). "Clinical practice. Calcium kidney stones." N Engl J Med **363**(10): 954-963.

Worcester, E. M., F. L. Coe, A. P. Evan, K. J. Bergsland, J. H. Parks, L. R. Willis, D. L. Clark and D. L. Gillen (2008). "Evidence for increased postprandial distal nephron calcium delivery in hypercalciuric stone-forming patients." Am J Physiol Renal Physiol **295**(5): F1286-1294.

Wu, X. R. (2015). "Interstitial calcinosis in renal papillae of genetically engineered mouse models: relation to Randall's plaques." Urolithiasis **43 Suppl 1**: 65-76.

Yu, A. S. (2011). "Electrophysiological characterization of claudin ion permeability using stably transfected epithelial cell lines." Methods Mol Biol **762**: 27-41.

Yu, A. S., M. H. Cheng, S. Angelow, D. Gunzel, S. A. Kanzawa, E. E. Schneeberger, M. Fromm and R. D. Coalson (2009). "Molecular basis for cation selectivity in claudin-2-based paracellular pores: identification of an electrostatic interaction site." J Gen Physiol **133**(1): 111-127.

Zelenchuk, L. V., A. M. Hedge and P. S. Rowe (2015). "SPR4-peptide alters bone metabolism of normal and HYP mice." Bone **72**: 23-33.

Zhai, X. Y., R. A. Fenton, A. Andreasen, J. S. Thomsen and E. I. Christensen (2007). "Aquaporin-1 is not expressed in descending thin limbs of short-loop nephrons." J Am Soc Nephrol **18**(11): 2937-2944.

Zhang, P., W. Nie and H. Jiang (2013). "Effects of vitamin D receptor polymorphisms on urolithiasis risk: a meta-analysis." BMC Med Genet **14**: 104.

Zhang, Y. G., S. Wu, R. Lu, D. Zhou, J. Zhou, G. Carmeliet, E. Petrof, E. C. Claud and J. Sun (2015). "Tight junction CLDN2 gene is a direct target of the vitamin D receptor." Sci Rep **5**: 10642.